AD-A115 224   AIR FORCE GEOPHYSICS LAB HANSCOM AFB MA   F/8 1/3
                A SURVEY OF MELTING LAYER RESEARCH.(U)
                JAN 82 R C SCHALLER, I D COHEN, A A BARNES
UNCLASSIFIED   AFGL-TR-82-0007   NL

1 of 2
AD A
115224

MICROCOPY RESOLUTION TEST CHART

NATIONAL BUREAU OF STANDARDS 1963 A

AD A115224

AFGL-TR-82-0007
AIR FORCE SURVEYS IN GEOPHYSICS, NO. 438

A Survey of Melting Layer Research

ROBERT C. SCHALLER, Lt Col, USAF
IAN D. COHEN, Capt, USAF
ARNOLD A. BARNES, Jr.
LAWRENCE C. GIBBONS, Capt, USAF

4 January 1982

DTIC
ELECTE
JUN 7 1982
D

METEOROLOGY DIVISION   PROJECT 2310
AIR FORCE GEOPHYSICS LABORATORY
HANSCOM AFB, MASSACHUSETTS 01731

AIR FORCE SYSTEMS COMMAND, USAF

82 06 07 233

This report has been reviewed by the ESD Public Affairs Office (PA)
and is releasable to the National Technical Information Service (NTIS).

This technical report has been reviewed and
is approved for publication.
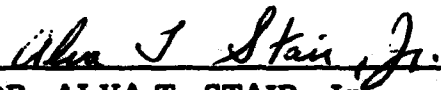
DR. ALVA T. STAIR, Jr
Chief Scientist

Qualified requestors may obtain additional copies from the
Defense Technical Information Center. All others should apply
to the National Technical Information Service.

REPORT DOCUMENTATION PAGE		READ INSTRUCTIONS BEFORE COMPLETING FORM
1. REPORT NUMBER AFGL-TR-82-0007	2. GOVT ACCESSION NO. AD-BA115 224	3. RECIPIENT'S CATALOG NUMBER
4. TITLE (and Subtitle) A SURVEY OF MELTING LAYER RESEARCH		5. TYPE OF REPORT & PERIOD COVERED Scientific. Interim.
		6. PERFORMING ORG. REPORT NUMBER AFSG, No. 438
7. AUTHOR(s) Robert C. Schaller, Lt. Col. USAF Ian D. Cohen, Capt. USAF Arnold A. Barnes, Jr. Lawrence C. Gibbons, Capt. USAF		8. CONTRACT OR GRANT NUMBER(s)
9. PERFORMING ORGANIZATION NAME AND ADDRESS Air Force Geophysics Laboratory (LYC) Hanscom AFB Massachusetts 01731		10. PROGRAM ELEMENT. PROJECT, TASK AREA & WORK UNIT NUMBERS 61102F 2310G502
11. CONTROLLING OFFICE NAME AND ADDRESS Air Force Geophysics Laboratory (LYC) Hanscom AFB Massachusetts 01731		12. REPORT DATE 4 January 1982
		13. NUMBER OF PAGES 102
14. MONITORING AGENCY NAME & ADDRESS(if different from Controlling Office)		15. SECURITY CLASS. (of this report) Unclassified
		15a. DECLASSIFICATION DOWNGRADING SCHEDULE

16. DISTRIBUTION STATEMENT (of this Report)

Approved for public release; distribution unlimited.

17. DISTRIBUTION STATEMENT (of the abstract entered in Block 20, if different from Report)

18. SUPPLEMENTARY NOTES

19. KEY WORDS (Continue on reverse side if necessary and identify by block number)

Melting layer	Liquid water content
Cloud physics	Particle size
Rain	Melting band
Snow	Ice crystals
Bright band	Radar reflectivity

20. ABSTRACT (Continue on reverse side if necessary and identify by block number)

   This report summarizes previous melting-layer research both within and outside AFGL and provides recommendations for future research in the melting layer. An extensive literature search provided a bibliography of previous research. This bibliography is included as an appendix. Several definitions of the top and bottom of the melting layer are presented and discussed. Aggregation and breakup appear to be the chief microphysical processes that determine the particle-size spectrum of snow and ice that enter the melting layer. cont.

DD FORM 1473
1 JAN 73

cont

20. Abstract (Continued)

Studies of the actual melting process and of the melting layer as seen by radar are presented. Microphysical and thermodynamic characteristics are discussed. Dynamic considerations are mentioned. Previously gathered aircraft data are reviewed, and recommendations are made for future aircraft and radar data-gathering efforts.

Accession For

NTIS GRA&I	☒
DTIC TAB	☐
Unannounced	☐
Justification	

By

Distribution/

Availability Codes

Dist	Avail and/or Special
A	

Contents

3

Contents

Illustrations

4

Table

A Survey of Melting Layer Research

1. INTRODUCTION

The purpose of this report is to summarize past outside research into the melting layer, state what has been done by the Cloud Physics Branch (LYC) of the Air Force Geophysics Laboratory (AFGL) up to December 1981, and to make recommendations for future research in this area.

Since the first description of the radar bright band was published 35 years ago (Ryde, 1946[1]) the vast majority of research into the melting of snow and ice parti- cles in stratiform clouds has been confined to radar studies of the melting (or bright) band (Mason, 1955;[2] Ludlam, 1980[3]). These studies have shown that the increase in radar reflectivity (hence, the term, bright band) was due to the change of phase of water from the solid to the liquid form.

1. Ryde, J. (1946) The attenuation of radar echoes produced at centimeter wave- lengths by various meteorological phenomena. Report of Conf. on Met. Factors in Radio Wave Propagation, London, Great Britain, pp. 169-189.

2. Mason, B.J. (1955) Radar evidence for aggregation and orientation of melting snowflakes, Quart. J. Royal Met. Soc. 81:262-264.

3. Ludlam, F. (1980) Clouds and Storms, The Pennsylvania State University Press, University Park, Pennsylvania.

Studies of icing phenomena (Great Britain Meteorological Office, 1965;[4] List and Dussault, 1967;[5] Medzhitov, 1964[6]), of cloud liquid water content (Pruppacher and Klett, 1980[7]), and of weather modification (List, 1980;[8] Cooper, 1980;[9] Hallett, 1980[10]) have pointed to the need for a study of the melting layer as a basic research project that will enhance our understanding of the atmosphere.

In recent years Department of Defense agencies have noted several problems that directly relate to the melting layer. The Air Force has observed the erosion of hypersonic vehicles passing through this layer, with a resulting degradation in vehicle performance. Also, certain conditions of precipitation, temperature, or humidity can cause an alteration of microwave signals and laser transmission, thereby causing problems with surveillance, weapons guidance systems, and communications. (It should be noted that even with the attenuation and scattering of communications signals, it is still possible to get the information through by changing the mode of transmission.)

Millions of dollars of damage due to the icing of control surfaces of operational aircraft is also characteristic of the melting layer. Since maximum liquid water content occurs in this layer, (Wexler, 1955[11]) the problem of engine ingestion of liquid water also leads to a need to study this region.

The U.S. Army, in its use of surface-to-surface and surface-to-air missiles has also stated a need to study icing conditions and liquid water content (Air Weather Service Geophysical Requirement 2-80 [12]).

4. Great Britain Meteorological Office (1965) Ice Accretion on Aircraft.

5. List, R., and Dussault, J. (1967) Quasi-steady-state icing and melting conditions and heat and mass transfer of spherical and spheroidal hailstones, J. Atm. Sci. 24:522-529.

6. Medzhitov, R. (1964) Cloud microstructure and icing of airplanes over Belorussia. Moscow Tsentralnyi Institut Prognozov, Trudy, 136:101-115.

7. Pruppacher, H., and Klett, J. (1980) Microphysics of Clouds and Precipitation, Reidel Publishing Co., Dordrecht, Holland, 705 pp.

8. List, R. (1980) An update on the status of the WMO precipitation enhancement project, Third WMO Scientific Conference on Weather Modification, Clermont-Ferrand, France, 21-25 July 1980, pp. 233-240.

9. Cooper, W.A. (1980) Estimation of rainfall using measurements from aircraft, Third WMO Scientific Conference on Weather Modification, Clermont-Ferrand, France, 21-25 July 1980, pp. 365-372.

10. Hallett, J. (1980) Some observations of supercooled water in cyclonic storms and implications from natural and artificial ice phase evolution, Third WMO Scientific Conference on Weather Modification, Clermont-Ferrand, France, 21-25 July 1980, pp. 471-476.

11. Wexler, R. (1955) The melting layer, Proc. First Conf. on Physics of Clouds and Precipitation Particles, pp. 306-314.

12. Air Weather Service 2-80 Geophysical Requirement (1980) Improved Cloud Data Handling and Analysis.

In order to satisfy the above, a study of the melting layer was begun by the Cloud Physics Branch in October, 1980. This report summarizes the results of this study through November, 1981.

2. HISTORICAL BACKGROUND

Pace (1980)[13] has provided the most comprehensive theoretical and experimental study of the melting layer done over the past 40 years, or since Findeisen (1940)[14] first looked at isothermal layers in the atmosphere at temperatures close to $0°C$ - layers that were caused by the cooling produced by melting snow.

After Ryde (1946)[1] published his analysis of radar echoes produced by various meteorological phenomena, most researchers confined their studies to that part of the melting layer best known as the bright band or melting band (Byers and Coome, 1947;[15] Austin and Bemis, 1950;[16] Browne and Robinson, 1952;[17] Imai, et al, 1955;[18] Wexler 1955;[11] Lhermitte and Atlas, 1963;[19] Ramana Murty, et al, 1965;[20] Ekpenyong and Srivastava, 1970[21]). Atlas (1964)[22] published a study of advances in radar meteorology and Battan (1973)[23] covered radar theory thoroughly.

13. Pace, J. (1980) Microphysical and Thermodynamic Characteristics Through the Melting Layer, Report No. AS126, Dept. of Atmospheric Science, University of Wyoming, Laramie, Wyoming, 204 pp.

14. Findeisen, W. (1940) The formation of the $0°C$-isothermal layer and fracto-cumulus under nimbostratus, Met. Zeit 57:49-54.

15. Byers, H.R., and Coome, R.D. (1947) The "Bright Line" in radar cloud echoes and its probable explanation, J. Meteor. 4(No. 3):75-81.

16. Austin, P.M., and Bemis, A. (1950) A quantitative study of the bright band in radar precipitation echoes, J. Meteor. 7:165-171.

17. Browne, I.C., and Robinson, N. (1952) Cross-polarization of the radar melting band, Nature 170:1078-1079.

18. Imai, I., Fujiwara, M., Ichimura, I., and Toyama, Y. (1955) Radar reflectivity of falling snow, J. Met. Res. 7:422-425.

19. Lhermitte, R., and Atlas, D. (1963) Doppler fallspeed and particle growth in stratiform precipitation, Proc. Tenth Conf. on Radar Met., Washington, D.C., pp. 297-302.

20. Ramana Murty, B., Roy, A., and Biswas, K. (1965) Radar echo intensity below the bright band, J. Atm. Sci. 22:91-94.

21. Ekpenyong, B., and Srivastava, R. (1970) Radar Characteristics of the Melting Layer — A Theoretical Study, Univ. of Chicago Dept. of Geophys. Sciences and Ill. Inst. of Tech. Dept. of Elec. Eng., Technical Report No. 16, Lab. for Atm. Probing, Chicago, Illinois.

22. Atlas, D. (1964) Advances in radar meteorology, Adv. in Geophysics 10:318-478.

23. Battan, L.J. (1973) Radar Observation of the Atmosphere, University of Chicago Press, Chicago, Illinois, pp. 324-330.

Further radar experiments led to studies of polarized radar signals. Polarization parameters throughout the area of the bright band were listed and compared by Browne and Robinson (1952),[17] Barge (1974),[24] Hendry and MacCormick (1974),[25] Hendry, et al (1976),[26] Battan (1977),[27] and Humphries and Barge (1979).[28]

The importance of drop breakup and aggregation in the melting band was studied by DuToit (1967),[29] Ohtake (1969),[30] Lhermitte and Atlas (1963),[19] Passarelli (1978),[31] Heymsfield (1979),[32] Humphries and Barge (1979),[28] Marshall and Gunn (1952),[33] and Mason (1971).[34] However, no agreement was reached by these researchers on the importance of drop breakup and aggregation.

Wexler et al, (1954)[35] were the first to perform extensive calculations concerning the thermodynamics of atmospheric cooling by melting particles. Macklin (1963),[36] Atlas, et al, (1969),[37] and Pruppacher and Klett (1980)[7] are others who pioneered this effort.

24. Barge, B.L. (1974) Polarization measurements of precipitation backscatter in Alberta, J. Rech. Atmos. 8:163-173.

25. Hendry, A., and MacCormick, G.C. (1974) Polarization properties of precipitation particles related to storm structure, J. Rech. Atmos. 8:189-200.

26. Hendry, A., MacCormick, G.C., and Barge, B.L. (1976) K-band and S-band observation of the differential propagation constraint in snow, IEEE Trans. Antennas and Propagat. AP-24:521-525.

27. Battan, L.J. (1977) Rain resulting from melting ice particles, J. Appl. Met. 16:595-604.

28. Humphries, R.G., and Barge, B.L. (1979) Polarization and dual-wavelength radar observation of the bright band, IEEE Trans. Georie Elect. GE-17(No. 4):190-195.

29. DuToit, P. (1967) Doppler radar observations of drop sizes in continuous rain, J. Appl. Met. 6:1082-1087.

30. Ohtake, T. (1969) Observations of the size distribution of hydrometeors through the melting layer, J. Atm. Sci. 26:545-557.

31. Passarelli, R.E., Jr. (1978) An approximate analytical model of the vapor deposition and aggregation growth of snowflakes, J. Atm. Sci. 35:118-124.

32. Heymsfield, G.M. (1979) Doppler radar study of a warm frontal region, J. Atm. Sci. 36:2093-2107.

33. Marshall, J.S., and Gunn, K.L.S. (1952) Measurement of snow parameters by radar, J. Meteor. 9:332-337.

34. Mason, B.J. (1971) The Physics of Clouds, Clarendon Press, London, Great Britain, 671 pp.

35. Wexler, R., Reed, R.J., and Honig, J. (1954) Atmospheric cooling by melting snow, Bul. Amer. Meteor. Soc. 35:48-51.

36. Macklin, W. (1963) Heat transfer from hailstones, Quart. J. Royal Met. Soc. 89:360-363.

37. Atlas, D., Tatehira, R., Srivastava, R., Marker, W., and Carbone, R. (1969) Precipitation-induced mesoscale wind perturbations in the melting layer, Quart. J. Royal Met. Soc. 95:544-560.

Many of the listed studies were attempts to deduce information about melting layer processes by interpreting the available data, often through the use of theoretical models of somewhat questionable validity. Pace (1980)[13] has resolved some of the problems by assembling an abundance of in situ data and developing a theoretical model deduced from such data.

3. CLOUD PHYSICS BRANCH STUDY

3.1 Objectives and Approach

The Cloud Physics Branch began its investigation into the melting layer in October 1980. The objectives of this basic research project are to determine the nature of the processes operating in the melting layer and to develop a model of the microphysics of the melting layer. The model will be built from the results of research on snowflakes and ice-crystal melting, radar reflectivity, and meso-scale dynamics within the layer.

The current study has been confined to stratiform clouds (both winter and summer) and is a study of the melting of ice and snow. It was decided not to look at hail and graupel at the present time because their occurrence is rare compared to that of ice and snow.

This study will not be restricted to looking only at the bright band because the bright band is only a portion of the entire melting layer. The bright band has been well-defined and often discussed, mainly in the light of radar reflectivity (Rayleigh and Mie scattering).

As a starting point and as background for this research, an exhaustive literature search and evaluation has been performed. A list of more than 100 references has been compiled and rated with regard to relevancy. The list and evaluation form Appendix A in this report.

3.2 Contracts

Several outside agencies and individuals have provided and are continuing to provide information for the present study. Professor Steven B. Newman of Central Connecticut State College carried out a ten-week research program at AFGL on the melting layer during the summer of 1981. A copy of his final report is included in Appendix B. He studied the problem of defining the boundaries of the melting layer and also developed a model of snowflake aggregation and breakup. He showed that at reasonable cloud ice contents (1.0 to 1.5 g/m^3) the aggregation and breakup of snowflakes just above the melting layer results in considerable ice multiplication and growth. The increase in both size and number concentration of snowflakes

11

entering the melting layer may play a considerable role in enhancing the radar echo intensity in the melting layer resulting in the radar bright band. Dr. Newman is continuing this research at Central Connecticut State College during the present academic year under a mini-grant from the Air Force Office of Scientific Research (AFOSR).

Professor Richard Passarelli and Mr. Kenneth Lo of M. I. T. have performed extensive studies into snowflake aggregation and breakup, using data collected by the AFGL MC-130 aircraft (Figure 1). A draft of their paper, entitled "A New Sampling Technique for Quantitative Airborne Studies of Snow Growth: Theory and Examples," is Appendix C. Professor Passarrelli has devised a new flight plan that permits one to observe the height evolution of snow-size spectra in a reference
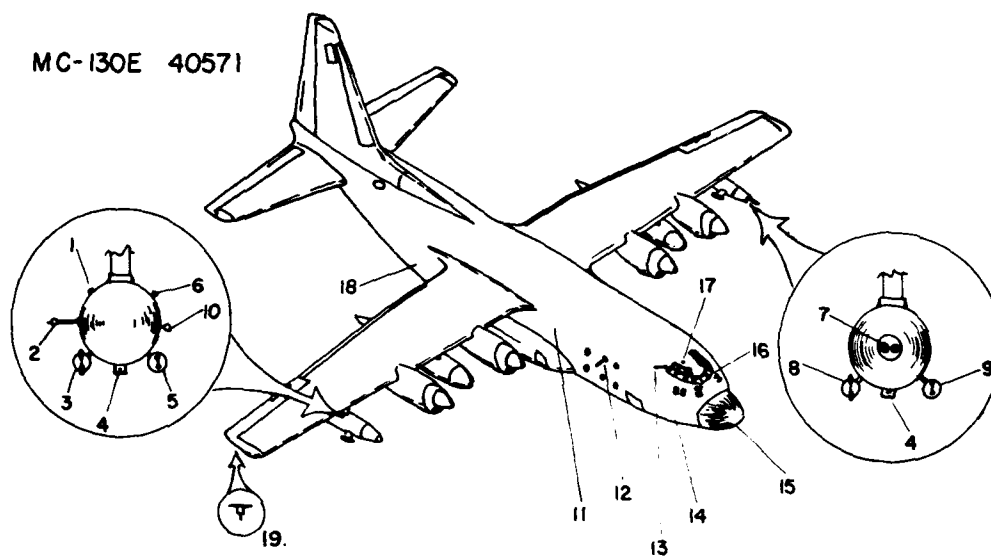
KEY

1. DEW POINT HYGROMETER PROBE
2. PMS I-D AXIAL SCATTER PROBE(2-30μ)
3. PMS I-D PRECIP. PROBE(300-4500μ)
4. HYDROMETEOR FOIL SAMPLER
5. PMS I-D CLOUD PROBE (20-300μ)
6. TOTAL AIR TEMPERATURE PROBE
7. EWER PROBE
8. PMS 2-D PRECIP. PROBE(200-6400μ)
9. PMS 2-D CLOUD PROBE (25-800μ)
10. JW CLOUD WATER PROBE

11. PDP-8/E COMPUTER & LINE PRINTER
12. FORMVAR HYDROMETEOR REPLICATOR
13. VISUAL HYDROMETEOR PROBE
14. I.N.S. & DOPPLER RADAR
15. AN/APQ-122 K_g & 5CM WEATHER RADAR
16. 16mm NOSE CAMERA
17. PROBE LIGHT
18. TELEMETRY
19. ICING PROBE

Figure 1. Cloud Physics MC-130E. This specially-instrumented aircraft was used to gather data for the Cloud Physics Branch until it was transferred to another Air Force unit in May, 1981

12

frame where the effects of horizontal gradients and temporal changes of the atmosphere are minimized. This reduces the evolution of snow-size distribution to a 1-D steady-state problem. The flight plan, termed Advecting Spiral Descent (ASD, also called, the Passarelli Spiral) requires an aircraft to start aloft in a mesoscale precipitation area. Then it spirals downward in a constant bank angle, descending at approximately the mean fallspeed of snow (Figure 2) and drifting with the wind. The advantage of ASD is that no a priori knowledge of the vertical wind profile is required. The analysis is performed by averaging spectra over a complete loop of the spiral, serving to average any horizontal inhomogeneities. Results show that snow growth is a well-behaved phenomenon and the ASD technique is sampling it in a coherent manner. The qualitative comparison between observation and theory suggests that snow growth evolves through at least three stages, namely deposition, aggregation, and breakup. Both the works by Newman and by Passarelli and Lo are showing how snow forming in the upper part of the storm (above the melting layer) feeds into the lower part of the precipitation system.
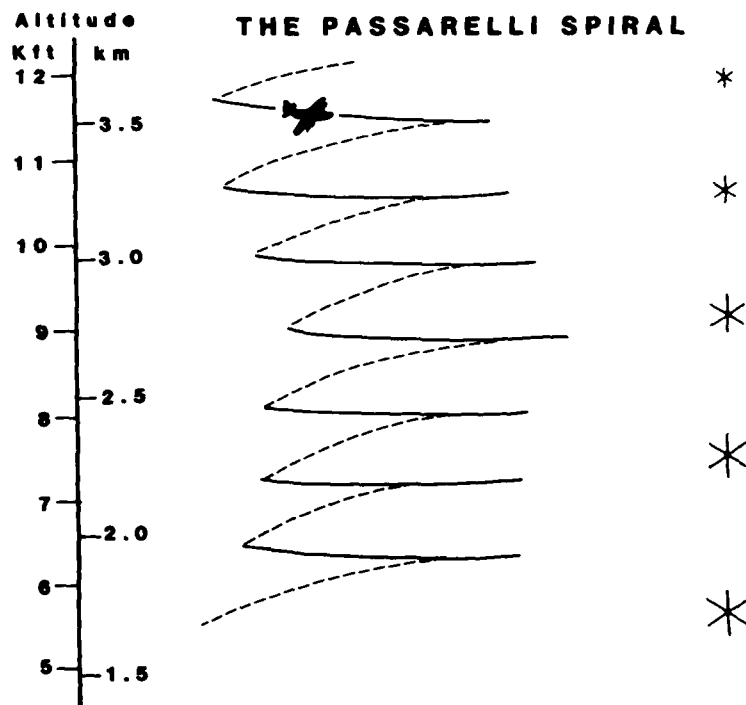
Figure 2. The Passarelli Spiral. This is an aircraft maneuver used to study melting snowflakes. It consists of a spiral descent at 200 ft/min. (approximately the fall velocity of a snowflake) from the top to the bottom of a cloud system

13
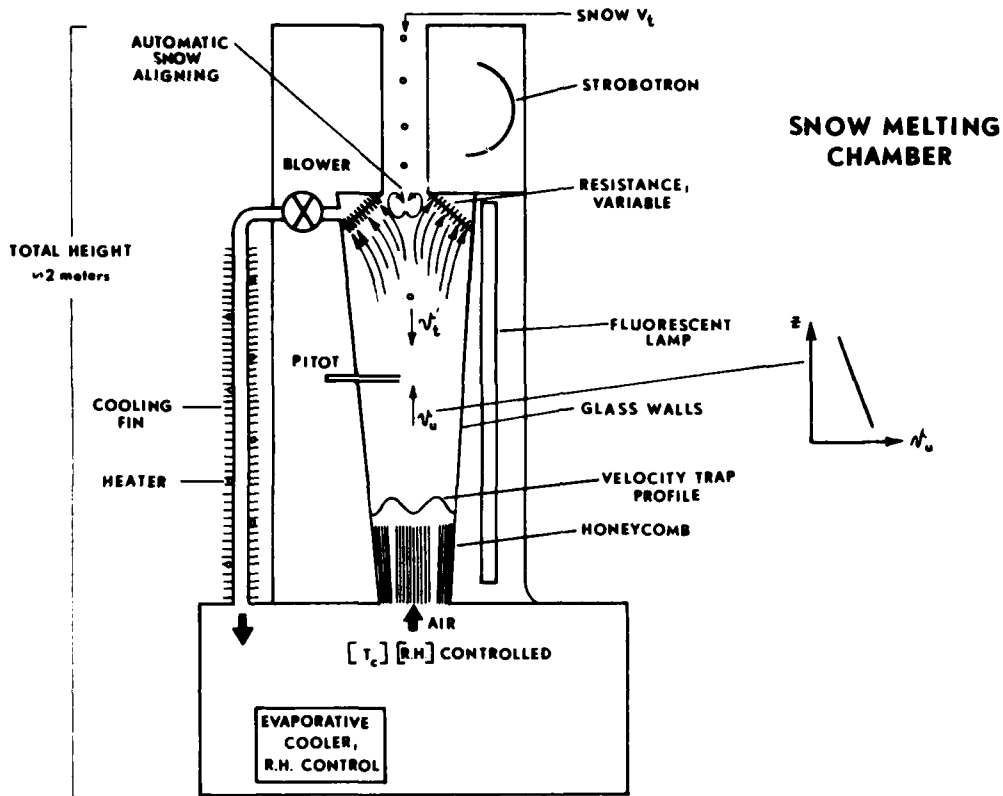
Figure 3. University of Utah Melting Chamber. The snowflake is suspended in the center of the chamber by the velocity trap. The snowflake is then observed and photographed as it melts

Since, in a successful melting layer study, experimental and theoretical studies of ice crystals and snowflake melting are in critical need, a contract has been awarded to Dr. Norihiko Fukuta at the University of Utah in Salt Lake City to construct a melting chamber (Figure 3). Dr. Fukuta will use the chamber to take photographs of melting snowflakes suspended in air. Dr. Fukuta's theory on the melting of ice and snow is discussed in Section 7 of this report. A complete summary of his theoretical ideas are included in Appendix D. Professor William B. Cotton of Colorado State University in Fort Collins, Colorado, is using a three-dimensional (3-D), time-dependent cloud physics model to investigate the physical basis for relationships between standard meteorological measurements (by radar, lidar, satellite, etc.) and the meaningful cloud physics parameters, such as the

14

vertical storm motions, the liquid water content, and the hydrometeor size distributions. Since this contract just began in November 1981, there are no results to report.

4. DEFINING THE TOP OF THE MELTING LAYER

Initially, it would seem logical to define the top of the melting layer at the 0°C-isotherm because that is the point at which melting should begin. However, is that necessarily true? Does melting really begin at the 0°C-isotherm, or does it start at that level where the wet-bulb temperature is 0°C (Newman, Appendix B)? The wet-bulb 0°C-isotherm is usually 100-200 m below the dry-bulb 0°C-line (Austin and Bemis, 1950;[16] Hooper and Kippax, 1950;[38] Browne, 1952;[39] Mason, 1955[2]). This question will be addressed below.

Another question that was posed was whether or not there was some melting before the snow reached the 0°C-isotherm because of contaminants, such as sea salt, which might have lowered the melting point of the snow or ice crystals. It is highly unlikely that this has any appreciable effect because of the small concentration of the contaminants in the atmosphere and because of the relative immobility of the molecules in the crystalline lattice.

Still another factor to consider is whether or not long wave radiation from the lower part of the atmosphere could be absorbed by particles so that melting might occur at atmospheric temperatures lower than 0°C-isotherm. Since snow is known as a good long wave radiator, this could be a significant process. Further discussion in this area is included in Section 7.

Other methods considered for defining the top of the melting layer were: 1) the top of the bright band; 2) when a certain portion of the mass has already melted; and 3) using fall speeds of the hydrometeors involved (Sweeney and Barnes, Appendix E).

For the purpose of this study, it was decided to define the top of the melting layer as the top of the 0°C-(dry-bulb)-isothermal layer. This isothermal layer is usually about 200-m deep. This same definition was arrived at independently by Pace (1980).[13] The isothermal layer is a result of the melting of ice and snow particles. This definition does not resolve the wet-bulb vs dry-bulb temperature question posed above, but will be studied further in this investigation.

---

38. Hooper, J., and Kippax, A. (1950) The bright band: a phenomenon associated with radar echoes from falling rain, Quart. J. Royal Met. Soc. 76:125-131.

39. Browne, I. C. (1952) Radar Studies of Clouds, Ph. D. Thesis, Cambridge University, England.

15

5. DEFINING THE BOTTOM OF THE MELTING LAYER

Attempting to determine the thickness of the melting layer posed some more problems. On cold days when snow is reaching the ground, the end of the melting layer has not occurred by the time the earth's surface is reached. Also, the base is a dynamic thing that can change with time. From a radar viewpoint, Sweeney and Barnes (Appendix E) consider the melting layer be broken into two zones after Wexler (1955).[11] Zone 1 stretches from the 0°C-isotherm to the peak of the radar reflectively in the bright band, and zone 2 from that peak to the point at which raindrops reach terminal velocity.

Professor Newman (Appendix B) has mentioned that defining the bottom of the melting layer as that level at which there is no more frozen precipitation may be setting a boundary that is too low in altitude for other purposes. He also notes that the $+5^{\circ}$C-level has been the most widely used threshold temperature for the bottom of the melting layer, but that the reason for this choice appears to be entirely arbitrary.

Many private discussions within the Cloud Physics Branch have led us to the conclusion that, in the present study, no real purpose would be served by trying to clearly define the bottom of the melting layer at this time. Indeed, since the best that could be accomplished right now is an arbitrary definition; setting such a definition may be too restrictive. Therefore, the Cloud Physics Branch has decided not to define the bottom of the melting layer at this stage of our investigation.

6. SNOW AND ICE ENTERING THE MELTING LAYER

As mentioned earlier, any complete study of the melting layer would have to include a description of the snow and ice that enter the layer from above.

Professor Newman (Appendix B) has used the aggregational growth equation of Rogers (1979)[40] to develop a simple aggregational model for snowflakes. He ignores growth by diffusion or accretion and gives aggregates a maximum diameter of 5 mm, at which size the snowflakes break up into smaller particles. He assumes that the aggregation rate increases as the flakes approach the 0°C-isotherm. Then he shows that aggregational growth and breakup yield greater numbers of larger snowflakes than were present before aggregation began. This factor may account for a large part of the radar bright band in the melting layer, especially when the larger snowflakes begin to melt.

---

40. Rogers, R.R. (1979) A Short Course in Cloud Physics, Pergammon Press, New York, 227 pp.

16

Lo and Passarelli (Appendix C) have gone farther than Newman in their study. Their model and data obtained from the AFGL MC-130 aircraft have shown that snow growth evolves through at least three stages: deposition, aggregation, and breakup. They use a 1-D, steady-state model of snow growth and compare it to the observed size spectra from the Passarelli Spiral (Figure 2). In other words the Passarelli Spiral aircraft maneuver can successfully trace a 1-D region in which the effects of spatial and temporal gradients are minimized. As Lo and Passarelli state, "this technique opens the door for more detailed quantitative comparisons between microphysical theory and observations."

Mr. Robert O. Berthel (1981)[41] of the Cloud Physics Branch has developed a mathematical model that enables us to study single ice crystals of known geometric forms by considering each crystal's spatial relationship to the assumed measuring instrument. A random number technique is used to define crystal orientation and several forms of single ice crystals have been investigated in terms of equivalent melted diameter of liquid water drops. He has demonstrated the reliability of PMS ice particle measurements by mathematical modeling with the use of a computer. Berthel's study is being extended and will be applied to the modeling of the melting layer.

7. MELTING OF ICE CRYSTALS AND SNOWFLAKES

As stated earlier in this report, the melting of ice crystals and snowflakes proceeds inward from the outer edges and surfaces. This is because the latent heat of fusion absorbed by the frozen surface is heat supplied from the outside environment (Fukuta, Appendix D).

There are three different mechanisms by which heat may be supplied to the ice crystal or snowflake during the melting process: radiative transfer, sensible heat conduction, and latent heat transfer by water vapor diffusion. Since there is almost a radiative balance between the cloud above and the falling melted crystals below the melting layer, we chose to ignore the radiative heat transfer. If an ice crystal or snowflake is placed in quiescent warm air without falling, there will be a temperature field established around the crystal and sensible heat conduction occurs from the environment to the crystal through the field. The latent heat transfer occurs in the same manner during vapor diffusion from the surface to the environment, in the opposite direction from the sensible heat transfer.

In the real atmosphere when the ice or snow crystal falls through the environment, the temperature and water vapor field around the crystal are deformed. The fields are modified the most at the distal points; this is why melting occurs from

---

41. Berthel, R.O. (1981) The Conversion of Aircraft Ice Crystal Measurements into Terms of Liquid Water Using Simulated Data, AFGL-TR-81-0173, AD A106 419, 46 pp.

17

the outside in towards the center. Since the water on the surface tends to take the shape with the smallest surface area (a sphere), the ice or snow crystal shrinks. This shape change leads to an increase in the fall speed; the change in fall speed alters the convective motion around the crystal, and the accompanying temperature and vapor fields are also modified.

Fukuta (Appendix D) first treats the problems of heat conduction and vapor diffusion to and from the ice surface in a quiescent air environment, then proceeds to add the effect of convective motion of air around the crystal caused by the fall. He then devises the mathematical equations for the melting of ice crystals of both oblate and prolate spheroids (plate and prism crystals). These equations are presented in Appendix D.

Fukuta then does the same type of calculation for snowflake melting, deriving an empirical expression to describe this phenomena. Again, the equations are presented in Appendix D.

8. ANALYSIS OF FLIGHT DATA

AFGL has used an instrumented MC-130E aircraft to gather data on clouds at various levels. The MC-130E is a four-engine turboprop transport. In recent years, it has been flown and maintained by the 4950th Test Wing of the Aeronautical Systems Division at Wright-Patterson AFB, Ohio. AFGL cloud sampling equipment on the airplane is described by Varley (1978).[42,43] The airplane has been used for cirrus studies (Barnes, 1980;[44] Cohen, 1981;[45,46] Cohen, 1979;[47] Cohen and Barnes, 1980;[48] Varley and Brooks, 1978;[49] Varley, 1978;[42,43] Varley and Barnes, 1979;[50]

42. Varley, D.J. (1978) Cirrus Particle Distribution Study, Part 1, Air Force Surveys in Geophysics No. 394, AFGL-TR-78-0192, AD A061 485, 71 pp.

43. Varley, D.J. (1978) Cirrus Particle Distribution Study, Part 3, AFGL-TR-78-0305, AD A066 975.

44. Barnes, A.A., Jr. (1980) Observations of ice particles in clear air, Journal de Recherches Atmospherique 14(No. 3-4):311-315, AFGL-TR-81-0347, AD A108 914.

45. Cohen, I.D. (1981) Development of a Large Scale Cloud System, 23-27 March 1978, AFGL-TR-81-0127, AD A106 417, Environmental Research Papers 739, 112 pp.

46. Cohen, I.D. (1981) Cirrus Particle Distribution Study, Part 8, AFGL-TR-81-0316, Air Force Surveys in Geophysics 437, (in press).

47. Cohen, I.D. (1979) Cirrus Particle Distribution Study, Part 5, AFGL-TR-79-0155, AD A077 361.

48. Cohen, I.D., and Barnes, A.A. (1980) Cirrus Particle Distribution Study, Part 6, AFGL-TR-80-0261, AD A096 772.

49. Varley, D.J., and Brooks, D.M. (1978) Cirrus Particle Distribution Study, Part 2, AFGL-TR-78-0248, AD A063 807.

50. Varley, D.J., and Barnes, A.A. (1979) Cirrus Particle Distribution Study, Part 4, AFGL-TR-79-0134, AD A074 763.

18

Varley, Cohen, and Barnes, 1980[51]) and studies of large scale systems (Varley, 1980;[52] Cohen, 1981[45]), and was originally instrumented for cloud physics measurements required for testing of ICBM reentry nosecones (Barnes, et al, 1974[53]).

8.1 Icing Flights

During the months of November 1979 to April 1980 and October 1980 to May 1981, one of the missions of the MC-130E was to investigate aircraft icing. About 25 flights were made in the layers just above the freezing level. Due to the proximity of this area to the melting layer, several flights were reexamined for possible use in the melting layer program. Flights in the icing program were usually conducted near a weather observing station that took rawindsonde observations. The rawindsonde observations provided temperature and dew-point observations that could be compared with those reported by the aircraft. Data were gathered at 1000-ft intervals. Each data pass consisted of about 3 to 6 min. of sampling time.

Several flights held promise of providing data for the melting layer project, but in most cases the data came from the area above the freezing level and thus are not useful for this project. Only one flight (made at Greensboro, North Carolina on 22 January 1980) had significant data at altitudes within the melting layer, but on that day the melting layer was unusually small, and the 1000-ft interval did not provide sufficient detail of the melting layer.

8.2 Snow Growth Flights

As previously mentioned, Lo and Passarelli (Appendix C) have developed a flight pattern to be used to study snow growth. It consists of a spiral descent at 200 ft per minute (approximately the fall velocity of a snowflake) from the top to the bottom of a cloud system (Figure 2). In some cases, this pattern has penetrated into the melting layer. The pattern provides a continuous vertical profile of the atmosphere.

Past experience has shown that a complete spiral is difficult to obtain, since the aircraft often cannot remain in the cloud due to dissipation of the cloud itself,

51. Varley, D.J., Cohen, I.D., and Barnes, A.A. (1980) Cirrus Particle Distribution Study, Part 7, AFGL-TR-80-0324, AD A100 269.

52. Varley, D.J. (1980) Microphysical Properties of a Large Scale Cloud System 1-3 March 1978, AFGL-TR-80-0002, Environmental Research Papers 690, AD A083 140, 100 pp.

53. Barnes, A.A., Nelson, L.D., and Metcalf, J.J. (1974) Weather Documentation at Kwajalein Missile Range, Preprints of the 6th Conference on Aerospace and Aeronautical Meteorology, American Meteorological Society, pp. 66-69; also Air Force Surveys in Geophysics, No.292, AFCRL, 12 September 1974, 14 pp. AFCRL-TR-74-0430, AD A000 925.

airspace restrictions, safety of flight, or time constraints. Of the spirals completed, only one (that of 7 March 1980) provided a good cross-section of the melting layer.

8.3 Other Flight Data

Several other programs have provided some cloud data. The Large Scale Cloud Systems program has provided a variety of data in clouds at various levels. Other programs have generally dealt with clouds at higher levels.

As a result of the flight programs we have previously conducted, we do have some aircraft data on the melting layer, but since previously we have not been concerned specifically with the melting layer, we do not have the solid body of aircraft data we need. The aircraft data we now have may supplement future data-gathering efforts, but it is not complete enough to stand by itself.

9. MICROPHYSICAL AND THERMODYNAMIC CHARACTERISTICS

9.1 Microphysical Characteristics

It seems clear that aggregation and breakup are the dominant microphysical processes occurring above the melting layer (Newman, Appendix B; Lo and Passarelli, Appendix C; Pace, 1980 [13]). Data assembled by Stewart and Marwitz (1980)[54] support not only this statement, but the fact that aggregation and breakup also occur in the isothermal layer below $0^{\circ}C$ that extends for approximately 200 m. Drop breakup of the melting particles also occurs below the bright band and is a definite factor that contributes to the decrease in reflectivity observed there (Newman, Appendix B; Sweeney and Barnes, Appendix E; Pace, 1980 [13]).

Vertical profiles of particle concentration observed by Stewart and Marwitz (1980)[54] imply that there is a significant source of ice crystals near the $-6^{\circ}C$-level. If the crystals were produced by the Hallett-Mossop process (1974),[55] the maximum would occur at $-5^{\circ}C$. However, the apparent discrepancy is explained by the fact that ice particles are transported upward by ascending air motions. Professor Newman (Appendix B) has developed a model that discusses the breakup of snowflakes in greater detail.

It has also recently been noted by Pace (1980)[13] that the level of maximum reflectivity is slightly below the level at which the largest particles occurred. This

---

54. Stewart, R., and Marwitz, J. (1980) Cloud Physics Studies in SCPP during 1979-80, Report No. AS125, Dept. of Atmospheric Science, University of Wyoming, Laramie, Wyoming, 96 pp.

55. Hallett, J., and Mossop, S. C. (1974) Production of secondary ice particles during the riming process, Nature 249:26-28.

can be explained by the fact that the development of a water coating on large snow-flakes and ice crystals is delayed relative to that on the smaller ones. Hence, the formation of a liquid water coating on the larger particles does not occur until after the temperature of the environment approaches approximately $1^{o}C$, the level of maximum reflectivity. In other words, it appears as though the intensity of the bright band within the melting layer is determined by the various characteristics (concentration, shape, manner of melting) of the largest particles present. The decrease of reflectivity below the bright band then must be due both to the collapse of the large aggregates as they melt and subsequent decrease in concentration due to faster fallspeeds, and also to particle breakup. He states that the existence of the melting phenomenon will not thermodynamically permit the existence of super-cooled water in the melting layer, that is, the existence of nonmelting-related supercooled water.

Fukuta[56] says that it is possible to obtain detailed microphysical knowledge of the melting layer by utilizing his theory (Appendix D) in numerical computations. He also states that the idea of liquid water accumulation in the melting layer is questionable due to the increase in fallspeeds as melting occurs. In other words, although melting results in an increase in liquid water content, the increase in fall velocities acts towards reducing that content. Further examination of these points will be done in the future.

9.2 Thermodynamic Characteristics

Pace (1980)[13] has developed a model to describe the evolution of the $0^{o}C$-isothermal layer. A general review of his work will be discussed here, the com-plete derivation is given in his report.

Pace's model equates the sensible heat extracted from the surrounding air to the latent heat absorbed by a flux of particles that melt as they fall into air warmer than $0^{o}C$. This analytical model is used to study the effects of variation in snow-fall rate, time, degree of saturation, and initial lapse rate on the depth of the iso-thermal layer. A numerical model derived from this analytical model is then used to examine the effects of variations in melting rate on the evolution of the melting layer.

Six simplifying assumptions are used: 1) Conditions in the cloud are horizon-tally homogeneous; 2) Snowfall rate is spatially and temporally constant; 3) Lapse rate below the original $0^{o}C$-level is initially linear; 4) The gas constant and speci-fic heat at constant pressure are equal to their dry air values; 5) Temperature and pressure do not vary in the vertical; and 6) All cooling affects the air within the

---

56. Fukuta, N. (1981) Private communication.

final depth of the isothermal layer. All of the above assumptions have only minor effects on the final numerical calculations, except for number six, which leads the model to predict deeper isothermal layers than would actually occur.

Fukuta[57] feels that an isothermal layer does not exist because the absorption of latent heat causes temperature variations below the $0^{o}C$-level. He also states that the existence of the melting phenomenon will not thermodynamically permit the existence of supercooled water in the melting layer, that is, the existence of nonmelting-related supercooled water. (The absence of supercooled water in the melting layer does not exclude aircraft icing since the ice and water will readily freeze to subzero parts of the aircraft that have been cold soaked.)

It is also clear that the proportion of ice and snow that melts at any temperature level depends on the temperature lapse rate, the ice-particle size distribution, ice-mass concentration, habits, and other factors. Pace (1980)[13] uses an empirical technique to take these factors into account as a first attempt at dealing with this complex problem. Professor Cotton at Colorado State University may be able to provide further insight into this area with his atmospheric model.[58]

Wexler (1955)[11] has used radar reflectivity to describe the amount of snow and ice that has melted. However, this is strictly an empirical technique which lacks adequate simultaneous in situ airborne measurements. Sweeney and Barnes (Appendix E) discuss Wexler's work.

10. DYNAMIC CONSIDERATIONS

Since the initial purpose of this melting layer study was to minimize the variability of important meteorological parameters, we are not at the present time concerned with melting layers within convective situations. Although, in those situations snow does appear in shafts, there is more cooling in some parts of the region than others, and there is turnover, turbulence, etc. The dynamic consider-ations will not be taken into account until much later. Future plans include the use of dual Doppler radar to investigate internal dynamics over a much broader area than that sampled at the same time by instrumented aircraft.

11. RECOMMENDATIONS

A comprehensive investigation of the melting layer is a valuable contribution to our knowledge of the structure and development of clouds and precipitation

57. Fukuta, N. (1981) Private communication.
58. Cotton, W.B. (1981) Private communication.

systems. Knowledge of the microphysical processes that occur in the melting layer will enable the Air Force to better predict icing conditions, and save money and lives by having aircraft avoid those conditions. By knowing where conditions of precipitation, temperature, and humidity (all of which can interfere with communication signals) occur, it will be possible to either avoid those areas or change the transmission characteristics in order to minimize interference. Both microwave and laser systems can benefit from that change. Rerouting of guided missiles to avoid areas of predicted icing or large liquid water content can also be accomplished. Since melting process can have a profound effect on both the structure of the cloud and its resultant surface precipitation pattern, the investigation of the melting layer should include aircraft, satellite, and ground-based observations.

11.1 Flight Program

Flight data aimed specifically at the melting layer are needed. We should compare temperature and dew-point to the visual and microphysical properties of the clouds. The following items should be examined:

a. Temperature: Firm upper and lower boundaries for the melting layer have never been established. By comparing the temperature observed by an aircraft with the types of particles present in the cloud at the same time, we can get an idea of the range of temperatures at which melting occurs.

b. Dew point: The dew point may have a greater effect on the melting layer than the temperature, since the ability of the atmosphere to transport heat varies with the amount of water vapor in a given sample of air. Again, the relation of the dew point to the melting layer is unknown. If necessary, another measure of moisture (for example, mixing ratio, relative or specific humidity, etc.) may be substituted for the dew point. (An instrument to measure water vapor even at supersaturation is being developed under contract for another branch work unit.)

c. Winds: Both vertical and horizontal air motion play a key role in the development of any storm system. Again, the effects of wind and wind shear on the size and extent of the melting layer are largely unknown.

d. Pressure altitude: This is necessary to measure the vertical extent of the melting layer, but it is also useful to compare the effects of altitude on the melting layer.

e. Turbulence: Turbulence is caused by changes in wind direction (in 3-D) and/or speed. Its frequency and severity often can tell us whether the clouds are convective in nature, as well as how rapidly the cloud structure is changing. Since turbulence is so important to the aviation industry, flight operations, and safety, it is, in itself, an important quantity.

23

f. Icing: Most icing will occur in the region above the melting layer, but since we have not fixed firm boundaries on either region, it would be helpful to study relations between these two regions.

g. Visibility: The visibility within and density of a cloud are of importance to both the aviator and the meteorologist. If we can determine any visual characteristics associated with the melting layer, this information would be most useful and would have applications to operations of some weapons systems.

h. Particle size distribution: The number and size of particles in a given sample of cloud tells much about its structure. We can learn much about such basic questions as to what physical processes occur in precipitation systems from a study of this information, which can be measured by state-of-the-art equipment.

i. Liquid water content: In addition to its usefulness as a measure of water in a cloud and potential precipitation intensity, this quantity can give insight into how much snow has melted. It can be deduced mathematically, and sometimes measured physically.

j. Particle shape and type: Good documentation of the shape of particles is essential to an understanding of the melting process.

k. Reflectivity: The ability of the droplets and crystals to reflect radar beams can help us define what radar is detecting. AFGL scientists have been developing relationships that enable us to compute reflectivity from microphysical data. We can then compare computed reflectivity with the reflectivity observed by radar.

l. Form factor: Plank (1971)[59] developed the form factor to help define a relationship between the mass of a particle and its radar reflectivity. The form factor measures the consistency of a sample of particles. If all of the particles in a given sample are about the same size, the form factor will approach 1, which is its maximum value. If there is a large variety of particle sizes, the form factor will approach zero (its minimum value). A consistently high-form factor, implies that a cloud is not changing rapidly, since most growth processes will produce a variety of particle sizes.

11.2 Radar Observations

The use of a ground-based sensor can complement the data gathered by an aircraft. We plan to use two Doppler radar systems to form a dual Doppler system over eastern Massachusetts. The use of these systems in conjunction with an aircraft will provide a better and more complete data set than any of the systems alone can provide.

59. Plank, V.G. (1977) Hydrometeor Data and Analytical-Theoretical Investigations Pertaining to SAMS Rain Erosion Program of the 1972-1973 Season at Wallops Island, Virginia, AFGL-TR-77-0149, Environmental Research Papers No. 603, AD A051 192, 239 pp.

The correlation of radar and aircraft observations will be necessary to fully explore the melting layer. An aircraft can give us a detailed look at a small portion of the atmosphere. Radar can not match the detail an aircraft can provide, but it can cover a much larger area. Combining the two can enable us to tell if what the aircraft instruments detect is representative of a larger area. It will also enable us to understand the data we get from the radars more completely.

The use of two Doppler radars (a dual Doppler system) will enable us to describe the horizontal wind fields. The Doppler radar can tell us whether an element of a cloud is moving toward or away from us and how fast. By using two such radars, we can pinpoint the motion of that cloud element. We plan to use the radar facilities of AFGL's Remote Ground Based Sensing Branch at Sudbury, Massachusetts and those of the Massachusetts Institute of Technology (MIT) at Cambridge, Massachusetts.

11.3 Flight Profile

The aircraft flight profile should concentrate on th. :elting layer itself. In recent years, we have used a descending spiral with a 15-degree bank and a 200-ft/minute rate of descent (previously referred to as an ASD or Passarelli spiral). This gives us a good vertical cross-section of whatever portion of the cloud on which we wish to concentrate. This spiral pattern will be useful in the melting layer program. It can be used in conjunction with level data passes to give a full cross-section of the melting layer.

Whenever feasible, sampling will be conducted in areas where coverage by both radars is possible. This will give us the full advantage of the unique sensing capabilities of the dual Doppler system.

References

1. Ryde, J. (1946) The attenuation of radar echoes produced at centimeter wave-lengths by various meteorological phenomena. Report of Conf. on Met. Factors in Radio Wave Propagation, London, Great Britain, pp. 169-189.

2. Mason, B. J. (1955) Radar evidence for aggregation and orientation of melting snowflakes, Quart. J. Royal Met. Soc. 81:262-264.

3. Ludlam, F. (1980) Clouds and Storms, The Pennsylvania State University Press, University Park, Pennsylvania.

4. Great Britain Meteorological Office (1965) Ice Accretion on Aircraft.

5. List, R., and Dussault, J. (1967) Quasi-steady-state icing and melting conditions and heat and mass transfer of spherical and spheroidal hailstones, J. Atm. Sci. 24:522-529.

6. Medzhitov, R. (1964) Cloud microstructure and icing of airplanes over Belorussia. Moscow Tsentralnyi Institut Prognozov, Trudy, 136:101-115.

7. Pruppacher, H., and Klett, J. (1980) Microphysics of Clouds and Precipitation, Reidel Publishing Co., Dordrecht, Holland, 705 pp.

8. List, R. (1980) An update on the status of the WMO precipitation enhancement project, Third WMO Scientific Conference on Weather Modification, Clermont-Ferrand, France, 21-25 July 1980, pp. 233-240.

9. Cooper, W.A. (1980) Estimation of rainfall using measurements from aircraft, Third WMO Scientific Conference on Weather Modification, Clermont-Ferrand, France, 21-25 July 1980, pp. 365-372.

10. Hallett, J. (1980) Some observations of supercooled water in cyclonic storms and implications from natural and artificial ice phase evolution, Third WMO Scientific Conference on Weather Modification, Clermont-Ferrand, France, 21-25 July 1980, pp. 471-476.

11. Wexler, R. (1955) The melting layer, Proc. First Conf. on Physics of Clouds and Precipitation Particles, pp. 306-314.

12. Air Weather Service 2-80 Geophysical Requirement (1980) Improved Cloud Data Handling and Analysis.

27

13. Pace, J. (1980) Microphysical and Thermodynamic Characteristics Through the Melting Layer, Report No. AS126, Dept. of Atmospheric Science, University of Wyoming, Laramie, Wyoming, 204 pp.

14. Findeisen, W. (1940) The formation of the $0^\circ C$-isothermal layer and fracto-cumulus under nimbostratus, Met. Zeit 57:49-54.

15. Byers, H.R., and Coome, R.D. (1947) The "Bright Line" in radar cloud echoes and its probable explanation, J. Meteor. 4(No.3):75-81.

16. Austin, P.M., and Bemis, A. (1950) A quantitative study of the bright band in radar precipitation echoes, J. Meteor. 7:165-171.

17. Browne, I.C., and Robinson, N. (1952) Cross-polarization of the radar melting band, Nature 170:1078-1079.

18. Imai, I., Fujiwara, M., Ichimura, I., and Toyama, Y. (1955) Radar reflectivity of falling snow, J. Met. Res. 7:422-425.

19. Lhermitte, R., and Atlas, D. (1963) Doppler fallspeed and particle growth in stratiform precipitation, Proc. Tenth Conf. on Radar Met., Washington, D.C., pp. 297-302.

20. Ramana Murty, B., Roy, A., and Biswas, K. (1965) Radar echo intensity below the bright band, J. Atm. Sci. 22:91-94.

21. Ekpenyong, B., and Srivastava, R. (1970) Radar Characteristics of the Melting Layer — A Theoretical Study, Univ. of Chicago Dept. of Geophys. Sciences and Ill. Inst. of Tech. Dept. of Elec. Eng., Technical Report No. 16, Lab. for Atm. Probing, Chicago, Illinois.

22. Atlas, D. (1964) Advances in radar meteorology, Adv. in Geophysics 10:318-478.

23. Battan, L.J. (1973) Radar Observation of the Atmosphere, University of Chicago Press, Chicago, Illinois, pp. 324-330.

24. Barge, B.L. (1974) Polarization measurements of precipitation backscatter in Alberta, J. Reck. Atmos. 8:163-173.

25. Hendry, A., and MacCormick, G.C. (1974) Polarization properties of precipitation particles related to storm structure, J. Rech. Atmos. 8:189-200.

26. Hendry, A., MacCormick, G.C., and Barge, B.L. (1976) K-band and S-band observation of the differential propagation constraint in snow, IEEE Trans. Antennas and Propagat. AP-24:521-525.

27. Battan, L.J. (1977) Rain resulting from melting ice particles, J. Appl. Met. 16:595-604.

28. Humphries, R.G., and Barge, B.L. (1979) Polarization and dual-wavelength radar observation of the bright band, IEEE Trans. Georie Ele . GE-17(No.4):190-195.

29. DuToit, P. (1967) Doppler radar observations of drop sizes in continuous rain, J. Appl Met. 6:1082-1087.

30. Ohtake, T. (1969) Observations of the size distribution of hydrometeors through the melting layer, J. Atm. Sci. 26:545-557.

31. Passarelli, R.E., Jr. (1978) An approximate analytical model of the vapor deposition and aggregation growth of snowflakes, J. Atm. Sci. 35:118-124.

32. Heymsfield, G.M. (1979) Doppler radar study of a warm frontal region, J. Atm. Sci. 36:2093-2107.

33. Marshall, J.S., and Gunn, K.L.S. (1952) Measurement of snow parameters by radar, J. Meteor. 9:332-337.

34. Mason, B.J. (1971) The Physics of Clouds, Clarendon Press, London, Great Britain, 671 pp.

35. Wexler, R., Reed, R.J., and Honig, J. (1954) Atmospheric cooling by melting snow, Bul. Amer. Meteor. Soc. 35:48-51.

36. Macklin, W. (1963) Heat transfer from hailstones, Quart. J. Royal Met. Soc. 89:360-363.

37. Atlas, D., Tatehira, R., Srivastava, R., Marker, W., and Carbone, R. (1969) Precipitation-induced mesoscale wind perturbations in the melting layer, Quart. J. Royal Met. Soc. 95:544-560.

38. Hooper, J., and Kippax, A. (1950) The bright band: a phenomenon associated with radar echoes from falling rain, Quart. J. Royal Met. Soc. 76:125-131.

39. Browne, I.C. (1952) Radar Studies of Clouds, Ph.D. Thesis, Cambridge University, England.

40. Rogers, R.R. (1979) A Short Course in Cloud Physics, Pergammon Press, New York, 227 pp.

41. Berthel, R.O. (1981) The Conversion of Aircraft Ice Crystal Measurements into Terms of Liquid Water Using Simulated Data, AFGL-TR-81-0173, AD A106 419, 46 pp.

42. Varley, D.J. (1978) Cirrus Particle Distribution Study, Part 1, Air Force Surveys in Geophysics No. 394, AFGL-TR-78-0305, AD A061 48S, 71 pp.

43. Varley, D.J. (1978) Cirrus Particle Distribution Study, Part 3, AFGL-TR-78-0305, AD A066 975.

44. Barnes, A.A., Jr. (1980) Observations of ice particles in clear air, Journal de Recherches Atmospherique 14(No. 3-4):311-315, AFGL-TR-81-0347, AD A108 914.

45. Cohen, I.D. (1981) Development of a Large Scale Cloud System, 23-27 March 1978, AFGL-TR-81-0127, AD A106 417, Environmental Research Papers 739, 112 pp.

46. Cohen, I.D. (1981) Cirrus Particle Distribution Study, Part 8, AFGL-TR-81-0316, Air Force Surveys in Geophysics 437, (in press).

47. Cohen, I.D. (1979) Cirrus Particle Distribution Study, Part 5, AFGL-TR-79-0155, AD A077 361.

48. Cohen, I.D., and Barnes, A.A. (1980) Cirrus Particle Distribution Study, Part 6, AFGL-TR-80-0261, AD A096 772.

49. Varley, D.J., and Brooks, D.M. (1978) Cirrus Particle Distribution Study, Part 2, AFGL-TR-78-0248, AD A063 807.

50. Varley, D.J., and Barnes, A.A. (1979) Cirrus Particle Distribution Study, Part 4, AFGL-TR-79-0134, AD A074 763.

51. Varley, D.J., Cohen, I.D., and Barnes, A.A. (1980) Cirrus Particle Distribution Study, Part 7, AFGL-TR-80-0324, AD A100 269.

52. Varley, D.J. (1980) Microphysical Properties of a Large Scale Cloud System 1-3 March 1978, AFGL-TR-80-0002, Environmental Research Papers 690, AD A083 140, 100 pp.

53. Barnes, A.A., Nelson, L.D., and Metcalf, J.J. (1974) Weather Documentation at Kwajalein Missile Range, Preprints of the 6th Conference on Aerospace and Aeronautical Meteorology, American Meteorological Society, pp. 66-69; also Air Force Surveys in Geophysics, No. 292, AFCRL, 12 September 1974, 14 pp. AFCRL-TR-74-0430, AD A000 925.

54. Stewart, R., and Marwitz, J. (1980) Cloud Physics Studies in SCPP during 1979-80, Report No. AS125, Dept. of Atmospheric Science, University of Wyoming, Laramie, Wyoming, 96 pp.

55. Hallett, J., and Mossop, S.C. (1974) Production of secondary ice particles during the riming process, Nature 249:26-28.

56. Fukuta, N. (1981) Private communication.

57. Fukuta, N. (1981) Private communication.

58. Cotton, W.B. (1981) Private communication.

59. Plank, V.G. (1977) Hydrometeor Data and Analytical-Theoretical Investigations Pertaining to SAMS Rain Erosion Program of the 1972-1973 Season at Wallops Island, Virginia, AFGL-TR-77-0149, Environmental Research Papers No. 603, AD A051 192, 239 pp.

Appendix A

Reference List and Evaluation

A1. RATING SCALE FOR MELTING LAYER REFERENCES

Ratings (indicated by the numbers in parentheses at the end of each reference) are based on the relevance of information to this study according to the following scale:

1. VERY RELEVANT — contains much relevant information
2. SOMEWHAT RELEVANT — some valuable information in segments
3. POSSIBLY RELEVANT — a few references that may be useful
4. NOT VERY RELEVANT — only remotely applicable
5. NOT RELEVANT AT ALL — not applicable

A2. REFERENCE LIST

A1. Aden, A. (1951) Electromagnetic scattering from spheres with sizes comparable to the wavelength, J. Appl. Phys. 22:601-605. (1)

A2. Affronti, F., and Ciattaglia, L. (1970) Detection of the bright band layer with the Meteor-50 radar, Rivista di Meteorologia Aeronautica, Rome 30:(No. 4):47-53. (1)

A3. Atlas, D., Kerker, M., and Hitschfeld, W. (1953) Scattering and attenuation by non-spherical atmospheric particles, J. Atm. and Terr. Phys. 3:108-119. (2)

31

A4. Atlas, D., Tatehira, R., Srivastava, R., Marker, W., and Carbone, R. (1969) Precipitation-induced mesoscale wind perturbations in the melting layer, Quart. J. Royal Met. Soc. 95:544-560. (1)

A5. Austin, P.M., and Bemis, A. (1950) A quantitative study of the bright band in radar precipitation echoes, J. Met. 7:165-171. (1)

A6. Bailey, J., and Macklin, W. (1968) Heat transfer from artificial hailstones, Quart. J. Royal Met. Soc. 94:93-98. (3)

A7. Battan, L. (1977) Rain resulting from melting ice particles, J. Appl. Met. 16:595-604. (3)

A8. Battan, L., and Theiss, J. (1976) Rain resulting from melting snow, Proc. Int. Conf. on Cloud Physics, Boulder, Colorado, pp. 567-571. (2)

A9. Battan, L, Theiss, J., and Kassander, A., Jr. (1964) Some Doppler radar observations of a decaying thunderstorm, Proc. Eleventh Weather Radar Conf. Boston, Massachusetts, pp. 362-365. (3)

A10. Bigg, E.K. (1953) The formation of atmospheric ice crystals by the freezing of droplets, Quart. J. Royal Met. Soc. 79:510-519. (2)

A11. Biswas, K., Ramana Murty, Bh.V., and Roy, A. (1960) Freezing rain at Delhi and associated melting band characteristics, Indian Journal of Meteorology and Geophysics, Spec. No. 13, (Symposium on Physics of Clouds and Rain in the Tropics) pp. 137-142. (1)

A12. Blanchard, D.C. (1957) The supercooling, freezing and melting of giant waterdrops at terminal velocity in air, Proc. Conf. on Physics of Cloud and Precip. Particles, Pergammon Press, New York, pp. 233-249. (3)

A13. Browne, I.C. (1952) Radar studies of clouds, Ph.D. Thesis, Cambridge University, England. (2)

A14. Browne, I.C., and Robinson, N. (1952) Cross-polarization of the radar melting band, Nature 170:1078-1079. (2)

A15. Byers, H., and Coons, R. (1947) The 'bright line' in radar cloud echoes and its probable explanation, J. Met. 4:75-81. (2)

A16. Cheng, R. (1978) Ice pellet melting — ejection of microdroplets, Bull. of the Amer. Met. Soc. 59:512-513. (4)

A17. Cunningham, R. (1947) A different explanation of the bright-line, J. Met. 4:163. (1)

A18. Doviak, R., and Weil, C. (1972) Bistatic radar detection of the melting layer, J. Appl. Met. 11:1012-1016. (4)

A19. Drake, J., and Mason, B.J. (1966) The melting of small ice spheres and cones, Quart. J. Royal Met. Soc. 92:500-509. (2)

A20. DuToit, P. (1967) Doppler radar observations of drop sizes in continuous rain, J. Appl. Met. 6:1082-1087. (2)

A21. Dyer, R. (1968) Doppler measurements in stratiform rain, Proc. Thirteenth Radar Met. Conf., Montreal, Quebec, pp. 144-147. (3)

A22. Dyer, R. (1970) Particle fall speeds within the melting layer. Proc. 14th Radar Met. Conf., Tucson, Arizona, pp. 157-160. (2)

A23. Dyer, R., Berthel, R., and Izumi, Y. (1981) Techniques for Measuring Liquid Water Content Along a Trajectory, AFGL-TR-81-0082, AD A102 922. (3)

A24. Ekpenyong, B., and Srivastava, R. (1970) Radar Characteristics of the Melting Layer — A Theoretical Study, Univ. of Chicago Dept. of Geophys. Sciences and Ill. Inst. of Tech. Dept. of Elec. Eng., Technical Report No. 16, Lab. for Adm. Probing, Chicago, Illinois. (1)

32

A25. Fernald, F., and Dennis, A. (1964) Measurement of Forward-heater Cross-sections in the Melting Layer, NASA-CR-57468:178-181. (1)

A26. Fleagle, R.J., and Businger, J.A. (1963) An Introduction to Atmospheric Physics, Academic Press, New York. (2)

A27. Fletcher, N.H. (1962) The Physics of Rainclouds, Cambridge University Press, England. (2)

A28. Fukuta, N. (1969) Experimental studies on the growth of small ice crystals, J. Atm. Sci. 26:522-531. (3)

A29. Fukuta, N., and Walter, L. (1970) Kinetics of hydrometeor growth from a vapor-spherical model, J. Atm. Sci. 27:1160-1172. (3)

A30. Fukuta, N. (1973) Thermodynamics of cloud glaciation, J. Atm. Sci. 30:1645-1649. (2)

A31. Fukuta, N., Neubauer, L., and Erickson, D. (1979) Final Report to NSF under Grant No. ENV 77-15346. (5)

A32. Fukuta, N., Guo, W., and Guo, T. (1974) Kinetics of hydrometeor growth-spheroidal model, Conf. on Cloud Physics, Tucson, Arizona, pp. 67-70. (4)

A33. Fukuta, N., Paik, Y., Saxena, W., Armstrong, J., Gorove, A., Guo, T., and Guo, W. (1973) Final Report to NSF under Grant No. GA-29525. (5)

A34. George, J.J. (1960) Weather Forecasting for Aeronautics, Academic Press, New York, pp. 410-415. (1)

A35. Great Britain Meteorological Office (1965) Ice Accretion on Aircraft. (2)

A36. Gunn, R., and Kinzer, G. (1949) The terminal velocity of fall for water droplets in stagnant air, J. Meteor. 6:243-248. (1)

A37. Gunn, K., and Marshall, J. (1958) The distribution with size of aggregate snowflakes, J. Meteor. 15:452-461. (1)

A38. Gupta, B., Mani, A., and Ventikeshwaran, S. (1961) Some observations of melting band in radar echoes at Poona, Indian J. Met. and Geophys. 12:317-322. (2)

A39. Gvelesviani, A., and Kartsivadze, A. (1968) On the melting of spherical hailstones, Proc. Int. Conf. on Cloud Physics, Toronto, Ontario. pp. 422-425. (3)

A40. Harrold, T., and Browning, K. (1967) Meso-scale wind fluctuations below 1500 metres, Meteorology Magazine 96:367-379. (3)

A41. Heymsfield, G. (1979) Doppler radar study of a warm frontal region, J. Atm. Sci. 36:2093-2107. (4)

A42. Hobbs, P.V. (1973) Ice in the atmosphere: a review of the present position, Physics and Chemistry of Ice, Royal Society of Canada, Ottawa, pp. 308-319. (1)

A43. Hoffer, T., and Mallen, S. (1968) A vertical wind tunnel for small droplet studies, J. Appl. Met. 7:290-292. (5)

A44. Hogg. D., Guiraud, F., and Burton, E. (1980) Simultaneous observations of cool cloud liquid by ground-based microwave radiometry and icing of aircraft, J. Appl. Met. 19:893-895. (2)

A45. Hooper, J., and Kippax, A. (1950) The bright band: a phenomenon associated with radar echoes from falling rain, Quart. J. Royal Met. Soc. 76:125-131. (1)

A46. Houze, R., Jr., Locatelli, J., and Hobbs, P. (1976) Dynamics and cloud microphysics of the rainbands in an occluded frontal system, J. Atm. Sci. 33:1921-1936. (2)

A47. Imai, I., Fujiwara, M., Ichimura, I. and Toyama, V. (1955) Radar reflectivity of falling snow, J. Met. Res., Tokyo 7:422-425. (1)

A48. Johnson, D. (1981) Analytical solution for cloud drop concentration, J. Atm. Sci. 38:215-218. (5)

A49. Kerker, M., Langleben, P., and Gunn, K. (1951) Scattering of microwaves by a melting spherical ice particle, J. Meteor. 8:424. (2)

A50. Knight, C.A. (1979) Observations of the morphology of melting snow, J. Atm. Sci. 36:1123-1130. (1)

A51. Kramers, H. (1946) Heat transfer from spheres to flowing media, Physica 12:61-80. (2)

A52. Labrum, N. (1952) The scattering of radio waves by meteorological particles, J. Appl. Phys. 23:1324-1330. (2)

A53. Lagourette, B. (1976) Study of dielectric properties of disperse microcrystals of ice near melting temperature, J. De Physique. 37:945-954. (3)

A54. Langleben, M. (1954) The terminal velocity of snowflakes, Quart. J. Royal Met. Soc. 80:174-181. (1)

A55. Lhermitte, R., and Atlas, D. (1963) Doppler fallspeed and particle growth in stratiform precipitation, Proc. Tenth Conf. on Radar Met., Washington, D.C. pp. 297-302. (1)

A56. List, R. (1963) General heat and mass exchange of spherical hailstones, J. Atm. Sci. 20:189-197. (3)

A57. List, R., and Dussault, J. (1967) Quasi-steady-state icing and melting conditions and heat and mass transfer of spherical and spheroidal hailstones, J. Atm. Sci. 24:522-529. (2)

A58. List, R., and Parsons, D. (1968) Simulation of the total heat transfer of spherical hailstones, Helvetica Physica Acta 41:1016-1020. (3)

A59. List, R., and Schemenauer, R. (1971) Free fall behavior of planar snow crystals, conical graupel and small hail, J. Atm. Sci. 28:110-115. (2)

A60. Lo, K., and Passarelli, R. (1981) A new sampling technique for quantitative airborne studies of snow growth: theory and examples, J. Atm. Sci. (in press). (1)

A61. Locatelli, J., and Hobbs, P. (1974) Fall speeds and masses of solid precipitation particles, J. Geophys. Res. 19:2185-2197. (1)

A62. Low, R.D. (1980) One-dimensional Cloud Microphysical Models for Central Europe and Their Optical Properties, OSD 1366, Atmospheric Sciences Laboratory, White Sands Missile Range, New Mexico. (2)

A63. Ludlam, F.H. (1958) The hail problem, Nubila 1:11-96. (3)

A64. Ludlam, F. (1980) Clouds and Storms, The Pennsylvania State University Press, University Park, Pennsylvania, 488 pp. (2)

A65. Macklin, W. (1963) Heat transfer from hailstones, Quart. J. Royal Met. Soc. 89:360-363. (3)

A66. Macklin, W. (1964) Factors affecting the heat transfer from hailstones, Quart. J. Royal Met. Soc. 90:84-90. (3)

A67. Magono, C. (1953) On the growth of snowflake and graupel, Science Reports of Yokohama University 3:33-40. (1)

A68. Magono, C., and Nakamura, T. (1965) Aerodynamic studies of falling snowflakes, J. Met. Soc. Japan 43:139-147. (1)

34

A69. Marier, D. (1967) The Sleet Bright Band, Report No. WBTM-ER-26, Weather Bureau Eastern Region Headquarters, Garden City, New York. (2)

A70. Mason, B.J. (1955) Radar evidence for aggregation and orientation of melting snowflakes, Quart. J. Royal Met. Soc. 81:262-264. (1)

A71. Maso , B.J. (1971) The Physics of Clouds, Clarendon Press, London, England. (2)

A72. Matsou, T., and Sasyo, Y. (1981) Empirical formula for the melting rate of snowflakes, J. Met. Soc. Japan 59:1-9. (1)

A73. Matsou, T. (1981) Melting of snowflakes below freezing level in the atmosphere, J. Met. Soc. Japan 59:10-25. (1)

A74. Matsou, T. (1981) Non-melting of snowflakes observed in subsaturated air below freezing level, J. Met. Soc. Japan 59:26-32. (1)

A75. McCormick, K. (1970) Reflectivity and attenuation observations of hail and the radar bright band, Proc. 14th Radar Met. Conf., Tucson, Arizona pp. 19-24. (2)

A76. Medzhitov, K. (1964) Cloud microstructure and icing of airplanes over Belorussia, Moscow Tsentralnyi Institut Prognozov, Trudy 136:101-115. (2)

A77. Ohtake, T. (1965) Preliminary observations of size distribution of snowflakes at just above and below the melting layer, Proc. Int. Conf. on Cloud Physics, Tokyo, Japan, pp. 271-275. (1)

A78. Ohtake, T. (1969) Observations of the size distribution of hydrometeors through the melting layer, J. Atm. Sci. 26:545-557. (1)

A79. Pace, J. (1980) Microphysical and Thermodynamic Characteristics through the Melting Layer, Report No. AS126, Dept. of Atmospheric Science, University of Wyoming, Laramie, Wyoming. (1)

A80. Pace, J., and Stewart, R. (1980) The effect of melting particles on the thermodynamic and microphysical characteristics of Sierra Nevada winter storms, VIII Int. Conf. on Cloud Physics, Clermont-Ferrand, France, pp. 563-564. (1)

A81. Passarelli, R. (1976) Coordinated Doppler radar and aircraft observations of riming growth and drop breakup in stratiform precipitation, Proc. Int. Conf. on Cloud Physics, Boulder, Colorado, pp. 500-505. (2)

A82. Passarelli, R. (1978) Theoretical and observational study of snow-size spectra and snowflake aggregation efficiencies, J. Atm. Sci. 35:882-889. (1)

A83. Pruppacher, H., and Klett, J. (1980) Microphysics of Clouds and Precipitation, Reidel Publishing Co., Dordrecht, Holland. (1)

A84. Pruppacher, H., and Neiburger, M. (1968) Design and performance of the UCLA wind tunnel, Proc. Int. Conf. on Cloud Physics, Toronto, Ontario, pp. 389-392. (5)

A85. Ramana Murty, B., Roy, A., and Biswas, K. (1965) Radar echo intensity below the bright band, J. Atm. Sci. 22:91-94. (1)

A86. Richter, J., and Hitney, H. (1980) The effects of atmospheric refractivity on microwave propagation, Atmospheric Water Vapor, Academic Press, New York, New York. (5)

A87. Rogers, R.R. (1976) A Short Course in Cloud Physics, Pergammon Press, New York, New York. (2)

35

A8£. Ryde, J. (1946) The attenuation of radar echoes produced at centimetre wavelengths by various meteorological phenomena, Report of Conf. on Met. Factors in Radio Wave Propagation, London, England pp. 169-189. (1)

A89. Sassen, K. (1975) Laser depolarization 'bright band' from melting snowflakes, Nature 255:316-318. (2)

A90. Sassen, K. (1976) Polarization diversity lidar returns from virga and precipitation: anomalies and the bright band analogy, J. Appl. Met. 15:292-300. (3)

A91. Sekhon, R., and Srivastava, R. (1970) Snow size spectra and radar reflectivity, J. Atm. Sci. 27:299-307. (1)

A92. Stewart, R., and Marwitz, J. (1980) Cloud Physics Studies in SCPP During 1979-80, Report No. AS125, Dept. of Atmospheric Science, University of Wyoming, Laramie, Wyoming. (1)

A93. Takeda, T., and Fujiyoshi, Y. (1978) Microphysical processes around melting layer in precipitating clouds as observed by vertical pointing radar, J. Met. Soc. Japan 56:293-303. (1)

A94. Vonnegut, B., and Moore, C. (1960) Visual analogue of radar bright band phenomenon, Weather 15:272-279. (3)

A95. Weiss, R., Locatelli, J., and Hobbs, P. (1977) Deduction of ice particle types in the vicinity of the melting layer from Doppler radar measurements, J. Appl. Met. 16:314-316. (1)

A96. Wexler, R. (1955a) An evaluation of the physical effects in the melting layer, Proc. Fifth Weather Radar Conf. Ft. Monmouth, New Jersey pp. 329-334. (1)

A97. Wexler, R. (1955b) The melting layer, Proc. First Conf. on Physics of Clouds and Precipitation Particles pp. 306-314. (1)

A98. Wexler, R., and Atlas, D. (1956) Factors influencing radar-echo intensities in the melting layer, Quart. J. Royal Met. Soc. 82:349-351. (1)

A99. Wexler, R., and Atlas, D. (1958) Moisture supply and growth of stratiform precipitation, J. Meteor. 15:531. (2)

A100. Wexler, R., Reed, J.R., and Honig, J. (1954) Atmospheric cooling by melting snow, Bulletin of the Amer. Meteor. Soc. 35:48-51. (2)

A101. Yokoyama, T., and Tanaka, H. (1980) Effects of coalescence in a melting layer in two-wavelength microwave backscattering, VIII Int. Conf. on Cloud Physics, Clermont-Ferrand, France pp. 235-237. (1)

A102. Zikmunda, J., and Vali, G. (1972) Fall patterns and fall velocities of rimed ice crystals, J. Atm. Sci. 29:1334-1347. (2)

A103. Zwack, P., and Anderson, C. (1970) Showers and continuous precipitation, Proc. 14th Radar Meteorology Conf., Tucson, Arizona pp. 335-338. (2)

Appendix B

An Investigation into the Nature of the
Melting Layer in Stratiform Clouds

Dr. Steven B. Newman
Physics-Earth Sciences Department
Central Connecticut State College

Abstract

Research into the nature of the melting layer in mixed stratiform clouds has
been conducted in the Cloud Physics Branch of the Air Force Geophysics Laboratory
(AFGL). An extensive reference list has been compiled, covering some 35 years
of published work concerning the melting layer and the radar bright band.

In addition, the problem of defining the boundaries of the melting layer have
been examined. It is postulated that the 0°C dry-bulb isotherm may not always be
the best threshold level for the top of the melting layer. Instead, the 0°C wet-bulb
level is examined, and a relationship between airmass stability and the height dif-
ference between these two levels is developed. The lower boundary of the melting
layer remains undefined, primarily due to lack of a concrete definition of the "end"
of melting.

A simple model of snowflake aggregation and breakup has been developed. It
is shown that at reasonable cloud ice contents, the aggregation and breakup of snow-
flakes just above the melting layer results in considerable ice multiplication, as
well as growth. The increase in both size and number concentration of snowflakes
entering the melting layer may play a considerable role in enhancing the radar
echo intensity in the melting layer resulting in the radar bright band.

37

B1. INTRODUCTION

The Air Force Geophysics Laboratory (AFGL) is the Air Force center for research in the environmental sciences. AFGL interacts with a family of 12 other research and development laboratories in the Air Force Systems Command (AFSC) to identify emerging research and technology needs and integrate scientific advances into Air Force technology.

The Meteorology Division of AFGL satisfies several requirements of operational commands by bringing together pertinent technologies to solve specific problems. Within the division, the Cloud Physics Branch is heavily involved in research in the area of melting layer processes and also in an aircraft icing program for improving forecasting of atmospheric icing conditions for both design and operational use by the Air Force.

B2. OBJECTIVES

The main objective of this research was to investigate some of the cloud microphysical processes associated with the melting layer in stratiform clouds. We have attempted to extend previously derived models of snowflake aggregation and melting and to investigate the interaction with the ambient atmosphere.

This research has not attempted to completely model the melting layer, but rather to provide a "first look" at some of the processes occurring within it. As such, it is limited to static or simplified dynamic models.

Compilation of an extensive melting layer reference list was also a major objective of this research, as was a first attempt to accurately define the upper and lower limits of the melting layer.

It should be noted that this research is only in its early stages, thus any conclusions that are drawn here must be regarded as purely preliminary in nature, and will doubtless need further study.

B3. LITERATURE SEARCH

Using a list of over 60 references already compiled by Ms. Walsh and Capt. Gibbons of the Cloud Physics Branch, the author completed an exhaustive search of the existing literature on the radar bright band and the melting layer. The excellent facilities of the AFGL Research Library, and the cross-referencing from citations as they were found and abstracted were used to prepare a list of approximately 90 books, papers, and monographs. This is probably the most extensive

38

reference list pertaining to the bright band and the melting layer ever compiled. It represents the sum total of what is presently known about the nature of these phenomena. The entire reference is reproduced here in Appendix A.[*] The author would appreciate hearing from anyone who might know of other references that are not included in this list.

B4. DEFINING THE MELTING LAYER

The definition of the melting layer has presented one of the major problems encountered thus far; although on the surface, such a definition would appear to be quite straightforward. Logically, one would choose, a priori, the 0°C dry-bulb isotherm as the upper boundary of the melting layer. Indeed, all the previous research we have seen does define the top of the melting layer in just this way. However, a possibility exists that melting may not actually begin when frozen precipitation particles fall past the 0°C dry-bulb level in clouds.

In most clouds, a relative humidity of 100 percent is not always maintained. In fact, many clouds have relative humidities that are *less than 100 percent*. In such cases, the wet-bulb and dry-bulb temperatures will not be equal at any given height, and the 0°C wet-bulb isotherm will be located somewhat below (in terms of height) the 0°C dry-bulb isotherm.

The Glossary of Meteorology defines the wet-bulb temperature thus:

WET-BULB TEMPERATURE — The temperature that an air parcel would have if cooled adiabatically to saturation at constant pressure by evaporation of water into it, all latent heat supplied by the parcel.

— Glossary of Meteorology

This is significant in that melting of snowflakes will not begin until the wet-bulb temperature rises above 0°C. This is because the snowflake or ice crystal behaves as a wet bulb, thus the air immediately surrounding the flake or crystal will be cooled, by evaporation, to the wet-bulb temperature.

Previous research (Austin and Bemis, 1950;[B1] Hooper and Kippax, 1950;[B2] Browne, 1952;[B3] Mason, 1955;[B4] Gupta, et al, 1961[B5]) indicates that the radar bright band is always found at some distance below the 0°C dry-bulb isotherm (Figure B1). The actual distance is found to be quite variable. Hooper and Kippax (1950)[B2] reported a gap of 330 ± 150 ft between the 0°C-isotherm and the radar bright band; while Gupta, et al, (1961)[B5] reported a gap of approximately 4700 ft.

Present research indicates that, for situations where the 0°C dry-bulb isotherm is located above ground level, the distance between the 0°C dry-bulb isotherm and the 0°C wet-bulb isotherm is directly related to the stability of the air

---

[*]This reference list in its latest revised form appears as Appendix A of this report.

Because of the large number of references cited above, they will not be listed here. See References, page 50.
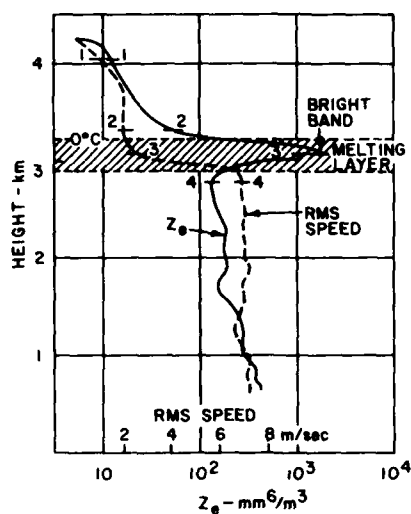
Figure B1. Profile of Radar Reflectivity
vs Height. Note that maximum radar re-
flectivity is found below the 0°-isotherm
(after Lhermitte and Atlas, 1963 [B6])

mass. Using the K-Index (George, 1960 [B7]) as a measurement of stability, we
have found a good relationship between this index and the distance between the 0°C
dry-bulb, and 0°C wet-bulb isotherms. These results are summarized in Fig-
ure B2. Note that high values of K (greater than 30) are indicative of strong air-
mass instability, with the likelihood of thunderstorms high. Values of K lower
than approximately 15 indicate very stable air. The solid line on the figure is the
best-fit curve to the data, and would call for a 1300-m difference for a K-Index of
0, and a 100-m difference for a K-Index of 40.

In a cloud with relative humidity near 100 percent, the gap between the 0°C wet-
bulb isotherm and the 0°C dry-bulb isotherm is on the order of 100 to 150 m. This
is within the range of values reported in the above mentioned literature. It is pos-
sible, then, that the top of the radar bright band may correspond well with the 0°C
wet-bulb isotherm, where melting has progressed to the point of providing a liquid
coating to the snowflakes. In fact, it is also possible that in the shallow layer

B6. Lhermitte, R., and Atlas, D. (1963) Doppler fallspeed and particle growth in
stratiform precipitation, Proc. Tenth Conf. on Radar Meteorology, Washington,
D.C. pp. 297-302.

B7. George, J.J. (1960) Weather Forecasting for Aeronautics, Academic Press,
New York, pp. 410-415.
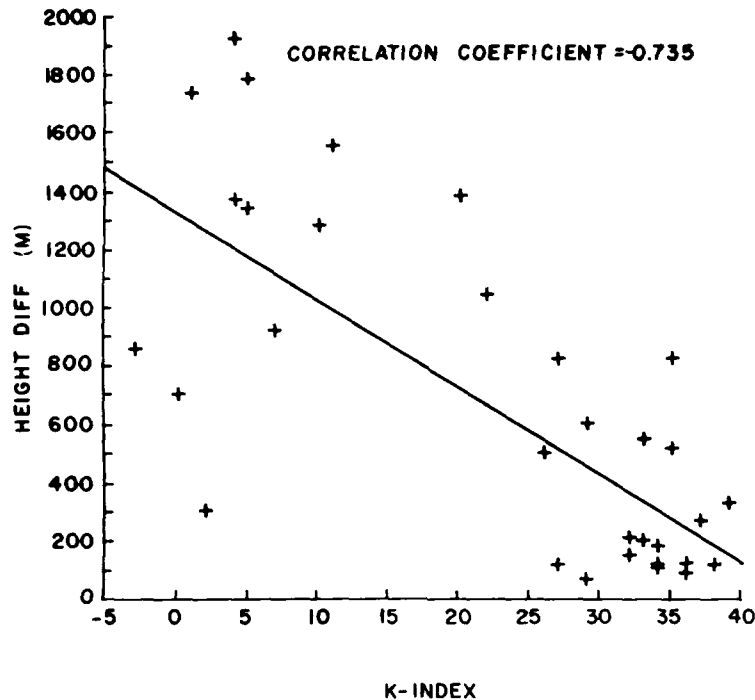
Figure B2. K-Index vs Height Difference Between 0°C Dry-bulb Isotherm and 0°C Wet-bulb Isotherm. Solid line represents best fit to date

between the 0°C dry-bulb and the 0°C wet-bulb levels, any water droplets present in the cloud may remain supercooled, even if the ambient temperature is slightly higher than 0°C.

Defining the top of the melting layer also presents a problem because it is not a constant height surface. As snowflakes begin melting, they take up latent heat from the surrounding atmosphere. The resultant cooling will cause the top of the melting layer to lower, locally, in altitude (Figure B3). This lowering will be non-uniform due to nonuniform melting rates and nonuniform precipitation areas in the cloud. In some cases, the effect can be expected to be highly localized, producing convective overturn in those areas where the local lapse rate becomes superadiabatic. Such overturn incidents could result in downbursts of cold air, or momentary occurrences of heavy precipitation at the ground.

Defining the bottom of the melting layer also presents some problems which, at the present time, have not been resolved. The radar bright band is rarely more than a few hundred meters thick, yet the melting layer is known to extend well below the lower boundary of the bright band.

41
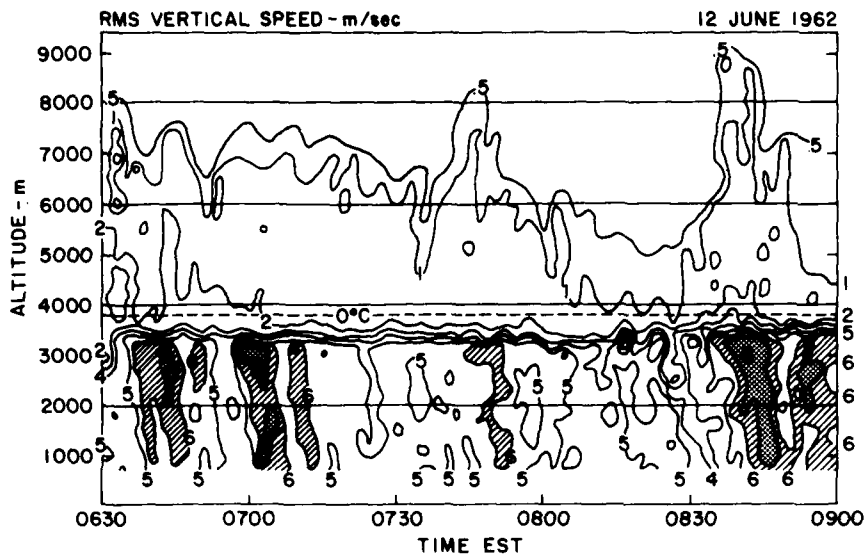
Figure B3. Time vs Height Profile of Radar Reflectivity. The bright band is easily seen. Note changes in the level of the bright band with time (after Lhermitte and Atlas, 1963 [B6])

If we define the bottom of the melting layer as the level at which there is no more frozen precipitation, then we may be setting a boundary that is too low in altitude. *Snowflakes are rarely observed* at temperatures above +4°C.[B8] A more logical method would be to establish a threshold level below which a given percentage of snowflakes and ice crystals will have completely melted. Although this is probably somewhere between +3°C and +5°C for total melting of 90 percent of the snowflakes,[B9] the +5°C-level has been the most widely used threshold temperature for the bottom of the melting layer. The reasons for this choice appear to be entirely arbitrary, without any supporting data.

Unfortunately, we do not have sufficient flight data with which to attempt any such definition ourselves. Only one or two flights actually penetrated the melting layer, and these were specifically studying icing processes just above the melting layer. More flights specifically aimed at studying the melting layer need to be made in order to obtain enough reliable data to accurately define melting layer boundaries, both upper and lower.

___

B8. Glass, M. (1981) Private communication.

B9. Cohen, I.D. (1981) Private communication.

B5. A SNOWFLAKE AGGREGATION MODEL

Lhermitte and Atlas (1963),[B6] as well as Mason (1955)[B4] have suggested that a possible explanation for the enhancement of the radar echo intensity in the melting layer is aggregation of snowflakes with ice crystals just above the 0°C-isotherm. Lo and Passarelli (1981)[B10] have found evidence of aggregation at temperatures much lower than had previously been thought possible. Observations by Hobbs (1973)[B11] indicate that, while very large aggregates may be found at ground level when temperatures are near 0°C, in clouds, aggregates of maximum dimension greater than 5 mm are uncommon. However, observations made during AFGL flights indicate that in the region between -3°C and 0°C, aggregates larger than 5 mm do exist. The model presented herein does not allow for such larger aggregates; however, further refinement will take these observations into account.

Using the aggregational growth equation given by Rogers (1979),[B12] a simple aggregation model has been developed. The equation for growth of a snowflake by aggregation is,

$$dm/dt = EM \pi R^2 \Delta u ,$$ (B1)

where E is the mean collection efficiency of the snowflake, R the snowflake radius, Δu the difference in fallspeed between the snowflakes and the icecrystals, and M is the cloud ice content, which can be related to the ice crystal number density, N, by

$$M = Nv \rho ,$$ (B2)

where v is the average ice crystal volume and ρ the average ice crystal density.

The cloud ice content differs from the cloud liquid water content in that no supercooled droplets are counted in deriving the value of M. Thus, use of M in the model means that any growth by diffusion or accretion is effectively ignored. Only growth by aggregation is considered.

B10. Lo, K., and Passarelli, R., Jr. (1981) A new sampling technique for quantitative airborne studies of snow growth: theory and examples, J. Atmos. Sci. (in press).

B11. Hobbs, P.V. (1973) Ice in the atmosphere: a review of the present position, in Physics and Chemistry of Ice, Whalley, Jones, and Gold, Ed., Royal Society of Canada, Ottawa, Canada, pp. 308-319.

B12. Rogers, R.R. (1979) A Short Course in Cloud Physics, Pergamon Press, New York.

Mason (1971)[B13] relates the diameter, D, of a stellar dendritic snowflake to its mass, m, by

$$m = 0.027 \ D^2 \quad . \tag{B3}$$

And, substituting into Eq. (B1) gives

$$1/R \ dR/dt = 4.63 \ EM \ \pi \Delta u \quad . \tag{B4}$$

Integration of Eq. (B4) from $R = R_0$ to $R = R_f$, and from $t = 0$ to $t = t_f$ yields,

$$R_f = R_0 \exp (4.63 \ EM \ \pi \Delta ut) \quad . \tag{B5}$$

In obtaining solutions for this expression, a number of simplifying assumptions have been made:

1. All snowflakes fall at a constant speed of 1 m/sec; while all ice crystals fall at a constant speed of 0.5 m/sec. These are valid assumptions, according to Magono (1953),[B14] and Rogers (1979),[B12] respectively; however, Passarelli (1978)[B15] has shown that the fallspeed of aggregating dendritic flakes is related to the diameter of the dendrite.

2. The lapse rate of temperature is constant during the model run.

3. Aggregates have a maximum dimension of 5 mm. Upon growing larger than this size they spontaneously break up into smaller particles. The model then resumes aggregational growth with a new 1-mm diameter snowflake, until it falls to the 0°C-level. If the particle again reaches 5 mm before reaching the 0°C-level, it breaks up once again, resulting in the same recycling process.

4. The snowflakes aggregate in the layer from -10°C to 0°C. Layer thickness depends on the lapse rate.

We examine the case of a snowflake with initial maximum dimension of 1 mm falling through the layer with constant lapse rates of -4°C/km, -5°C/km and -6°C/km. Solution of Eq. (B5) for 10-s intervals of growth are shown in Figures B4 through B6. Cloud ice contents are 1.0 and 1.5 g/m^3, respectively, for each lapse rate.


B13. Mason, B.J. (1971) The Physics of Clouds, Clarendon Press, London, England.

B14. Magono, C. (1953) On the growth of snowflake and graupel, Science Reports of Yokohama National University, Sect. I, (No. 3), pp. 33-40.

B15. Passarelli, R., Jr. (1978) Theoretical and observational study of snow-size spectra and snowflake aggregation efficiencies, J. Atmos. Sci. 35:882-889.
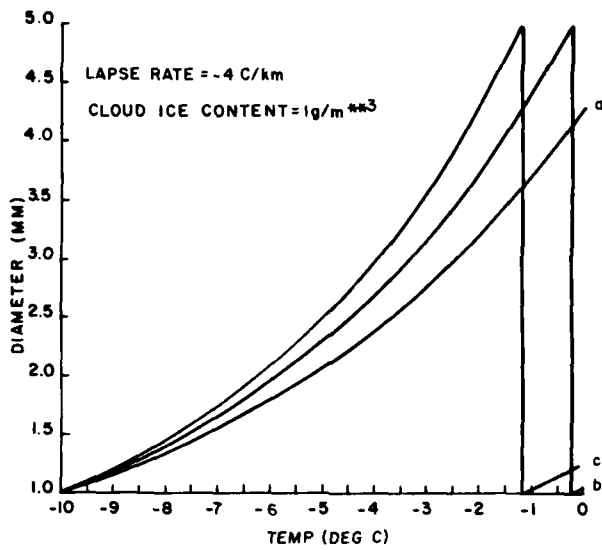
(a) Cloud Ice Content is 1.0 g/mm^3
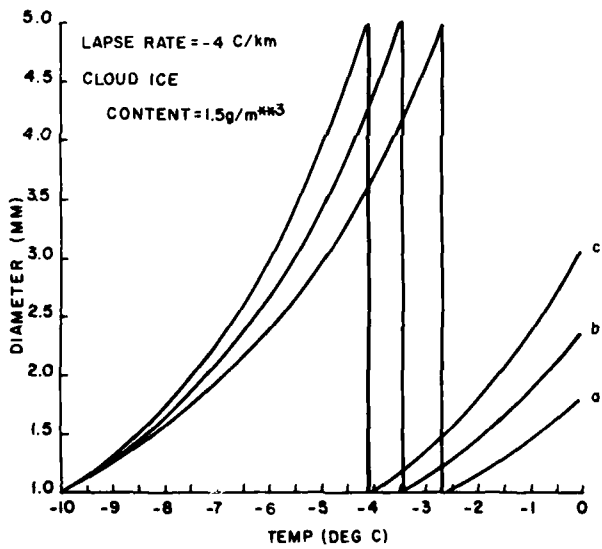
(b) Cloud Ice Content is 1.5 g/mm^3

Figure B4. Aggregational Growth and Breakup of a 1.0 mm-diameter Snowflake Falling Through the Layer from -10°C to 0°C. Lapse rate is constant at -4°C/km. Curves are for mean collection efficiencies of a) 0.8, b) 0.9, and c) 1.0

45
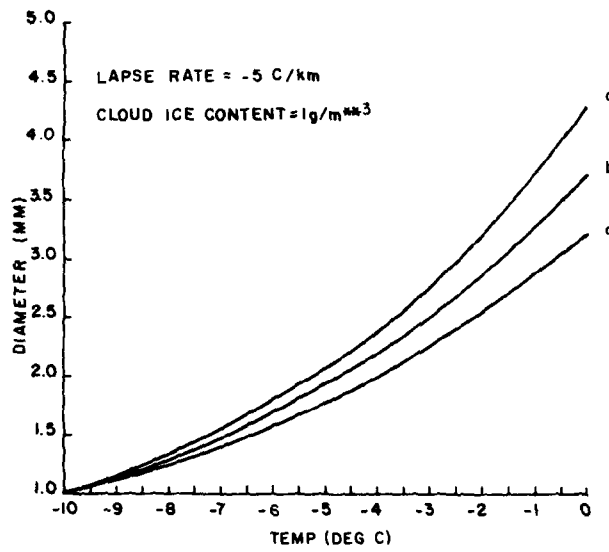
(a) Cloud Ice Content is 1.0 g/mm^3
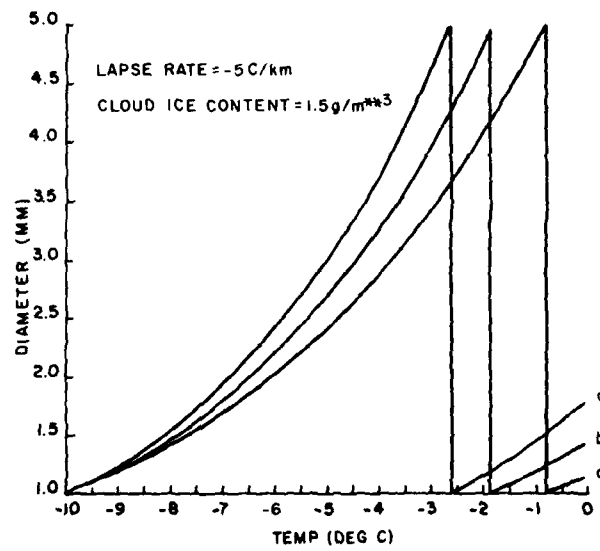
(b) Cloud Ice Content is 1.5 g/mm^3

Figure B5. Aggregational Growth and Breakup of a 1.0 mm-diameter Snowflake Falling Through the Layer from -10°C to 0°C. Lapse rate is constant at -5°C/km. Curves are for mean collection efficiencies of a) 0.8, b) 0.9, and c) 1.0

46
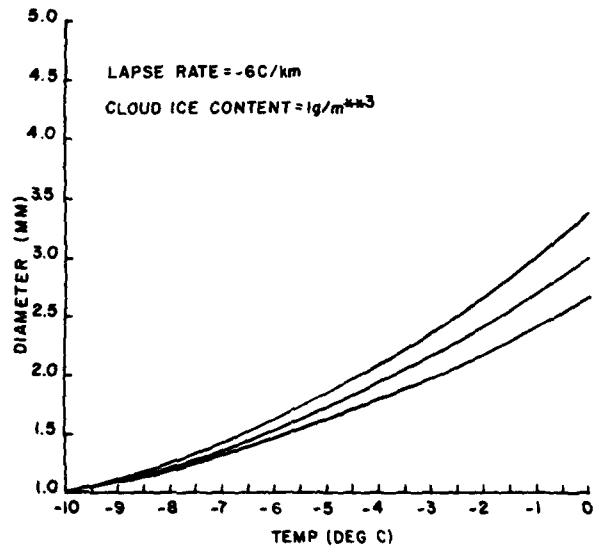
(a) Cloud Ice Content is 1.0 g/mm^3
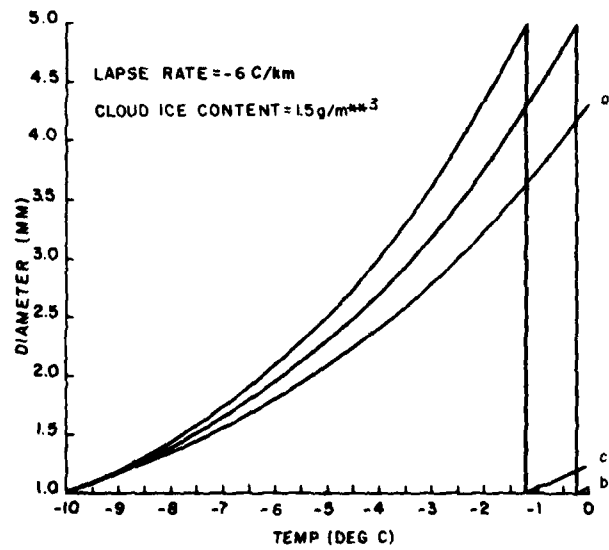
(b) Cloud Ice Content is 1.5 g/mm^3

Figure B6. Aggregational Growth and Breakup of a 1.0 mm-diameter Snowflake Falling Through the Layer from -10°C to 0°C. Lapse rate is constant at -6°C/km. Curves are for mean collection efficiencies of a) 0.8, b) 0.9, and c) 1.0

47

Note that the aggregation rate increases as the flakes approach the freezing level (curves become more vertical). This is to be expected as the growing flakes sweep out a greater area and collide more frequently with ice crystals.

At lapse rates of $-5^{\circ}C/km$ and $-6^{\circ}C/km$, breakup does not occur when the cloud ice content is 1.0 g/mm^3 (Figures B5(a) and B6(a)). However, breakup is seen to occur at all three lapse rates when the cloud ice content is 1.5 g/mm^3. Figure B4(b) illustrates how the growth then continues from 1-mm diameter until the freezing level is reached. The number of small particles that result each time a growing aggregate breaks up cannot be determined at the present time. However, if the flake were to splinter entirely into 1-mm diameter particles, there would be 25 for every 5-mm diameter snowflake undergoing breakup. It is reasonable to assume that some of the broken fragments will be larger, and some will be smaller than 1 mm, but in any case, aggregation and breakup appears to be a powerful mechanism for ice multiplication. Also note that the size of the ice particles entering the melting layer after resumption of growth is considerably larger than those that began the aggregation process, ranging from 1.75 to 3.25 mm in diameter for the case of $-4^{\circ}C/km$ lapse rate and 1.5 g/mm^3 cloud ice content.

Thus aggregational growth and breakup will yield greater numbers of larger snowflakes than were present before aggregation began. This in itself may account for a large part of the radar echo enhancement (bright band) in the melting layer, especially when these flakes become water-coated.

B6. RECOMMENDATIONS

The research done here during the summer of 1981 represents only the initial phase of an extensive study of melting layer processes being conducted by AFGL. Most of what is known about the melting layer comes from ground-based radar observations. In more recent years, Doppler radar has been utilized to give profiles of particle fallspeeds.

However, there is a singular lack of in situ data concerring the microphysics of the melting layer. The five or six flights by the MC-130E that we looked at provided very little data, as they were mostly confined to altitudes above the $0^{\circ}C$-isotherm. In the one or two flights that did penetrate the melting layer, only limited data were obtained as the time in the melting layer was short.

At this time, AFGL does not have a research aircraft, either Air Force operated or under contract. Such an aircraft is necessary to continue the research and gather enough reliable data in the melting layer to allow reasonable conclusions regarding its nature to be drawn. Among the important parameters that can be studied with new flight data are:

1. Cloud ice content
2. Liquid water content
3. Droplet size distribution
4. Ice crystal number density
5. Snowflake aggregation and breakup

The last parameter has been shown to be an important ice multiplication mechanism; however, the aggregation model developed herein is relatively simple and contains many assumptions. A larger data base would allow refinement of the model to a point where growth of snowflakes by other mechanisms (accretion, diffusion, etc.), as well as more realistic assumptions, could also be considered, and the growth of a snowflake could be more fully and accurately modeled.

Also, we need to understand more fully how a snowflake melts when it falls past the 0°C-level. Exactly what happens to it? Does it retain its shape until fully melted? How does its fallspeed change? What effect does collision with water droplets have when it is partially melted? Such studies can be done in the laboratory, possibly augmented by in-cloud observations. Some of these studies are currently being done for AFGL under contract.

In addition, I believe that more radar observations of the melting layer must be made. There is some disagreement as to the effect of particles in the melting layer on the polarization of the returning radar pulse. This is an area that needs further study.

The first description of the radar bright band was published approximately 35 years ago (Ryde, 1946[B16]). The research being conducted at AFGL represents one of the first major attempts in those 35 years to describe the melting layer by studying it from the inside as well as the outside.

Acknowledgments

B16. Ryde, J. (1946) The attenuation of radar echoes produced at centimetre wavelengths by various meteorological phenomena, Report of Conf. on Meteor. Factors in Radio Wave Propagation, London, England, pp. 169-189.

References

B1. Austin, P.M., and Bemis, A. (1950) A quantitative study of the bright band in radar precipitation echoes, J. Meteor. 7:165-171.

B2. Hooper, J., and Kippax, A. (1950) The bright band: a phenomenon associated with radar echoes from falling rain, Quart. J. Roy. Meteor. Soc. 76:125-131.

B3. Browne, I.C. (1952) Radar studies of clouds, Ph.D. Thesis, Cambridge University, England.

B4. Mason, B.J. (1955) Radar evidence for aggregation and orientation of melting snowflakes, Quart. J. Roy. Meteor. Soc. 81:262.

B5. Gupta, B., Mani, A., and Ventikeshwaran, S. (1961) Some observations of melting band in radar echoes at Poona, Ind. J. Meteor. and Geophys. 12:317-322.

B6. Lhermitte, R., and Atlas, D. (1963) Doppler fallspeed and particle growth in stratiform precipitation, Proc. Tenth Conf. on Radar Meteorology, Washington, D.C., pp. 297-302.

B7. George, J.J. (1960) Weather Forecasting for Aeronautics, Academic Press, New York, pp. 410-415.

B8. Glass, M. (1981) Private communication.

B9. Cohen, I.D. (1981) Private communication.

B10. Lo, K., and Passarelli, R., Jr. (1981) A new sampling technique for quantitative airborne studies of snow growth: theory and examples, J. Atmos. Sci. (in press).

B11. Hobbs, P.V. (1973) Ice in the atmosphere: a review of the present position, in Physics and Chemistry of Ice, Whalley, Jones, and Gold, Ed., Royal Society of Canada, Ottawa, Canada, pp. 308-319.

B12. Rogers, R.R. (1979) A Short Course in Cloud Physics, Pergamon Press, New York.

B13. Mason, B.J. (1971) The Physics of Clouds, Clarendon Press, London, England.

B14. Magono, C. (1953) On the growth of snowflake and graupel, Science Reports of Yokohama National University, Sect. I, (No. 3), pp. 33-40.

50

B15.   Passarelli, R., Jr. (1978) Theoretical and observational study of snow-size spectra and snowflake aggregation efficiencies, J. Atmos. Sci. 35:882-889.

B16.   Ryde, J. (1946) The attenuation of radar echoes produced at centimetre wavelengths by various meteorological phenomena, Report of Conf. on Meteor. Factors in Radio Wave Propagation, London, England, pp. 169-189.

Appendix C

A New Sampling Technique for Quantitative Airborne
Studies of Snow Growth: Theory and Examples

by

K. Kenneth Lo and Richard E. Passarelli, Jr.
Department of Meteorology and Physical Oceanography
Massachusetts Institute of Technology
Cambridge, Massachusetts 02139

The following article describes the Passarelli Spiral, or Advecting Spiral Descent (ASD), which has been used to observe snow growth in the atmosphere. This spiral flight plan will be used to gather data and to investigate microphysical processes operating in the melting layer. All of the research reported in this article, the work at MIT as well as the C-130 flights, data reduction, and analysis performed by Cloud Physics Branch, were funded by the AFOSR/AFGL basic research task in cloud physics. Professor Passarelli is the principal investigator under contract F19628-80-C-0021.

Abstract

In studies of precipitation growth, comparisons between theory and observations are difficult to perform because of the difficulty in obtaining a complete four-dimensional (4-D) (space and time) description of the kinematic, thermodynamic, and microphysical properties of the natural atmosphere. A new flight plan has been devised that permits one to observe the height evolution of snow-size spectra in a reference frame where the effects of horizontal gradients and temporal changes of the atmosphere are minimized. Consequently, the evolution of snow-size distribution is reduced to a 1-D steady-state problem. The flight plan, termed Advecting Spiral Descent (ASD), requires an aircraft to start aloft in a mesoscale precipitation area. Then it spirals downward in a constant bank angle, descending at approximately the mean fallspeed of snow. The spiral drifts with the winds. The advantage of ASD is no a priori knowledge of the vertical wind profile is required. The analysis is performed by averaging spectra over a complete loop of the spiral, serving to average any horizontal homogeneities. Several examples of data are given along with a brief comparison with theoretical results. The results show that snow growth is a well-behaved phenomenon and the ASD technique is sampling it in a coherent manner. The qualitative comparisons between observations and theory suggest snow growth evolves through at least three stages, namely deposition, aggregation, and breakup. This technique has potential applications in physical studies of cloud seeding and has already provided considerable insight into the physical processes of snow growth.

C1. INTRODUCTION

The ultimate test of a theoretical model of a physical process is how well the model can describe the natural occurrence of the process. In studies of precipitation growth, such comparisons are difficult to perform because of the difficulty in obtaining a complete 4-D (space and time) description of the kinematic, thermodynamic, and microphysical properties of the natural atmosphere. The rather detailed descriptions of the atmosphere that can be obtained from microphysical/dynamic models are typically beyond our observational capability for verification.

The theoretical modeling of snow growth by one of the authors (Passarelli, 1978a,[C1] 1978b[C2]) raised the question of how to verify the model results using measurements of snow-size spectra obtained by a single aircraft equipped with laser imaging probes. In this paper we present a flight plan that permits one to observe the height evolution of snow-size spectra in a reference frame where the effects of horizontal gradients and temporal changes in the microphysical and

C1. Passarelli, R.E., Jr. (1978a) The evolution of snow-size spectra in winter storms, Ph.D. Thesis, The University of Chicago, 100 pp.

C2. Passarelli, R.E., Jr., (1978b) An approximate analytical model of the vapor deposition and aggregation growth of snowflakes, J. Atmos. Sci. 35:118-124.

dynamic properties of the atmosphere are minimized. In eifect, the aircraft is constrained to drift with a region of falling snow in a Langrangian frame of reference tied to the average particle motion. In this reference frame the evolution of the size distribution of snow reduces to a simple 1-D steady-state problem so that a single aircraft can provide sufficient data for comparison with results from simple 1-D microphysical models.

First, we present a simple sedimentation model of falling sno√ to provide the physical rationale behind the flight plan, followed by a description of the aircraft track. Several examplei √f data are given along with a brief comparison with theoretical results. A more complete comparison between theory and observation will be presented in a later paper.

The results from the new technique show that snow growth is a very well-behaved phenomenon whose evolutionary processes can, to a large extent, be observed with current instrumentation. The technique has potential applications in physical studies of cloud seeding and has already provided considerable insight into the physical processes of snow growth.

C2. THE PHYSICAL RATIONALE BEHIND THE SAMPLING PROCEDURE

The change in the size distribution of snow at any point in time and space is governed by advection (air motion and particle fallspeed), primary particle growth (deposition or evaporation and riming of supercooled drops), the redistribution of mass within the size distribution (aggregation and breakup), and the production of new ice particles (nucleation). The question addressed here is whether a single aircraft can sample the atmosphere in such a way so as to separate the effects of advection from these microphysical processes.

Perhaps the most desirable situation for a single aircraft study of snow growth is that of widespread, steady-state snow. In the absence of horizontal gradients, horizontal advective processes make no contribution to changes in the size distribution. An aircraft can merely sample the atmosphere at various heights, at leisure, provided that conditions are steady. The particle growth can then be inferred from the height change in the size distribution. Unfortunately, even in widespread storms there are usually mesoscale areas of precipitation that move and change with time. Horizontal gradients in the properties of the atmosphere coupled with the effects of advection, fallspeed dispersion, and wind shear create a difficult sampling problem even if conditions are steady.

To illustrate this, consider a simple two-dimensional (2-D) sedimentation model of a finite, horizontally homogeneous, steady, line source of snow aloft which is 10-km wide and located 5 km above the earth's surface in an atmosphere having

55

constant shear (for example, Marshall, 1953[C3]). We assume, that no particle growth occurs and that updrafts are weak compared to fallspeeds. A particle starting from the source at height (Z_o) will fall and be deflected from its initial horizontal position (X_o) with respect to the source, that is, the particle trajectory is

$$X = X_o + \frac{S}{2} \frac{(Z_o - Z)^2}{V_f} \tag{C1}$$

where X is the horizontal position of the particle with respect to the source, S is the shear, Z is the height below the source, and V_f is the fallspeed. Neglecting horizontal gradients in the wind, all particles having the same fallspeed will have parallel trajectories. Figure C1 is a scale drawing of the precipitation "trails" for two particle fallspeeds (80 cm s^{-1} and 130 cm s^{-1}) assuming a constant wind shear of 10^{-3} s^{-1}. Note that the reference frame is fixed to the source. The width of the region occupied by particles of a given fallspeed is always equal to the width at the source. However, because particles of different fallspeeds define different trajectories, size sorting occurs and horizontal gradients develop. The region occupied by the large (130 cm s^{-1}) particles is indicated by horizontal hatching and the region occupied by the small (80 cm s^{-1}) particles is indicated by vertical hatching. The right-hand side of this precipitation trail contains no small particles while the left-hand side contains no large particles. However, the region of overlap for these two fallspeeds has uniform properties which are identical to the source region. If the particle fallspeeds are bounded by these hypothetical limits then the complete size distribution (all fallspeeds) will be constant in the region of overlap. The properties of the snow in the central region in Figure C1 are identical to those corresponding to an infinite line source aloft.
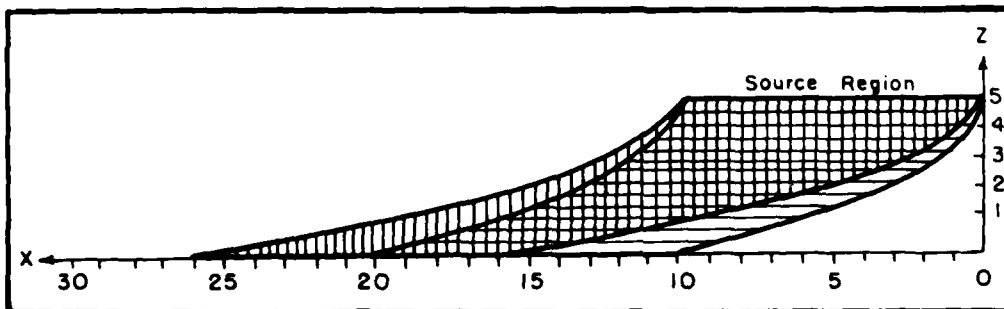

Figure C1. Particle Trajectories From Steady-state Line Source, Scales in km. Note that the reference frame is fixed to the source

C3. Marshall, J.S. (1953) Precipitation trajectories and patterns, J. Meteor. 10:25-29.

This example illustrates that for steady, finite, upper level source regions in which the dynamic and microphysical properties are relatively constant in horizontal space, there will be a limited region below which behaves as if there were an infinite, horizontally homogeneous source aloft. In this region the effects of horizontal advection can be ignored and snow growth can be treated as a 1-D (height) steady-state problem. Of course the smaller the horizontal gradients, the greater the depth over which this assumption will remain valid.

The problem of temporal variability of the source region can be examined in a similar manner. Let us again consider only two fallspeeds, 80 and 130 cm s^{-1}, and use the identical geometry and shear as in the previous case, however, let the steady source act for only 3125 s. During this time, the small flakes fall to 2.5 km and the large flakes fall to 4.0 km. Figure C2 shows the regions occupied by the two populations after the source shuts-off at 3125 s, and 6250 s when the first small flake hits the ground. After 3125 s there is a large region in which the snow has the steady-state properties of the initial source. At 6250 s, 3125 s after the source is turned off, there is still a region close to the surface that has the steady-state properties of the source. Recall that this region also has the properties of a horizontally infinite source.
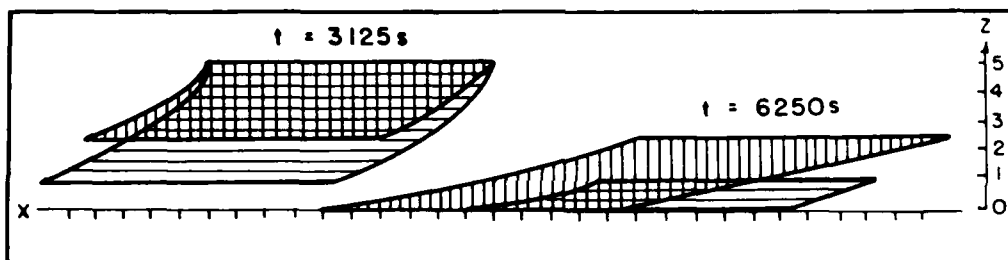
Figure C2. Particle Trajectories From Time-dependent Line Source, Scales in km. Note that for a source that varies slowly in time, there can be a region below that behaves as if the source were infinite and steady

This example illustrates that for a source that varies slowly in time, there can be a region below that behaves as if the source were infinite and steady. The center of this region falls at a rate equal to the average particle fallspeed. Ideally, if one could use an aircraft to follow this region, then the snow growth problem reduces to a 1-D (height) steady-state problem. We will refer to this region as the 1-D region.

The primary assumption in both of these analyses was that the fallspeeds lie between finite limits. Also the lower limit cannot be zero. These are fairly good assumptions for snow since observations show that the fallspeed of snow is only a

weak function of particle size. This is particularly true of unrimed cyrstals and aggregates (for example, Locatelli and Hobbs, 1974[C4]).

To illustrate the narrow dispersion of snowflake fallspeeds we can consider a specific example of an exponential distribution of equivalent melted diameters and a power law fallspeed-melted diameter relationship, that is,

$$N(D_m) = N_o e^{-\lambda D_m} \tag{C2}$$

$$V_f = aD_m^b \tag{C3}$$

where $N(D_m)\Delta D_m$ is the concentration of particles in the melted diameter interval $[D_m, D_m + \Delta D_m]$, N_o, and λ are the distribution parameters, V_f is the fallspeed, and a and b depend on the snowfall type. One can show that the relative dispersion (standard deviation/mean) of the mass flux as a function of fallspeed depends on b only,

$$\frac{\sigma}{\tilde{V}} = \left[\frac{\Gamma(4+3b)\, \Gamma(4+b)}{\Gamma^2(4+2b)} - 1 \right]^{1/2} \tag{C4}$$

where σ is the standard deviation of the mass flux-fallspeed distribution, $\tilde{V}$ is the mean mass flux fallspeed and Γ represents gamma function. For aggregate snow $b \sim 0.3$ (Langleben, 1954[C5]) so that the relative dispersion is only 15 percent. In the sedimentation examples, we used 80 and 130 cm s^{-1} as the fallspeed limits. The ± 2 fallspeeds are 74 and 137 cm s^{-1}, assuming a mean mass flux fallspeed of 105 cm s^{-1} and b = 0.3. Thus for snow, the vast majority of the mass flux is contained within a narrow range of fallspeeds.

Summarizing the discussion of the simple sedimentation models we can say that there is a region below a time-dependent, horizontally finite source that behaves as if the source were steady and infinite. This 1-D region exists provided that the fallspeed dispersion is finite (lower bound not equal to zero). The sampling scheme, which is suggested by these analyses, is to start at the center of such a source region and then follow the motion of an "average" particle as it falls and is advected by the horizontal wind. Observations of the particle-size distribution in this reference frame can then be interpreted by means of a 1-D (height) steady-state model of particle growth.

The technique has the greatest chance of success in regions of large-scale winter storms in which vertical air velocities, horizontal gradients, and temporal

C4. Locatelli, J. D., and Hobbs, P. V. (1974) Fallspeeds and masses of solid precipitation particles, J. Geophys. Res. 79:2185-2197.

C5. Langleben, M. P. (1954) The terminal velocity of snow aggregates, Quart. J. Roy. Meteor. Soc. 80:174-181.

variations are small. If these conditions prevail then there is usually very little, if any, supercooled water so that riming growth is not significant (for example, Passarelli, 1978b;[C2] Herzegh and Hobbs, 1980[C6]). The precipitation is in the form of snow and ice crystals and nucleation, deposition, aggregation, and possibly breakup are the microphysical processes, which can act to change the size distribution.

C3. THE AIRCRAFT FLIGHT TRACK

C3.1 Flight Procedure

Having defined an optimal region for studying snow growth in the natural atmosphere, we propose the following flight profile for sampling with a single aircraft. Starting aloft in a mesoscale precipitation area, the aircraft is placed in a constant bank angle ($\sim 15^\circ$) and a constant descent rate (~ 1 ms^{-1}). The aircraft spirals downward at approximately the mean fallspeed of snow and the loops of the spiral drift with the wind. Ideally, if conditions are quasi-steady and the properties of the atmosphere are fairly uniform over a length scale somewhat larger than the diameter of the loops, then the aircraft will remain in a 1-D region. We call this flight track the Advecting Spiral Descent (ASD).

An important advantage of the ASD in sampling a 1-D region is that one does not require an a priori knowledge of the vertical wind profile. The aircraft adjusts automatically to the wind shear since the loops of the spiral are flown relative to the air (bank angle constant) rather than relative to the ground. In principle, knowing the wind as a function of height and an average fallspeed one could construct a series of horizontal passes that would accomplish the same task, but the procedure is relatively complex in four-dimensions as compared to the ASD approach.

The analysis of particle size spectra sampled via the ASD technique can be performed by averaging spectra over a complete loop of the spiral. A loop is defined as when the aircraft completes a 360° turn. This serves to average any horizontal inhomogeneities. Ideally, one would like horizontal inhomogeneities to be minimal over the radius of the loops.

Another approach is to compare particle size spectra at various heights that occurred in the same sector of different loops (for example, using magnetic heading). Ideally, if all the loops are the same size and the aircraft performs a 1 ms^{-1} ASD, then each point of the aircraft trajectory corresponds to the trajectory of a 1 ms^{-1} particle. After turning 360° (completing the next loop) the aircraft should

C6. Herzegh, P.H., and Hobbs, P.V. (1980) The mesoscale and microscale structure and organization of clouds and precipitation in midlatitude cyclones. II: Warm frontal clouds, J. Atmos. Sci. 37:597-611.

59

encounter the same 1 ms^{-1} particle at a lower altitude. This is stretching the technique to the ultimate limit. In practice, as discussed in the next section, the loops get smaller as the aircraft descends so that the aircraft does not actually "reencounter" the same 1 ms^{-1} particle. Nevertheless, the observed point-to-point correlations can be quite high as we shall show.

C3.2 The ASD Flight Characteristics

During a coordinated turn at a constant bank angle, the aerodynamic lift, gravitational, and centrifugal forces are balanced. One can show that the radius of a turn, r is

$$r = \frac{(TAS)^2}{g} \cot \theta \qquad (C5)$$

where TAS is the aircraft true air speed, θ is the bank angle, and g is the gravitational acceleration. The turn radius as a function of bank angle for various true air speeds is plotted in Figure C3. During a descent, a pilot will usually maintain a constant indicated air speed (IAS), which is related to the true air speed by

$$\rho_o (IAS)^2 = \rho (TAS)^2 \quad , \qquad (C6)$$

where ρ_o is the density of air at a standard temperature and pressure ($0^\circ C$ and 1013 mb) and ρ is the actual air density. In a descent where the bank angle and indicated air speed remain constant, the true air speed is less at lower levels and the radius of the loops decreases in accordance with

$$r = \frac{\rho_o}{\rho} \frac{(IAS)^2}{g} \cot \theta \quad . \qquad (C7)$$

Hence, if ρ doubles over the depth of the spiral, the turn radius will decrease by one half.

Ideally, one would like to have the turn radius as small as possible to minimize the effects of horizontal inhomogeneities. Practically, the turn radius is dictated by the pilot's ability to safely maintain a given bank angle for long periods of time in instrument flight conditions. A bank angle of 30° is probably a maximum upper limit. In the examples that follow, we used $15^\circ - 20^\circ$ of bank.

60
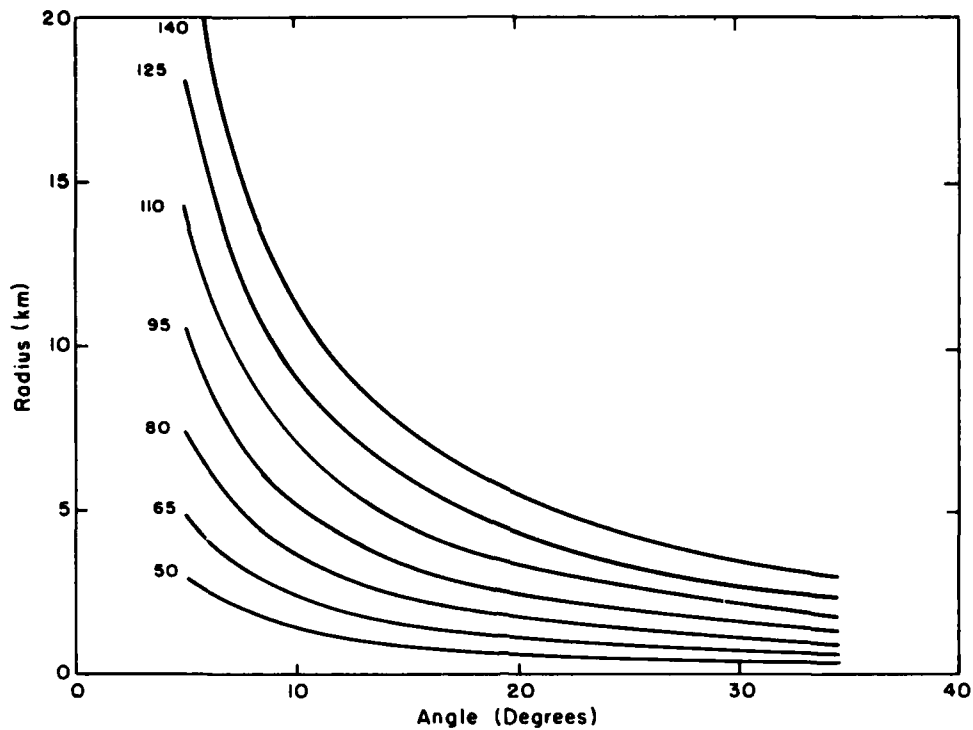
Figure C3. Turn Radius as a Function of Bank Angle for Various True Air Speeds (given in m/s) During the Advecting Spiral Descent (ASD) in Passarelli Spiral

C4. EXAMPLES OF ASD DATA

C4.1 Data and Instrumentation

To illustrate the technique we present data from the AFGL instrumented C-130 cloud physics aircraft that is equipped with a variety of sensors. Only the data from the Particle Measurement Systems (PMS) 200-Y probe will be discussed here. This is a 1-D laser imaging probe that counts and sizes particles into 15 size categories ranging from 300 μm to 4500 μm, each 300 μm wide. Three flights are presented. Two were made off the coast of Washington (25 and 26 February 1980) and one off the coast of New Hampshire (8 March 1980). One ASD was performed on each day and these will be referred to as spirals 1, 2, and 3, respectively.

All three spirals took place in cyclonic storms. Spiral 1 was flown just ahead of the front and spiral 2 was flown approximately 100-km east of the low pressure center. Spiral 3 was flown after the cold front had passed. The soundings indicated that the atmosphere was approximately moist adiabatic and saturated in all

61

cases. The height and temperature ranges for the three spirals are given in
Table C1. No significant supercooled water was detected in any of the storms.

Table C1. Three Advecting Spiral Descents

Storms	Spiral Top		Spiral Bottom	
	Height	Temperature	Height	Temperature
1	6740 m	-29 C	3060 m	-6 C
2	6940 m	-26 C	2320 m	0 C
3	3450 m	-21 C	1730 m	-5 C

C4.2 Loop Averaged Spectra

Snow-size spectra averaged over a complete loop are shown in Figure C4 for
the first spiral. The spectra are labeled consecutively from the top to the bottom
loops of the spiral. The spectra are approximately exponential in form such that

$$N(D) = N_o e^{-\lambda D} \quad , \tag{C8}$$

where $N(D)dD$ is the concentration in the size interval $[D, D+dD]$, N_o shall be
referred to as the intercept and λ the distribution slope.

The spectra from the first spiral show an initial monotonic increase in the
intercept while the slope remains relatively constant through loop 12, after which
there is a rapid decrease in both the slope and intercept during loops 13 and 14.
The remainder of the loops show essentially no change. Note that the vertical
separation between successive loops is 200 m.

Because of the quasi-exponential behavior it is convenient to characterize the
spectra by N_o and λ, which can be done via a least squares fit. Figure C5 shows
data from the three spirals in $\log_{10} N_o$ - $\log_{10} \lambda$ (hereafter, N_o - λ space). The
loop numbers are indicated next to the data points, which are connected sequenti-
ally by a line. Environmental temperatures are indicated for places where signi-
ficant changes occur.

This type of spectral display is convenient because a straight line in N_o -λ
space corresponds to a constant moment of an exponential distribution, since the
j^{th} moment of a spectrum is

$$M_j = \int_0^\infty D^j N_o e^{-\lambda D} \, dD = \frac{N_o \Gamma(j+1)}{\lambda^{j+1}} \quad . \tag{C9}$$

62
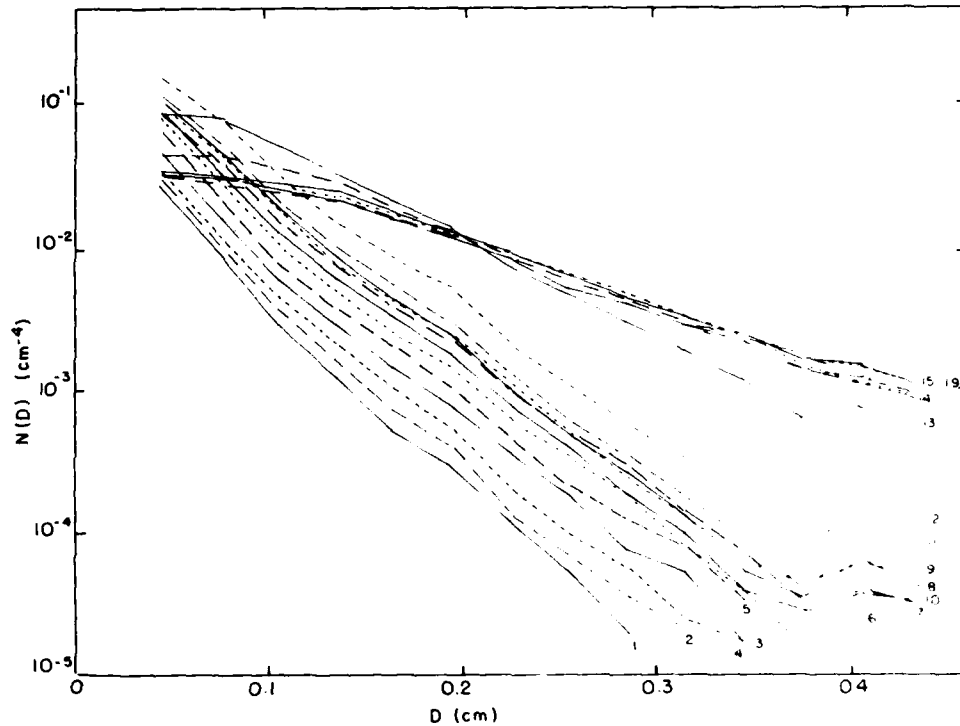
Figure C4. Snow Size Spectra for Spiral 1 (25 February 1980) Averaged Over the Various Loops. Numbers on the right indicate loop numbers

Hence in logarithmic N_o-λ space, the moment M_j is constant along any straight line having slope (J+1).

The behavior of the spectra in Figure C4 can be discussed in terms of the "trajectory" of the spectral evolution in N_o-λ space in Figure C5. The first spiral is characterized by a gradual increase in N_o and a slight decrease in λ such that the slope of the N_o-λ trajectory is negative, implying that all spectral moments are increasing. At loop 12 the spectral evolution changes dramatically and both N_o and λ decrease. Eventually N_o and λ assume approximately constant values. The second spiral shows a similar pattern of three stages of evolution. Stage 1 is characterized by an increase in N_o accompanied by relatively little change in λ. Stage 2 is characterized by a rapid decrease in both N_o and λ. Stage 3 is marked by an apparent cessation of spectral evolution. The third spiral only reveals stages 2 and 3.

The N_o-λ trajectories for the second stage of growth are roughly parallel for all three spirals, having slopes ranging from 1.80 to 1.95. This suggests that

63
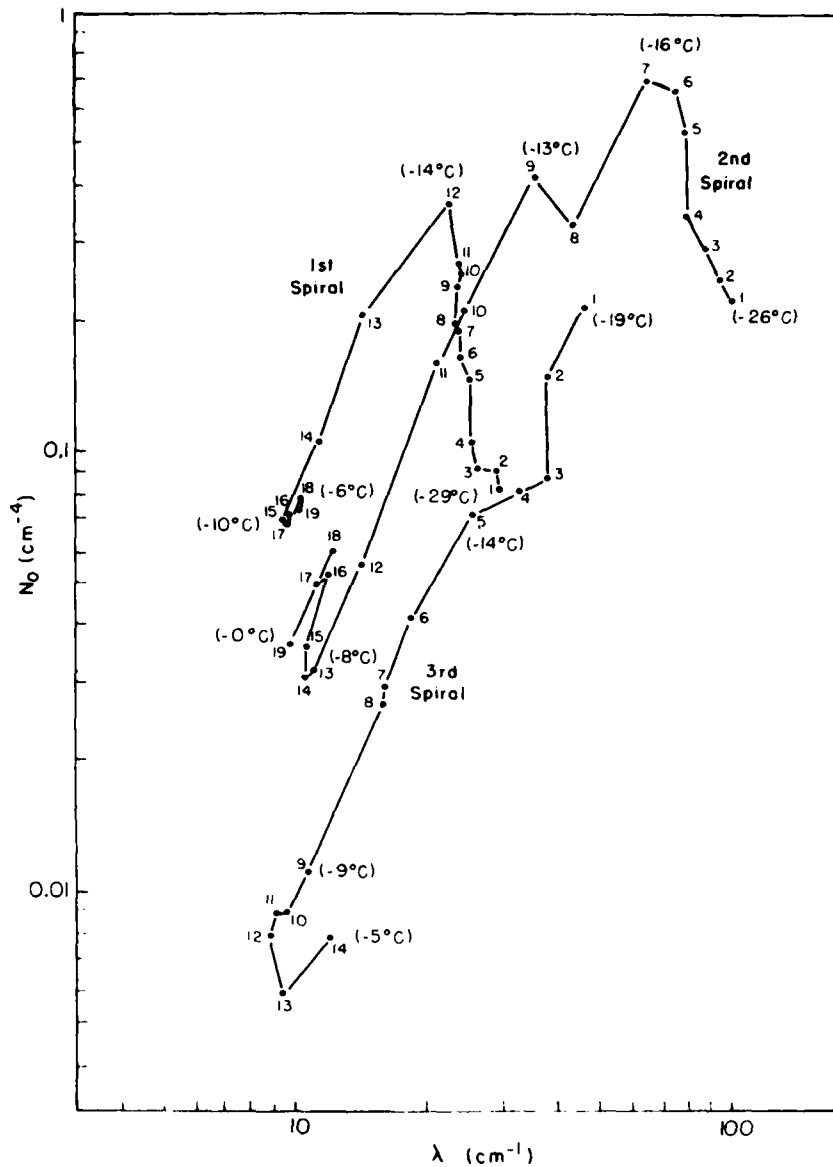
Figure C5. N_0-λ Trajectories for the Three Spirals. See text for details

during this phase of spectral evolution, the "total diameter" is a conservative property of the distribution. These three cases also suggest that the distribution slope, λ, has a minimum value of ~ 10 cm^{-1}, which characterizes the third stage of evolution.

C4.3 Horizontal Gradients in the Microphysical Structure

In order to examine the horizontal gradients in the size distributions, the mean diameter from the 200-Y spectra as a function of aircraft magnetic heading is plotted in Figure C6 for the first and second spirals. Each loop is represented by a separate graph and the loops are stacked vertically in accordance with their height. The loop in which the spectra transformed from first to second stage growth (the peak in the N_o-λ trajectory) is indicated by a star in each case. Note that before the transition, the mean diameter is essentially uniform within each loop and gradually increases with depth. (Not all upper level loops are shown.) However, after the transition, horizontal inhomogeneities develop very rapidly. Note that the features are correlated from one loop to the next.

In order to examine the point-to-point behavior of the spectra we arbitrarily divide each loop into four quadrants bounded by the cardinal directions. Ideally the spectral evolution can be studied by examining the height evolution of spectra averaged over a particular quadrant rather than over an entire loop. Figure C7 shows an example of the N_o-λ evolution for the second spiral for the four quadrants. The N_o scale is different for each quadrant in order to separate the four quadrants. Note that the four N_o-λ trajectories all show the same general features. However, the W-N quadrant starts rapid stage 2 growth earlier than the other quadrants (for example, examine loops 9 and 10).

Figure C7 illustrates that even if we examine portions of a loop the spectral evolution is coherent. This is consistent with the previous discussions. Also, the rapid development of horizontal gradients of mean diameter are apparently related to the fact that spectra in different regions undergo the transition from stage 1 to stage 2 at different heights.

C5. DISCUSSION OF SPECTRAL EVOLUTION

The regular behavior of the size spectra suggests that the ASD technique is sampling a "well behaved" physical process in a coherent manner. There is good qualitative agreement between the observed spectral evolution and Passarelli's (1978a,[C1] 1978b[C2]) analytical model of deposition and aggregation. In this section we will discuss the physical implications of the observations and present some comparisons with model results.

The effect of deposition growth on the size distribution is characterized by how the rate of change of the particle diameter depends on the particle diameter, for example,

$$\frac{dD}{dt} \propto D^{\gamma} \quad . \tag{C10}$$
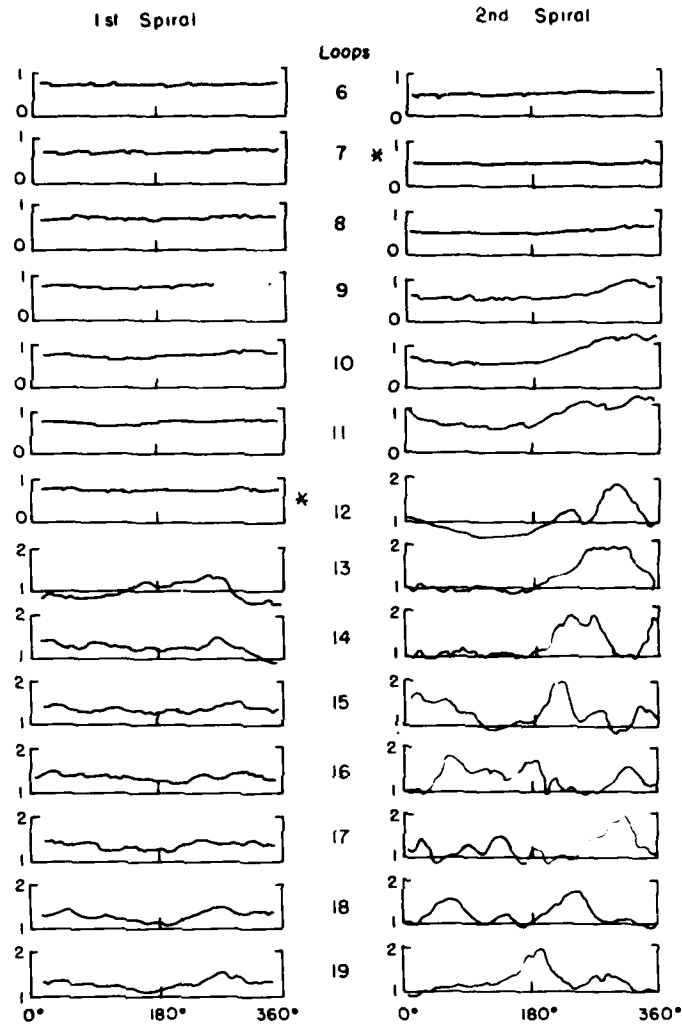
Figure C6. Average Diameter as a Function of Magnetic
Heading for Spirals 1 and 2. Diameters are given in cm.
Left-hand side is for spiral 1, right-hand side is for
spiral 2
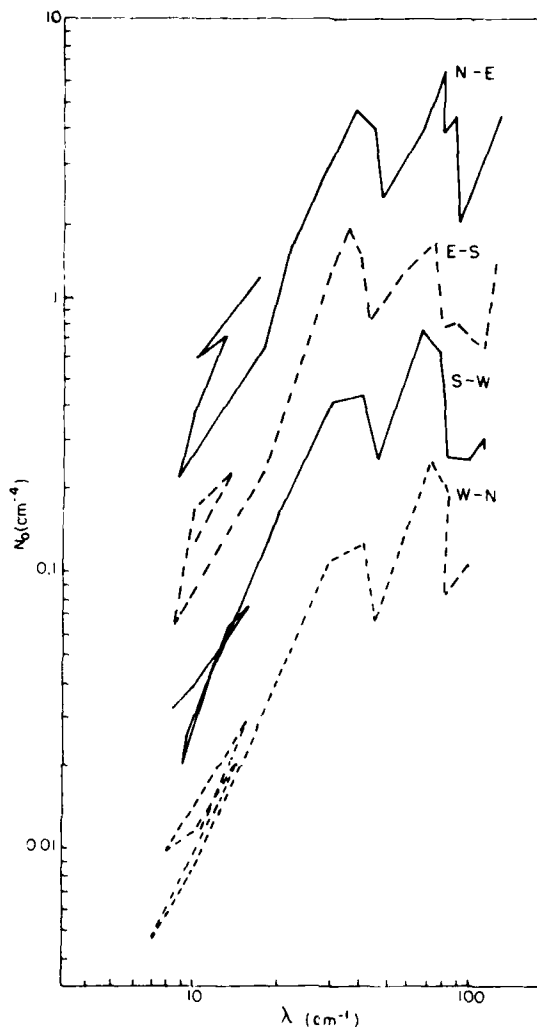
Figure C7. N_O-λ Evolution for the Cardinal
Quadrants of Spiral 2. N_O scale being differ-
ent for each quadrant in order to separate the
four quadrants. The scales on the left apply-
ing to quadrants N-E and S-W respectively,
the scales on the right applying to quadrants
E-S and W-N, respectively

67

For $\gamma > 0$, larger particles grow more quickly in diameter space and one would expect the distribution slope to decrease. For $\delta < 0$ deposition growth will cause the distribution to steepen. For snow, the particle mass varies, approximately, with the square of the particle diameter and the rate of change of mass is directly proportional to the particle diameter so that $\gamma \sim 0$. To a first approximation, all sizes will grow at the same rate in diameter space and the distribution slope will remain constant. The intercept will increase since the smaller, more numerous particles will grow into larger sizes. In the absence of a source of small particles, a lower limit to the size distribution will develop.

The first stage of particle growth (observed for spirals 1 and 2) is consistent with deposition growth. This is not to say that aggregation was not occurring, but that deposition was dominating. Note that during the first stage, the increase in N_o and the relatively slow decrease in λ suggests that the concentration increases. This is probably due to the growth of small particles into detectable sizes. The source of these small particles is either nucleation and/or secondary production.

The second stage of growth (in which both N_o and λ decrease) was observed for all three spirals. This is characteristic of aggregation that depletes small particles and creates large ones. The ASD data for spirals 1 and 2 show a very sudden transition from the dominance of deposition to aggregation. During the deposition growth phase the particles are small and collisions are rare. Eventually deposition produces sufficient number of large particles for aggregation to commence. Once started, the large particles produced by aggregation accelerate the aggregation process and rapidly deplete the smaller particles. This accounts for the sudden transition and the very rapid evolution of the size distribution after the transition. Note that on both spirals 1 and 2 the transition occurs at -15°C which is in the dendritic growth temperature range. This implies that the tendency for dendrites to form aggregates (for example, Jiusto and Weikmann, 1973[C7]) may play a role in the transition to aggregation growth. However, as we shall show, the model calculations do not require a change in the particle geometry or collection efficiency to simulate the first two stages of growth.

The most puzzling behavior is the apparent sudden end to aggregation. The spectra cease evolution when the slope reaches ~ 10 cm^{-1}. This suggests that the depletion of small particles is balanced by a production mechanism, and that large particles produced by aggregation are somehow depleted. This is consistent with a breakup mechanism. Another possibility is that the cessation of evolution is merely an instrumental artifact, but we are at a loss to explain how this could account for the observation that all three spirals evolve to the same limiting slope.

C7. Jiusto, J., and Weickmann, H.K. (1973) Types of snowfall, Bull. Amer. Meteor. Soc. 54:1148-1162.

68

The concept of snowflake breakup is very reasonable when one considers that 1 cm aggregates are quite common, but 10 cm aggregates do not exist. This suggests either that breakup is limiting aggregation growth or that aggregation is never sufficiently rapid to produce ultra-giant aggregates. The modeling results presented in the next section suggest that without breakup, aggregation would lead to continuing spectral evolution beyond the observed limiting value of the distribution slope.

The fact that all three spirals evolve to the same slope suggests a collisional breakup mechanism. This hypothesis is drawn from previous work on drop coalescence and breakup, which demonstrates that coalescence and collisional breakup lead to equilibrium distributions that have the same slope, regardless of the precipitation rate (Gillespie and List, 1976;[C8] Srivastava, 1978 [C9]).

Recent studies of ice particle breakup (Hobbs and Farber, 1972;[C10] Vardiman, 1978 [C11]) emphasize that the coexistence of dense, rapidly falling graupel along with fragile aggregates and crystals may be necessary for collisional breakup. However, our observations suggest that the presence of graupel is not necessary.

Another feature of the data which could be explained by breakup is the tendency for the small particle concentration to increase downwards. This was detected by a 1-D imaging probe for the small sizes (20 μm to 300 μm). The downward increase in the particle concentration occurred for spirals 1 and 2 and is surprising since aggregation and deposition deplete small particles. In the absence of supercooled liquid water and at the higher temperatures at the low levels it is not likely that nucleation could have been producing the small particles in concentrations of order 10 li^{-1}. Herzegh and Hobbs (1980)[C6] reached the same conclusion based on similar observations in similar storms, that is, breakup must be the source of these numerous small ice particles.

To illustrate the spectral evolution when only deposition and aggregation are acting we shall use Passarelli's (1978a,[C1] 1978b [C2]) steady-state analytical model. Briefly the model assumes that the rate-of-change of mass of a particle due to deposition is proportional to the particle diameter. The collection kernel is assumed to be

C8. Gillespie, J.R., and List, R. (1976) Evolution of raindrop size distributions in steady-state rainshafts, Preprints Int'l Conf. Cloud Phys., Boulder Colorado, Amer. Meteor. Soc. pp. 472-474.

C9. Srivastava, R.C. (1978) Parameterization of raindrop size distributions, J. Atmos. Sci. 35:108-117.

C10. Hobbs, P.V., and Farber, R.J. (1972) Fragmentation of ice particles in clouds, J. Rech. Atmos. 6:245-258.

C11. Vardiman, L. (1978) The generation of secondary ice particles in clouds by crystal-crystal collision, J. Atmos. Sci. 35:2168-2180.

$$K(D_1, D_2) = \frac{\pi}{4} \bar{E} (D_1 + D_2)^2 \mid V_1 - V_2 \mid \quad , \tag{C11}$$

where D_1 and D_2 are the diameters of the two coalescing particles, $\bar{E}$ is an average collection efficiency, and V_1 and V_2 are the particle fallspeeds. The original model assumes that the particles are spherically symmetric and have a constant bulk density. We retain the assumption of spherical symmetry, which is implicit in the collection kernel, but permit the density to be a function of size and express the mass-diameter relation as

$$m = \alpha D^\beta \quad , \tag{C12}$$

where α and β are functions of the snowfall type. The fallspeed-diameter relation is also assumed to be a power law,

$$V = aD^b \quad , \tag{C13}$$

where a and b depend on the snowfall type. The spectrum is constrained to be exponential and all these assumptions are used to derive moment conservation equations for the total mass and total square of the mass of the size distribution. This yields two nonlinear first order differential equations that are solved to obtain N_o and λ as functions of height below a reference level. The solutions are evaluated by assuming that the vertical air velocity and temperature as a function of height are known and that the atmosphere remains saturated with respect to ice. All water vapor excess (deficit) above (below) ice saturation goes to deposition (evaporation).

The reader should see Passarelli (1978a,[C1] 1978b[C2]) for details. The only change here is the use of an arbitrary power law mass-diameter relation. This analytical model, which constrains the size distribution to remain exponential, has been compared to a full numerical model which employs the same physics, and a full discretized spectrum (Leighton, 1980[C12]). The quantitative agreement was very good.

Figure C8 shows an N-λ space evaluation of the model for the following physical parameters:

C12. Leighton, H.G. (1980) A comparison of a numerical and an approximate analytical model of the growth of snowflakes, J. Atmos. Sci. 37:1409-1411.

$$E = 0.5$$
$$a = 95.0$$
$$b = 0.14$$
$$\alpha = 2.9 \times 10^{-3}$$
$$\beta = 1.9$$
$$w = 15.0$$

Locatelli and Hobbs values for dendritic aggregates,

where all units are cgs and w is the updraft speed, which was assumed to be constant. The atmosphere was assumed to be moist adiabatic with respect to ice. The spacing of the points is 200 m. The initial conditions for spiral 1 were used and the spiral 1 data points are shown for comparison.
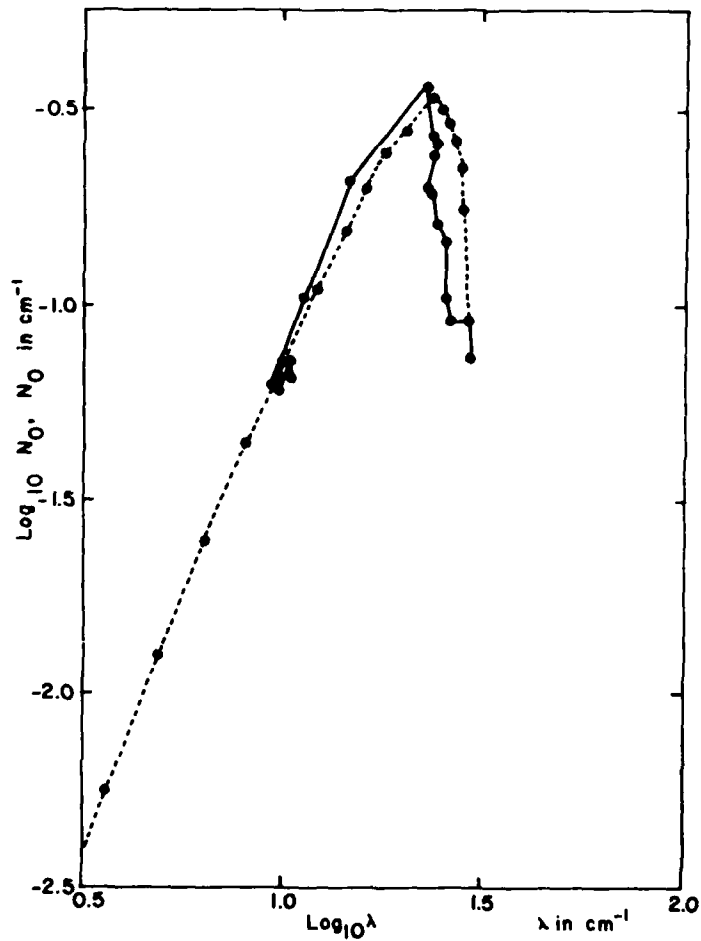

Figure C8. Model Evaluation for Spiral 1. Solid line for observations, dashed line from model results. See text (Appendix C) for details

The model adequately depicts the depositional and aggregational stages of growth. However, it cannot simulate the presumed breakup equilibrium and predicts a continual decrease in both N_0 and λ past the point where the observed spectra cease to evolve.

Reasonable fits to the other spirals can be obtained by adjusting the various physical parameters. Note that in evaluating the model for actual data, the observed N_0 and λ can be used to specify the total mass as a function of height for a known mass-size relation. The updraft can then be computed from the observed mass profile. However, without breakup in the model it is premature to launch into a detailed comparison. This will be the subject of another paper.

C6. RELATED OBSERVATIONAL STUDIES

Some recent observational studies of snow-size spectra have shown a spectral behavior similar to the ASD results, although the scatter is typically much greater. Passarelli (1978a,[C1] 1978b [C2]) employed similar instrumentation but a different vertical sampling scheme. The aircraft was placed in either a constant ascent or descent while flying at constant headings. Particle size distributions were averaged over 15 s intervals. The spectra from flights on 6 March 1975 and 10 March 1975 are shown in N_0 - λ space in Figure C9. While spectra obtained via the ASD technique show a very systematic behavior with height, the spectra obtained on these two days do not. The spectra apparently lie on a line corresponding to the second stage, but the position is random (Passarelli, 1978a [C1]). Note that the spectra for each day are very well differentiated in N_0 - λ space, which probably reflects the very different environmental conditions on the two days.

Passarelli (1978c,[C13] 1978d [C14]) also averaged particle size spectra over horizontal passes of 10-km length at various altitudes. The data for a flight on 26 November 1975 are also shown in Figure C9. The passes were spaced at 600 m and timed at 10 min apart — approximately the time required for snow to fall from one level to the next. The results show both a first stage and a second stage. Vertical incidence radar measurements on this day indicated fairly steady precipitation while the aircraft was sampling.

C13. Passarelli, R.E., Jr. (1978c) Theoretical and observational study of snow-size spectra and snowflake aggregation efficiencies, J. Atmos. Sci. 35:882-889.

C14. Passarelli, R.E., Jr. (1978d) An analytical model of snowflake growth, Con. on Cloud Phys. and Atmos. Elect. Issaquah, Wash. Amer. Meteor. Soc. pp. 142-147.
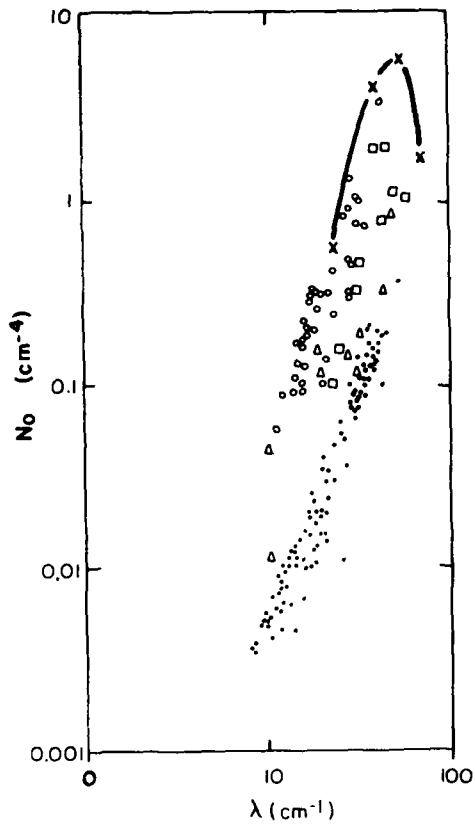
o	6 Mar 1975	(Passarelli 1978a)
•	10 Mar 1975	(" ")
x—x	26 Nov 1975	(" 1978d)
Δ	22 Jan 1976	(Houze et al, 1980)
□	8 Dec 1976	(" et al 1980)

Figure C9. Related Observational Studies.
See Section C6 for detail

Houze et al (1979,[C15] 1980[C16]) employed a similar technique by flying level passes, although no attempt was made to follow snow from level to level. The spectra for flights on 22 January 1976 and 8 December 1976 are also shown in Figure C9. The data are more scattered, perhaps because transient environmental conditions are manifested when the falling snow is not being followed. Still the observed spectra are within the values from the other cases. Although the height for each spectrum is not indicated, Houze et al (1979)[C15] show that N_o and λ decrease with decreasing temperature. Based on the general trend that temperature decreases with increasing altitude, it can be inferred that N_o and λ decrease with increasing altitude, which is in agreement with the second-stage concept.

It is revealing that all observed values indicate that the slope λ, is always greater than 10 cm^{-1}. This is in accord with the ASD results that suggest particle breakup. No matter what the height and environmental conditions are, the observed N_o values are within three orders of magnitude and the λ values are within one order of magnitude. Comparing the different sampling techniques, the ASD is more suited to show the height evolution of N_o and λ.

C7. SUMMARY AND CONCLUDING REMARKS

The qualitative agreement between the 1-D, steady-state model of snow growth and the observed size spectra suggests that the ASD technique can successfully trace a 1-D region in which the effects of spatial and temporal gradients are minimized. This technique opens the door for more detailed quantitative comparisons between microphysical theory and observation.

The qualitative comparison presented here shows that snow growth evolves through at least three distinct stages, which we have chosen to name the deposition, aggregation, and breakup stages. Initially deposition dominates. When a sufficient number of large particles has been generated aggregation becomes dominant and produces rapid changes in the size-distribution. Breakup eventually limits the production of large aggregates. We note that the breakup hypothesis, while reasonable in the light of the data and the fact that ultra-giant (10 cm) aggregates do not exist, is just that — an hypothesis. More work needs to be done to verify this.

The observed spectral evolution has some interesting implications. The transition from deposition to aggregation should be detectable by vertical incidence radar. The transition should be marked by an increase in the height, derivatives

C15. Houze, R.A., Jr., Hobbs, P.V., Herzegh, P.H., and Parsons, D.B. (1979) Size distributions of precipitation particles in frontal clouds, J. Atmos. Sci. 36:156-162.

C16. Houze, R.A., Jr., Parsons, D.B., and Herzegh, P.H. (1980) Reply, J. Atmos. Sci. 37:699-670.

of the radar reflectivity, and mean fallspeed. Deposition will generate a fairly
gradual increase in these quantities, while during the aggregational stage there
should be a rapid increase.

Another interesting aspect of the observations is the rapid aggregational
growth that should produce changes in the mean particle fallspeed. If it were
possible to perturb the deposition-aggregation transition by injecting artificial ice
nuclei, then it might be possible to exploit this for the redistribution of snowfall.
The ASD technique could be used to check this hypothesis.

There is a definite need for a larger data base and a more complete model of
snow growth. These tasks are currently underway and will be reported in a later
paper. Since there are a number of aircraft equipped to undertake these measure-
ments, it is hoped that a climatology of spectral behavior can be obtained through
the efforts of independent investigators.

Acknowledgments

References

C1. Passarelli, R.E., Jr.   (1978a) The evolution of snow-size spectra in winter
     storms, Ph. D. Thesis. The University of Chicago, 100 pp.

C2. Passarelli, R.E., Jr.   (1978b) An approximate analytical model of the vapor
     deposition and aggregation growth of snowflakes, J. Atmos. Sci.
     35:118-124.

C3. Marshall, J.S. (1953) Precipitation trajectories and patterns, J. Meteor.
     10:25-29.

C4. Locatelli, J.D., and Hobbs, P.V. (1974) Fallspeeds and masses of solid
     precipitation particles, J. Geophys. Res. 79:2185-2197.

C5. Langleben, M.P. (1954) The terminal velocity of snow aggregates, Quart.
     J. Roy. Meteor. Soc. 80:174-181.

C6. Herzegh, P.H., and Hobbs, P.V. (1980) The mesoscale and microscale structure and organization of clouds and precipitation in midlatitude cyclones. II: Warm frontal clouds, J. Atmos. Sci. 37:597-611.

C7. Jiusto, J., and Weickmann, H.K. (1973) Types of snowfall, Bull. Amer. Meteor. Soc. 54:1148-1162.

C8. Gillespie, J.R., and List, R. (1976) Evolution of raindrop size distributions in steady-state rainshafts, Preprints Int'l Conf. Cloud Phys., Boulder, Colorado, Amer. Meteor. Soc. pp. 472-474.

C9. Srivastava, R.C. (1978) Parameterization of raindrop size distributions, J. Atmos. Sci. 35:108-117.

C10. Hobbs, P.V., and Farber, R.J. (1972) Fragmentation of ice particles in clouds, J. Rech. Atmos. 6:245-258.

C11. Vardiman, L. (1978) The generation of secondary ice particles in clouds by crystal-crystal colli ion, J. Atmos. Sci. 35:2168-2180.

C12. Leighton, H.G. (1980) A comparison of a numerical and an approximate analytical model of the growth of snowflakes, J. Atmos. Sci. 37:1409-1411.

C13. Passarelli, R.E., Jr. (1978c) Theoretical and observational study of snow-size spectra and snowflake aggregation efficiencies, J. Atmos. Sci. 35:882-889.

C14. Passarelli, R.E., Jr. (1978d) An analytical model of snowflake growth, Conf. on Cloud Phys. and Atmos. Elect. Issaquah, Wash. Amer. Meteor. Soc. pp. 142-147.

C15. Houze, R.A., Jr., Hobbs, P.V., Herzegh, P.H., and Parsons, D.B. (1979) Size distributions of precipitation particles in frontal clouds, J. Atmos. Sci. 36:156-162.

C16. Houze, R.A., Jr., Parsons, D.B., and Herzegh, P.H. (1980) Reply, J. Atmos. Sci. 37:699-670.

Appendix D

Theories of Ice Crystal and Snowflake Melting

N. Fukuta
Department of Meteorology
University of Utah
Salt Lake City, Utah

D1. INTRODUCTION

When ice melts, the latent heat of fusion is absorbed by the ice and the heat is normally supplied from outside. So, melting proceeds inwards from the outer edges and surfaces of the ice.

In melting of snow crystals and snow flakes during their fall through zones of temperature higher than $0^{\circ}C$, the manner in which the heat is supplied to the ice surfaces controls the melting process. Heat may be transported to the ice surfaces through the air by the following three mechanisms: radiative transfer, sensible heat conduction, and latent heat transfer by water vapor diffusion. While the atmospheric ice melting proceeds, the cloud above and the falling melted crystals below the melting layer sustain a radiative balance in the zone. Under such a balance at a temperature as low as $0^{\circ}C$, the radiative heat transfer to the melting layer may be ignored. The heat transfer to the surface of a melting ice crystal in

the atmosphere may therefore be described by two other mechanisms: sensible and latent heat transfers.

If an ice crystal is placed in quiescent warm air without fall, a temperature field will be established around the crystal and sensible heat conduction occurs from the environment to the crystal through the field. The latent heat transfer takes place in an identical manner but in the opposite direction during water vapor diffusion from the surface to the environment. These processes are reasonably well understood with respect to ice crystal growth in a supercooled environment although their directions are reversed.

The atmospheric ice melting happens while an ice crystal falls. This ice crystal fall results in sheared air motions (convection) around the crystals, thereby deforming the temperature and water vapor fields. The fall motion of an ice crystal modifies the field most extensively at the distal points if the crystal shape were plate-like or prism-like. The distal points are for this reason the zones of fastest ice crystal melting. As ice melting proceeds, formed water should show a tendency of taking a shape of smallest surface area. Since the shape that takes the smallest surface area for a given volume is a sphere, the ice crystal shrinks from the distal points. This shape change of ice crystal during the melting leads to an increase in the fall speed. The fall speed increase in turn alters the convective air motion around the crystal and further modifies the accompanied temperature and vapor fields.

The fall speed change during the melting, although it is beyond the scope of present study, will provide important leads to estimation of ice and water content variation as a function of altitude and to interpretation of radar reflectivity data in the bright band.

We shall attempt formulation of this atmospheric ice melting process first with single crystals, and then with snowflakes.

D2. SINGLE ICE CRYSTAL MELTING

D2.1 Description of the Problem and the Approach

There are two basic shapes of atmospheric single ice crystals: plate and prism. In order to permit a smooth theoretical treatment of various factors in atmospheric ice melting, it is necessary to stimulate the two basic ice crystal shapes with simple geometrical bodies. A common practice in this regard is to use rotational spheroids, oblate for plate crystal and prolate for prism crystal. For simplicity, from now on we shall discuss the oblate spheroid. Treatment with a prolate spheroid can be easily obtained in an identical manner as we shall discuss later.

78

First of all, it is possible to treat the problems of heat conduction and vapor diffusion, respectively, to and from the ice crystal in a quiescent air environment, and then to add the effect of convective motion of air around the crystal which is caused by the fall. In stationary air, the heat conduction and vapor diffusion around the rotational oblate spheroid can be conveniently expressed by a spheroidal coordinate as shown in Figure D1. Since the effects of condensation and thermal accommodation coefficients are negligible for the ice crystal size in question, the isotherms of heat conduction and the isobars of vapor diffusion correspond to the set of confocal spheroids outside the ice crystal. Similarly, the flow lines of heat and vapor are included in the set of confocal hyperboloids of two sheets. Since the coordinate is an orthogonal system, the set of spheroids and the set of hyperboloids cross each other at right angles. An analytic solution for heat or water vapor flux at an arbitrary point of this crystal surface is available.
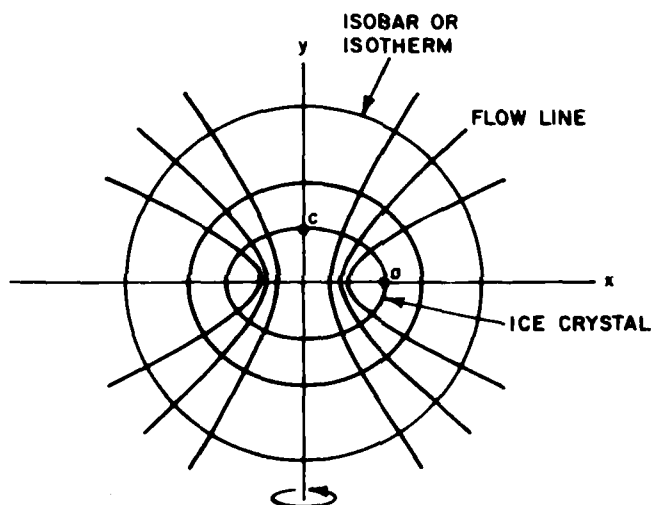
Figure D1. Rotational Oblate Coordinate for Heat Conduction and Vapor Diffusion Around a Stationary Ice Crystal in Air

The thermal flux at the distal points of ice spheroid is the largest and, as the crystal melts, the surface tension forces the formed water to gather mostly at proximal areas, letting the water lenses sandwich the crystal (see Figure D2). Under such a double system, the heat transfer by the sensible and latent heat fluxes suddenly becomes complex. There exists a clear need of proper

79
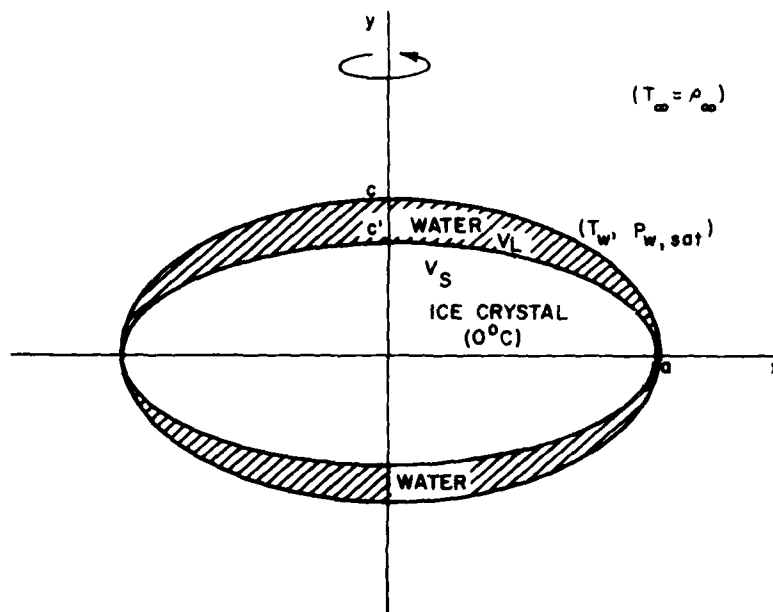
Figure D2. A Double Rotational Oblate Spheroid Model for a Partially Melted Ice Crystal. Both water and ice spheroids are in contact at the distal point, a, due to the surface tension effect of formed water

simplification. By examining the thermal conductivity in air (K_a), ice (K_i), and water (K_w);

$$K_a = 5.73 \times 10^{-6} \text{ cal (cm} \cdot \text{s} \cdot {}^oK)^{-1} \quad (0^oC)$$

$$K_i = 4.99 \times 10^{-3} \text{ cal (cm} \cdot \text{s} \cdot {}^oK)^{-1} \quad (0^oC)$$

$$K_w = 1.10 \times 10^{-3} \text{ cal (cm} \cdot \text{s} \cdot {}^oK)^{-1} \quad (0^oC)$$

$$K_w = 1.40 \times 10^{-3} \text{ cal (cm} \cdot \text{s} \cdot {}^oK)^{-1} \quad (20^oC)$$

$$1.52 \times 10^{-3} \text{ cal (cm} \cdot \text{s} \cdot {}^oK)^{-1} \quad (50^oC) \quad .$$

It may be seen that $K_w > 200 \, K_a$ at around 0^oC. This is to say that the heat conduction is slower in air under steady-state than in water. So, in addition to simulating water lenses sandwiching melted ice with a rotational oblate spheroid (see Figure D2), we assume that this double spheroid consisting of water and ice spheroids

80

behaves in the same manner as an identical ice spheroid as far as heat and water vapor fields of the surrounding air are concerned.

When this crystal falls, the convective air motion further changes the heat conduction to the spheroid. However, the overall effect of this air ventilation is known. It is clear that the ventilation effect is zero at the proximal points and is largest at the distal points. For this reason, we proceed to assume that the ventilation effect is proportional to the heat flux at the distal points.

With these assumptions, we shall attempt to estimate the rates of a, c, and c' changes.

D2.2 Melting of Plate-like Ice Crystal

D2.2.1 FORMULATION OF THE THEORY

When an ice crystal melts, the rate of heat absorption relates to the rate of melting in the following manner

$$\frac{dQ}{dt} = L_f\left(\frac{dm}{dt}\right) , \tag{D1}$$

where Q is the heat, t the time, L_f the latent heat of fusion, and m the mass of melted ice. Since the heat is supplied by two mechanisms, that is, sensible and latent heat (vapor diffusion) transfers,

$$\frac{dQ}{dt} = \frac{1}{dt}\left(dQ_s + dQ_1\right) , \tag{D2}$$

where subscript s stands for sensible and 1 for latent. Using analogy to the electrostatic field around a conductor condensor of oblate shape, (analogy was also used for the temperature and vapor fields of a growing ice crystal in a quiescent air environment), we have

$$\frac{dQ}{dt} = 4\pi C \ K_a\left[(T_\infty - T_w) - DL_c \ (\rho_\infty - \rho_{w,sat})\right] , \tag{D3}$$

where C is the electrostatic capacitance of the outer water oblate spheroid enveloping oblate ice spheroid, being given as

$$C = \frac{ae}{\sin^{-1}e} , \quad e = (1 - c^2/a^2)^{1/2} , \tag{D4}$$

81

in which a is the major axis and c the minor axis of the outer oblate spheroid, and T_∞, ρ_∞, and T_w, $\rho_{w,\,sat}$ are the temperature and vapor density in the environment and those at the water spheroid, respectively. D is the diffusivity of water vapor in air, L_c the latent heat of water condensation. Since T_w and $\rho_{w,\,sat}$ are not known, Eq. (D3) is, strictly speaking, not a solution. When $(dQ/dt) = 0$ or the sensible heat carried in by heat conduction is totally taken away by water evaporation followed by vapor diffusion away from the surface, it is possible to solve for T_w and ρ_w, such as in the cases of ice crystal or water-drop evaporation by vapor diffusion mechanism. Unfortunately, this is not the case in the present process. Instead of being zero, (dQ/dt) is the amount expended by ice melting per unit time. As we have seen in the preceding section, the thermal conductivity of water is more than 20 times larger than that of air. Furthermore, the thickness of the water layer is much smaller than that of air layer through which heat conduction must proceed. So, it may be reasonable to assume that

$$T_w = T_o \quad \text{and} \quad \rho_{w,\,sat} = \rho_o \,, \tag{D5}$$

where ρ_o is the saturation vapor density at $T = T_o$ and T_o is the melting point of ice or $0^\circ C$. Since ice melting normally takes place in air whose temperature is not far above $0^\circ C$ and whose relative humidity is high, and air flow condition around the falling and melting ice crystals is gentle, this assumption is not expected to create a large amount of error.

So far, we have obtained the expression for heat flux that is used for ice melting when the ice-containing oblate water spheroid is placed in quiescent air. When the spheroid falls through the air, the air motion changes the thermal and vapor fields around it (see Figure D3). This ventilation affects the fields differently but there are reasons to believe the difference is small and the normal practice is to set both corrections the same. Let us describe the ventilation correction by f_v. Then, we can modify Eq. (D3);

$$\frac{dQ}{dt} = 4\pi C f_v \left[K_a (T_\infty - T_o) + DL_c (\rho_\infty - \rho_o) \right] . \tag{D6}$$

The above equation already includes $T_w = T_o$, $\rho_w = \rho_o$ approximation, and it consists of known quantities only.

The above treatment has clarified heat transfer to a ventilated water spheroid containing a melting ice spheroid. Now, we try to understand the shape change inside the water spheroid during the melting. The right-hand term of Eq. (D1) may be expressed as

a

b
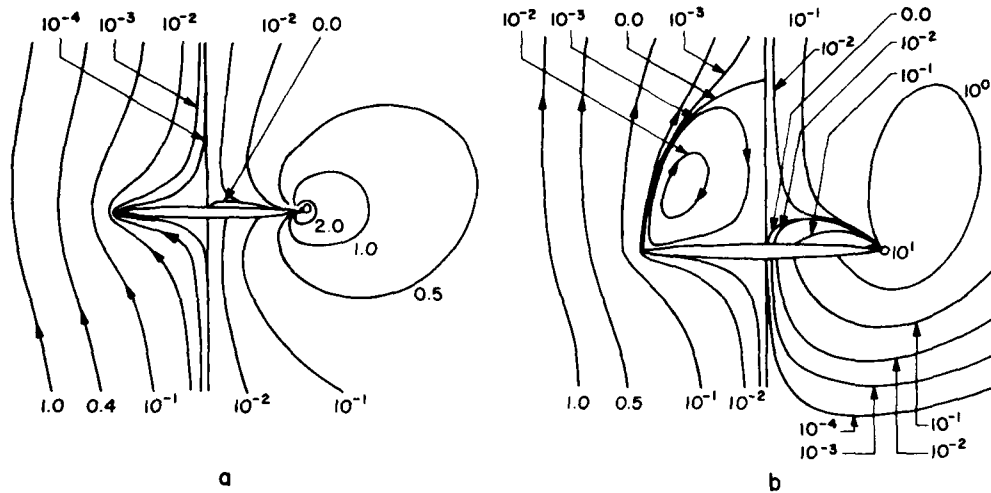
Figure D3. Numerically Computed Stream Function and
Vorticity Distribution Around an Oblate Spheroid of c/a = 0.05
at a) N_{Re} = 1.0 and b) N_{Re} = 20 (Pruppacher and Klett, 1980[D1])

$$Lf \frac{dm}{dt} = Lf \rho_L \frac{dV_L}{dt} ,$$ (D7)

where V_L and ρ_L are, respectively, the volume and the density of liquid water. If
we can ignore evaporation loss of water, the volume of the outer water spheroid

$$V = V_L + V_s ,$$ (D8)

where V_s is the volume of the ice spheroid, and

$$V = \frac{4}{3} \pi a^2 c ,$$ (D9)

and

$$V_s = \frac{4}{3} \pi a^2 c' ,$$ (D10)

D1. Pruppacher, H. and Klett, J. (1980) Microphysics of Clouds and Precipitation,
Reidel Publishing Co., Dordrecht, Holland.

83

(see Figure D2). Then from Eqs. (D8), (D9), and (D10)

$$V_L = V - V_s = \frac{4}{3} \pi a^2 (c - c') .$$ (D11)

Then

$$dV_L = dV - dV_s = \frac{4}{3} \pi \left[2a (c - c') da + a^2(dc - dc') \right] .$$ (D12)

From mass conservation ignoring the mass loss by evaporation,

$$\rho_L V_L + \rho_s V_s = m_o ,$$ (D13)

where m_o is the mass of ice crystal before melting.

It is known that the sensible heat flux to the surface of a stationary spheroid has the following relationship

$$\frac{\text{(Heat flux on the a-axis)}}{\text{(Heat flux on the c-axis)}} = \frac{a}{c} .$$

An identical relationship holds for the latent heat transfer by vapor diffusion. Therefore the above relationship is valid to the net heat flux. Since these heat fluxes are used to melt ice crystal at corresponding positions,

$$\frac{\text{(Net heat flux on the a-axis)}}{\text{(Net heat flux on the c-axis)}} = \frac{a}{c} = \frac{da}{dc'} .$$ (D14)

Note that although da corresponds to the change on the a-axis, dc', not dc, does that on the c-axis because c' represents a dimension of the ice crystal spheroid.

With the convective air motion around the falling ice crystal, the ventilation effect enhances the melting. As discussed above, the ventilation effect is assumed to be the same for both sensible and latent heat (vapor diffusion) conductions. The factor f_v relates the total effect of ventilation to the stationary heat and vapor fields. It is clear that there is no ventilation effect on the c-axis but the effect is at its maximum on the a-axis. The effect on the a-axis must be proportional to $(f_v - 1)$. Taking the proportionality constant A_1, Eq. (D14) may be modified as

$$\frac{da}{dc'} = \frac{a}{c} \left[A_1 (f_v - 1) + 1 \right] .$$ (D15)

In this treatment, we leave A_1 determination for experiments.

84

We now have three relationships for variation of a, c, and c', that is, Eqs. (D12), (D13), and (D15). Eq. (D6) adds the heat flux effect or introduces time variation to the quantities involved. So, we shall solve for da, dc, and dc' using Eqs. (D12), (D13), and (D15), using a fixed-time interval Δt to incorporate the net heat flux effect. In order to solve these equations, we convert Eq. (D13) in the following form,

$$\rho_L \, dV_L + \rho_s \, dV_s = 0,$$

or inserting Eq. (D12) and the differential form of Eq. (D10), we have

$$2a \left[- (\rho_L - \rho_s)c' + c\rho_L \right] da + a^2 \rho_L \, dc - a^2 (\rho_L - \rho_s) \, dc' = 0 \ . \tag{D16}$$

The dV_L term in Eq. (D12) is caused by the net heat flux Eq. (D6). So

$$dV_L = \frac{1}{\rho_L L_f} \, dQ \ , \tag{D17}$$

and from Eq. (D6)

$$dQ = A_2 \, Cf_v \ , \tag{D18}$$

where

$$A_2 = 4\pi \left[K_a \, (T_\infty - T_o) + DL_c (\rho_\infty - \rho_o) \right] \Delta t \ . \tag{D19}$$

In other words, dQ is the amount of heat used to melt the ice crystal in Δt time. This introduction of time interval Δt permits numerical computation as a function of time allowing incorporation of effects of time dependent variables. Eq. (D12) be··mes

$$\frac{A_2 \, Cf_v}{\rho_L \, L_f} = \frac{4}{3} \pi \left[2a \, (c - c') \, da + a^2 \, dc - a^2 \, dc' \right] \ . \tag{D20}$$

Using Eqs. (D15), (D16), and (D20) we can solve for da, dc, and dc';

$$da = -\frac{3}{4\pi ac} \frac{A_2 A_3 C}{L_f \rho_s} \left[A_1 (f_v - 1) - 1 \right] , \tag{D21}$$

85

where

$$A_3 = \frac{f_v}{\frac{2c'}{c}\left[A_1(f_v - 1) + 1\right] - 1} \quad , \tag{D22}$$

$$dc = \frac{3}{4\pi a^2} \frac{A_2 A_3 C}{L_f L \rho_s}\left\{\frac{2}{c}\left[-(\rho_L - \rho_s)c' + c\rho_L\right]\left[A_1(f_v - 1) + 1\right] - (\rho_L - \rho_s)\right\} \quad , \tag{D23}$$

and

$$dc' = \frac{-3}{4\pi a^2} \frac{A_2 A_3 C}{L_f \rho_s} \quad . \tag{D24}$$

D2.2.2 COMPUTATION SCHEME

With these solutions, it is now possible to compute melting of an ice crystal with the shape of rotational oblate spheroid falling in air with vertical temperature and relative humidity distributions.

Computation Scheme

Initial Conditions

$a = a_o$, $c = c_o$, $c' = c_o$, $T = T_o$, P, ρ_∞, v, m_o

Associated Conditions

f_v, c, ρ_s, K_a, L_c, L_f, D, A_1

dQ (18)

da (21), dc (23), dc' (24)

$a(= a_o + da)$, $c(= c_o + dc)$, $c'(=c_o + dc')$

$V + dV_L$, $V_s + dV_s$, $V + dV$

$\pi(a + da)(c + dc)$, $\pi(a + da)(c' + dc')$, $\pi(a + da)^2$

$V + dV$

Next Time Step

86
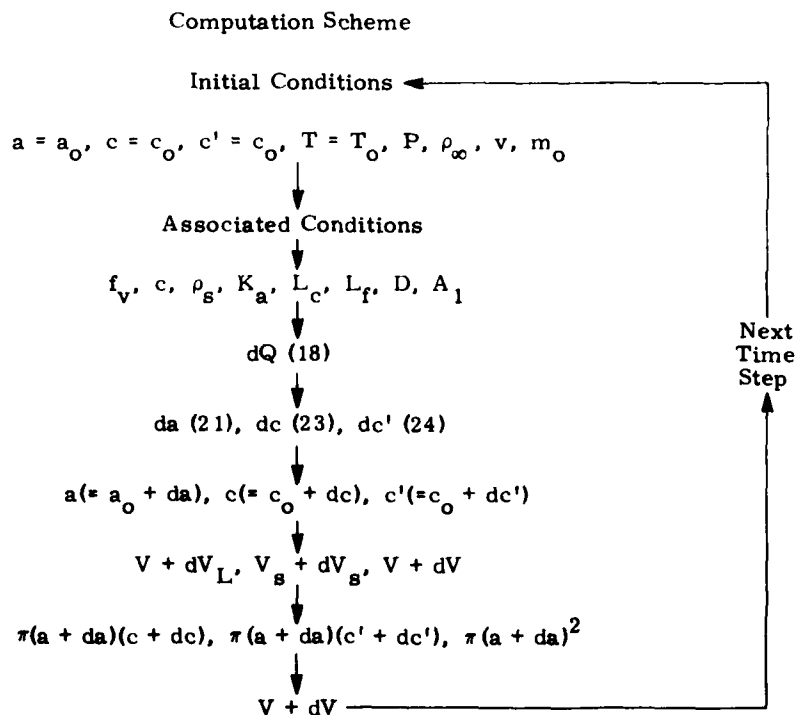
D2.2.3 VENTILATION COEFFICIENT OF VAPOR DIFFUSION AND HEAT CONDUCTION

According to Pruppacher and Klett (1980),[D1] the simplified ventilation coefficient for oblate spheroidal shaped ice crystal, f_v, is given as

$$f_v = 1 + 0.142X^2 + 0.054X^4 \ln (0.893X^2) , \tag{D25}$$

where

$$X = (N_{Sc})^{1/3} (N_{Re})^{1/2} \leq 0.71 \text{ or } N_{Re} \leq 0.63 \text{ with } N_{Sc} = 0.71 ,$$

where N_{Sc} is the Schmidt number given as

$$N_{Sc} = \frac{\nu}{D} = (\nu; \text{ kinematic viscosity}),$$

and N_{Re} is the Reynolds number given as

$$N_{Re} = \frac{2va}{\nu} ,$$

and

$$f_v = 0.937 + 0.178X , \tag{D26}$$

for $X \geq 0.71$ or $N_{Re} \geq 0.63$.

When $X \geq 1$, f_v varies linearly with X, and in our present model, X is expected to fall in this range. These authors state that for $N_{Re} \leq 100$,

$$f_v = 0.86 + 0.28X \ (X \geq 1.0) , \tag{D27}$$

agrees with experimental data to within 8 percent. So, Eq. (D27) appears to be our best choice for the ventilation coefficient.

For the terminal velocities of oblate spheroid ice crystals, Pruppacher and Klett (1980)[D1] list the following empirical relationship; for $c/a = 0.2$,

$$\log N_{Re} = B_o + B_1X + B_2X^2 , \tag{D28}$$

where $X = \log (C_D N_{Re}^2)$ and $B_0 = -1.3300$, $B_1 = 1.0217$, $B_2 = -0.049018$, and C_D is the hydrodynamic drag force coefficient, and for $c/a = 0.5$,

$$\log N_{Re} = B_0 + B_1 X + B_2 X^2 + B_3 X^3 , \tag{D29}$$

where $B_0 = -1.3247$, $B_1 = 1.0396$, $B_2 = -0.047556$, and $B_3 = -0.002327$. For an oblate spheroid,

$$C_D N_{Re}^2 = \frac{32 a^2 c (\rho_s - \rho_a)\rho_a g}{3\eta} = \frac{8 m_o \rho_a g}{\pi \eta^2} \tag{D30}$$

where ρ_a is the density of air, g the gravity acceleration, and η, the dynamic viscosity of air. They indicate that these equations are applicable for $N_{Re} \leq 100$ and beyond this level of the Reynolds number, oscillations will occur and eventually becomes a gliding-tumbling motion.

D3. SNOWFLAKE MELTING

Snowflake melting has been recently tackled by Matso and Sasyo (1981).[D2] Considering uncertainties involved in the process, their theory appears to be the best one we have at this moment. So, we briefly will review it.

The rate of heat transfer by the sensible heat conduction and vapor diffusion (latent heat transfer) can be expressed as, similar to Eq. (D3)

$$\frac{dQ}{dt} = 4\pi R f_v \varepsilon \left[K_a (T_\infty - T_w) - D L_c (\rho_\infty - \rho_{w,sat}) \right] , \tag{D31}$$

where R is the radius of snowflake, ε a factor involving the effects of various physical properties of the snowflake on the heat transfer rate. ε is assumed to be constant. For the Reynolds number between 10 and 1800

$$f_v = 1 + 0.275 N_{Pr}^{1/3} N_{Re}^{1/2} , \tag{D32}$$

where N_{Pr} is the Prandtl number being given as

$$N_{Pr} = \nu / K_a . \tag{D33}$$

D2. Matsuo, T., and Sasyo, Y. (1981) Empirical formula for the melting rate of snowflakes, J. Met. Soc. Japan 59:1-9.

$N_{Pr}^{1/3}$ does not vary much in our range of atmospheric conditions and so is taken to be 0.87. This reduces Eq. (D32) to

$$f_v = 1 + 0.24 \, N_{Re}^{1/2} \; . \tag{D34}$$

Observations show that during the melting of a snowflake, the water penetrates inwards. The ice crystal is exposed at least at the beginning of melting. The heat flux of the two kinds matches the rate of ice melting, or

$$-L_f \, 4\pi R^2 \, \rho_i dR = 4\pi R \epsilon f_v \, (K_a \Delta T + DL_c \, \Delta\rho) \, \Delta t \; , \tag{D35}$$

where $\Delta T = T_\infty - T_w$, $\Delta\rho = \rho_{w,\,sat} - \rho_\infty$ and ρ_i is the density of ice-skeleton. Equation (D35) with simplifications discussed above reads

$$-\frac{dR}{dt} = \frac{K\Delta T}{L_f \rho_i} \, \frac{1}{R} \, \epsilon \left[1 + 0.24 \left(\frac{2Rv}{\nu} \right)^{1/2} \right] \; . \tag{D36}$$

They report the solution of Eq. (D36) as

$$t = \frac{2L_f \rho_i}{\alpha^4 K\Delta T} \, \frac{1}{\epsilon} \left[\frac{1}{3} \alpha^3 \, (R_o^{3/2} - R^{3/2}) \right.$$

$$- \frac{1}{2} \alpha^2 \, (R_o - R) + \alpha (R_o^{1/2} - R^{1/2})$$

$$\left. - \ln \frac{1 + \alpha R_o^{1/2}}{1 + \alpha R^{1/2}} \right] \; . \tag{D37}$$

where $\alpha = 0.24 \, (2v/\nu)^{1/2}$ and R_o is the initial snowflake radius. Their integration was carried out under the condition $v = const.$, but in our case, v is coupled with R and this consideration is necessary when integration of (D36) is performed.

In the range $10^{-2} \le N_{Re} \le 300$, the following empirical expression may be used to relate the fall velocity to the size (Pruppacher and Klett, 1980)[D1]

$$Y = B_o + B_1 X + \ldots B_6 X^6 \; . \tag{D38}$$

89

where

$$B_o = -0.318657 \times 10^1$$

$$B_1 = +0.992696$$

$$B_2 = -0.153193 \times 10^{-2}$$

$$B_3 = -0.987059 \times 10^{-3}$$

$$B_4 = -0.578878 \times 10^{-3}$$

$$B_5 = +0.855176 \times 10^{-4}$$

$$B_6 = -0.327815 \times 10^{-5}$$

and

$$X = \ln (C_D N_{Re}^2) \text{ and } \ln N_{Re} = Y.$$

References

D1. Pruppacher, H., and Klett, J. (1980) Microphysics of Clouds and Precipitation, Reidel Publishing Co., Dordrecht, Holland.

D2. Matsuo, T., and Sasyo, Y. (1981) Empirical formula for the melting rate of snowflakes, J. Met. Soc. Japan, 59:1-9.

Appendix E

A Radar View of the Melting Layer

by

Hugh J. Sweeney
Cloud Physics Branch
Air Force Geophysics Laboratory
Hanscom Air Force Base
Bedford, Massachusetts

and

Arnold A. Barnes, Jr.
Cloud Physics Branch
Air Force Geophysics Laboratory
Hanscom Air Force Base
Bedford, Massachusetts

E1. BACKGROUND INFORMATION

The purpose of this appendix is to review the melting layer as described by observers using weather radar systems.

Ekpenyong and Srivastava (1970)[E1] carried out a theoretical study of the radar characteristics of the melting layer with the following assumptions:

E1. Ekpenyong, B., and Srivastava, R. (1970) Radar Characteristics of the Melting Layer — A Theoretical Study, Univ. of Chicago Dept. of Geophys. Sciences and Ill. Inst. of Tech. Dept. of Elec. Eng., Technical Report No. 16, Lab. for Atm. Probing, Chicago, Illinois.

1. The melting layer is assumed to have a steady thermal structure with a constant lapse rate that does not vary with time.

2. A steady supply of snowflakes of prescribed size distribution is maintained at the 0°C-level, that is, at the top of the melting region.

3. There is no aggregation or breakup of snowflakes in the melting region.

4. Snowflakes have spherical shapes.

5. The melted water forms a coat around the snowflake.

6. Growth by collision and coalescence with cloud drops and by condensation of water vapor is ignored.

They concluded that the comparison of their theoretical results with observations indicated that aggregation and breakup of melting snowflakes is a distinct possibility. The results of Lo and Passarelli (Appendix C) would indicate that any storm strong enough to have a distinct bright band would have aggregation and probably breakup operating above the melting layer. We would expect these processes to continue operating as the snow falls into and through the melting layer.

Ekpenyong and Srivastava[E1] also conclude that the temperature lapse rate may be larger than assumed in their model in the lower parts of the melting layer.

Snowflakes and aggregates are known to be non-spherical and these authors suggest that polarization measurements be made "in order to assess the effects of the non-spherical geometry of the scatterers."

Wexler (1955)[E2] suggests breaking the melting layer into two zones.

1. Zone 1 extends from the 0°C-isotherm to the peak of the radar reflectivity in the bright band.

2. Zone 2 extends from the peak of the radar reflectivity in the bright band to that point at which the snowflake is completely melted (that is, raindrops reach terminal velocity and radar reflectivity becomes nearly constant with height (Figure E1)).

E2. CALCULATIONS

In Zone 1 assume that melting takes place from the outside-in. The snow particles are becoming smaller but K^2 (K is the complex index of refraction) is changing from that for ice (0.18) to that for water (0.93);

$$|K|^2 = \left| \frac{\epsilon^2 - 1}{\epsilon^2 + 2} \right|^2 .$$

E2. Wexler, R. (1955) An evaluation of the physical effects in the melting layer, Proc. Fifth Weather Radar Conf. pp. 329-334.
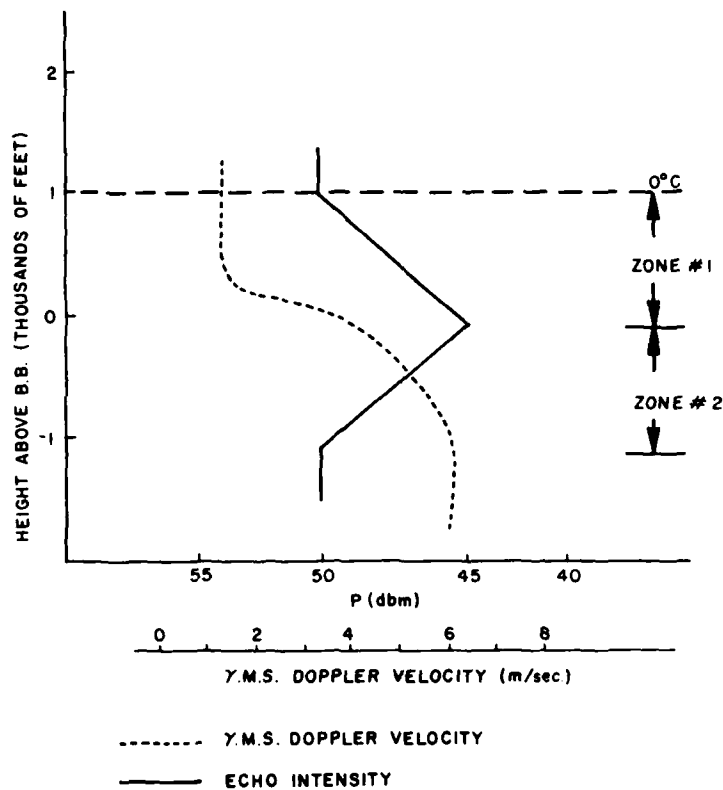
Figure E1. Defining the Zones of the Melting Layer

where

ε = dielectric constant,

K = complex index of refraction,

and

$$|K_w|^2 = 0.930, \qquad |K_i|^2 = 0.18 .$$

Let us assume that the mass of the snowflakes does not change as it melts. We define

D_m ≡ diameter of equivalent melted water drops.

D_o ≡ diameter of snowflakes.

Z ≡ D_m^6 .

93

For large snow, (which generally occurs at the top of the melting layer) Cunningham (1978)[E3] found that

$$D_m = 0.4 \, D_o{}^{0.782} \ .$$

Now the radar received power (P_r) is given by

$$P_r = C r^{-2} \, |K|^2 \, Z \ ,$$

where
$\qquad$ C = radar constant for individual radars.
$\qquad$ r = distance between radar and particle.
For a completely melted snowflake,

$$P_r(\text{water}) = C r^{-2} |K_w|^2 \, D_m{}^6$$

and for the unmelted snowflake,

$$P_r(\text{ice}) = C r^{-2} |K_i|^2 \, (0.4 \, D_o{}^{0.782})^6$$

$$= C r^{-2} |K_i|^2 \, D_m{}^6 \ .$$

The increase in signal strength due to melting of the snowflake is

$$\frac{P_r(\text{water})}{P_r(\text{ice})} = \frac{|K_w|^2}{|K_i|^2} = \frac{0.93}{0.18} = 5.17$$

or 7.1 dB. Note that this derivation depends on the assumption that the returned radar signal is a function of the water mass of the snowflake.

When a snowflake falls into the melting layer it usually melts from the outside-in, acquiring a film of water encircling the ice aggregate. According to Ekpenyong and Srivastava (1970)[E1] when one-third of the original volume of ice has melted into this film of water, the particle looks like a water drop to the radar, that is, the index of refraction has changed from that for ice to that for water.

E3. Cunningham, R.M. (1978) Analysis of particle spectral data from optical array (PMS) 1-D and 2-D sensors, Preprints, Fourth Symposium on Meteorological Observations and Instrumentation, 10-14 April 1978, Denver, Colorado, pp. 345-350.

If at this point, there is any air inside the circumscribed sphere making the diameter of the circumscribed sphere greater than D_m and if the radar scattering process is to any extent a surface phenomenon as opposed to a mass property, then there could be an increase of P_r above and beyond that due to the ice/water phase change.

If one-third of the mass has melted then $(D_n)^3 \equiv 2/3 (D_o)^3$ and the partially melted snowflake has a diameter of

$$D_n = (2/3)^{1/3} D_o = 0.87 D_o .$$

If it is encircled with water, then

$$P_r(n) = C r^{-2} \left| K_w \right|^2 D_n^6$$

$$= C r^{-2} \left| K_w \right|^2 (0.87 D_o)^6$$

$$= C r^{-2} \left| K_w \right|^2 (0.87 (D_m/0.4)^{1.28})^6$$

and

$$\frac{P_r(n)}{P_r(\text{water})} = (0.87 (D_m/0.4)^{1.28})^6 (1/D_m^6) = 494 \times D_m^{1.68} .$$

For D_m greater than 0.025 mm there would be an increase in signal.
For $D_o = 10$ mm, 1.0 cm-diameter snow, the increase would be

$$\frac{P_r(n)}{P_r(\text{water})} = \frac{(0.87 D_o)^6}{D_m^6} = 2152$$

or 33 dB. Since this type of increase is not seen when using 5 and 10 cm-wavelength radars, we must conclude that the return power is a mass and not a surface phenomenon for these wavelengths.

This means that the power received remains constant as the particle continues to melt and shrink while it falls through the melting layer. This holds true even as the particle reaches the final stages of melting, speeds up and rapidly approaches its terminal velocity. Then, the increase in velocity is about 5 to 1 (a typical case) and the concentration decreases in the same ratio. This change alone will account for a 7 dB decrease in echo intensity for the radar sampled volume at the bottom of the melting layer (Figure E2).

95
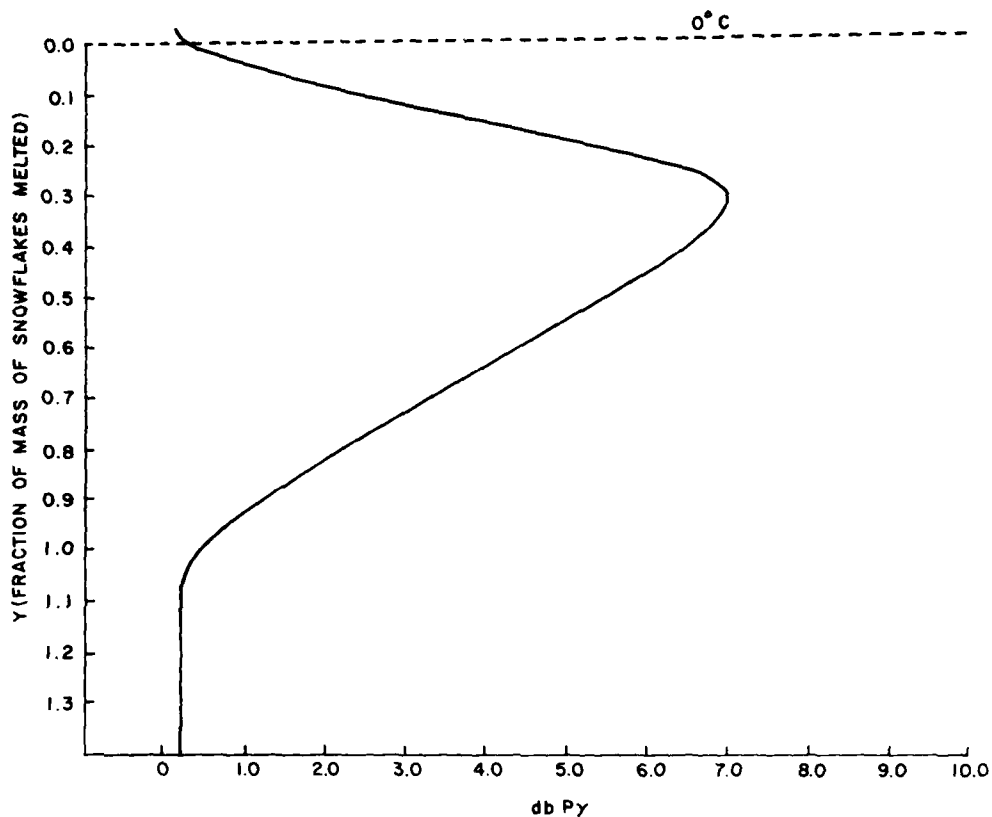
Figure E2. Power Received vs Mass Melted

E3. DISCUSSION

E3.1 *General*

In the basic melting layer model presented above, the bright-band radar signal is generated by ice aggregate particles melting within the layer. The increase in *echo intensity (zone 1) is caused by the change in value of the complex index of re-*fraction from that of ice to that of water. The decrease in signal intensity in zone 2 is attributed to the increase in fall velocity as the particles complete melt-ing (Figure E3). Not all of the processes involved are completely defined by accepted equations. Many of the parameters of the melting layer can be generated *mathematically once one knows the particle size distribution entering the melting* layer and the temperature lapse rate within the layer, but we know this is not a

96
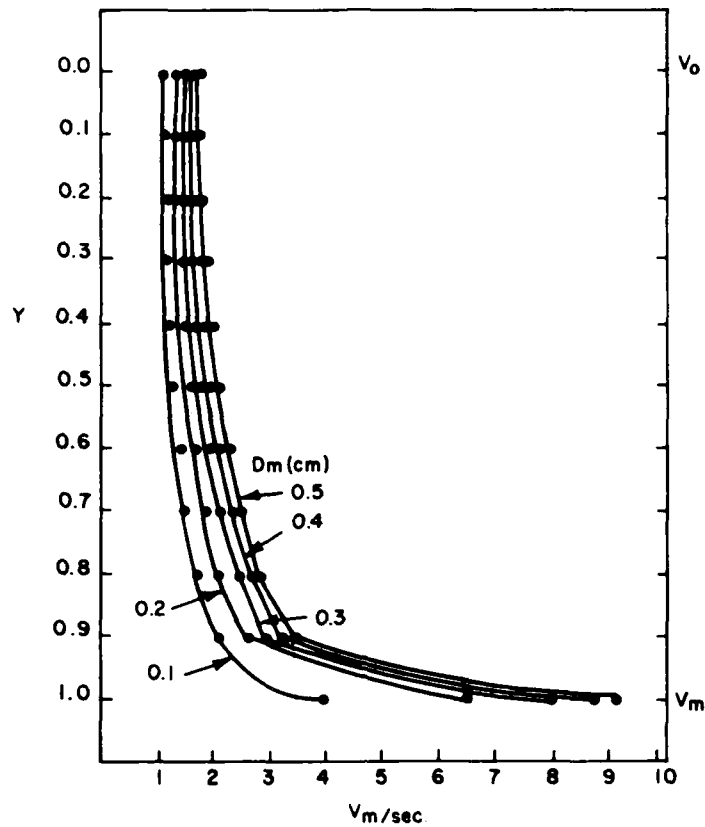
$$D_m = 0.4 \, D_0^{0.782}$$

$$V_0 = 207 \, D_m^{0.31}$$

$$V_m = 965 - 1030 \, e^{(-6D)}$$

$$Y = (D^3 - D_s^3) / D_m^3$$

$$V = V_0 \left[1 - (1 - V_0^3 / V_m^3) Y\right]^{-1/3}$$

$$V = \text{FALL SPEED OF PARTIALLY MELTED SNOWFLAKES}$$

Figure E3. Melted Mass vs Fall Velocity. Note that the fall velocity is approximately 1.0 m/sec as melting starts, then reaches approximately 5.0 m/sec as melting is almost complete

steady-state system and the internal dynamics of the melting layer must be included. In a melting layer with a steady-state thermal structure, the melting process described earlier contributes approximately 7 dB of signal intensity to the radar echo.

Numerous radar studies of the bright band show that at times the signal enhancement exceeds 7 dB. In these cases, other processes must contribute to signal enhancement. Some such possible processes are discussed.

97

AD-A115 224   AIR FORCE GEOPHYSICS LAB HANSCOM AFB MA   F/G 1/3
               A SURVEY OF MELTING LAYER RESEARCH.(U)
               JAN 82   R C SCHALLER, I D COHEN, A A BARNES
UNCLASSIFIED   AFGL-TR-82-0007   NL

2 of 2

END
DATE
FILMED
07-82
DTIC
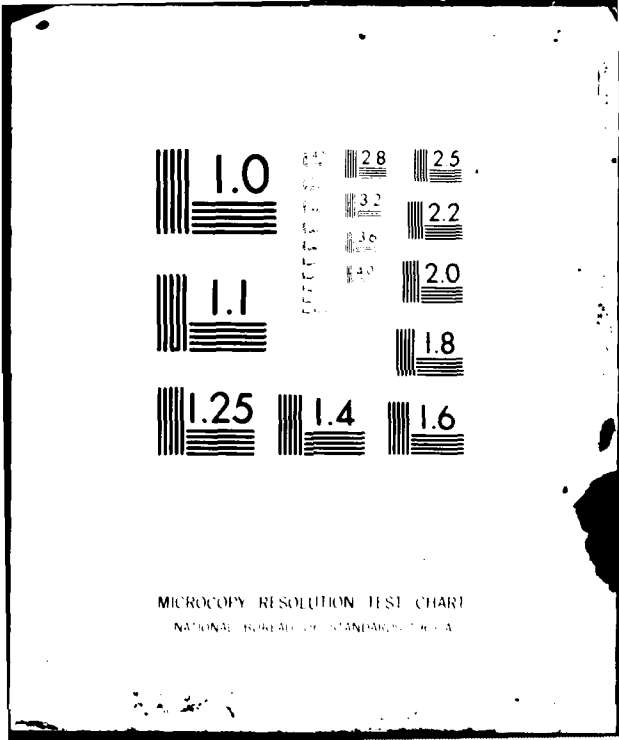
MICROCOPY RESOLUTION TEST CHART

NATIONAL BUREAU OF STANDARDS 1963 A

E3.2 Processes in Zone 1

Any process that causes a growth in the mass of a particle in zone 1 would affect Z, the radar reflectivity. This is because Z depends on M^2. Possible processes here are aggregation, collision, coalescence, and deposition. No calculation of the relative magnitude of these effects has been performed.

Another possible process in zone 1 is concerned with signal-strength variations due to the shape and orientation of scatterers in the bright band illuminated by polarized radiation. In conventional radar systems, the only component of the received signal that reaches the receivers is that which is polarized in the same plane as the incident wave so that Γ_x (intensity at the same polarization) is a measure of the echo intensity to be expected. Labrum (1952)[E4] has shown that the increase in Γ_x is introduced when the particles begin to collapse. When they are one-third melted, the collapse begins. It ends when they become spherical in shape as water drops.

E3.3 Processes in Zone 2

If the bright-band signal decreases more than 6 dB in zone 2 of this model, there must be some process leading to this extra decrease. One possibility is a breakup of water droplets with diameters in excess of 5 mm, a very realistic possibility. A breakup of 5 mm water droplets into five equi-volume droplets would result in a decrease in intensity of approximately 7 dB.

E3.4 Summary

The increase in the radar signal intensity in the so-called bright band can be explained by the following processes:

1. The complex index of refraction for ice crystals $\left|K_i\right|^2 = 0.180$ on melting changes to $\left|K_w\right|^2 = 0.930$ for water.

2. Any process that causes a growth in the mass of particles or aggregation in the melting zone would increase Z, the radar reflectivity.

3. The shape and orientation of the large snow aggregates near the top of the bright band could increase the radar echo intensity.

The following processes tend to decrease the radar echo intensity in the bright-band.

1. The increase in fall velocity of the melted particles decreases the number of scatters in the radar beam.

2. The breakup of water particles with large diameters decreases Z, the radar reflectivity.

E4. Labrum, N. (1952) The scattering of radio waves by meteorological particles, J. Appl. Phys. 23:(No.12):1324.

Those particles that attain a shape or orientation that enhances the radar echo intensity lose that enhancement when they melt and collapse to spherical shapes as water drops.

The size of the particles in the melting layer in this review are assumed to be small in size compared to the radar wavelength, that is, we assume Rayleigh scattering. The correctness of this assumption is very evident in calculations with partially melted snow. For a surface rather than a mass relationship, the returned radar signal was calculated to be much larger than actually observed, while for a mass relationship theory agrees well with observations.

References

E1. Ekpenyong, B., and Srivastava, R. (1970) Radar Characteristics of the Melting Layer — A Theoretical Study, Univ. of Chicago Dept. of Geophys. Sciences and Ill. Inst. of Tech. Dept. of Elec. Eng., Technical Report No. 16, Lab. for Atm. Probing, Chicago, Illinois.

E2. Wexler, R. (1955) An evaluation of the physical effects in the melting layer, Proc. Fifth Weather Radar Conf. pp. 329-334.

E3. Cunningham, R.M. (1978) Analysis of particle spectral data from optical array (PMS) 1-D and 2-D sensors, Preprints, Fourth Symposium on Meteorological Observations and Instrumentation, 10-14 April 1978, Denver, Colorado, pp. 345-350.

E4. Labrum, N. (1952) The scattering of radio waves by meteorological particles, J. Appl. Phys. 23(No. 12):1324.

Appendix F

Abbreviations

ABRES	Advanced Ballistic Reentry System
AF	Air Force
AFCRL	Air Force Cambridge Research Laboratory
AFGL	Air Force Geophysics Laboratory
AFOSR	Air Force Office Scientific Research
AFWL	Air Force Weapons Laboratory
ASD	Advecting Spiral Descent
CYCLES	CYCLonic Extratropical Storms
DRI	Desert Research Institute
DPSI	Digital Programming Services Inc.
EWER	Evaporate the Water that aggravates Erosion of Reentry
ICBM	InterContinental Ballistic Missile
KMR	Kwajelein Missile Range
LSCS	Large Scale Cloud Systems
LWC	Liquid Water Content
McIDAS	Man-Computer Interactive Data Access System

101

MRI	Meteorological Research Inc.
PMS	Partical Measuring Systems Inc.
SASC	Systems and Applied Science Corporation
TWCI	Total Water Content Instrument
Z	Radar Reflectivity
1-D	One-Dimensional PMS Probe
2-D	Two-Dimensional PMS Probe